FCT DOCUMENT COVER SHEET

Name/Title of Deliverable/Milestone/Revision No. Accelerated Testing of Selected Filler Compositions (Milestone M2SF-19SN010305021)

Work Package Title and Number Direct Disposal of Dual Purpose Canisters - SNL/SF-19SN01030502

Work Package WBS Number WBS: 1.08.01.03.05

Responsible Work Package Manager Mark J. Rigali (Name/Signature)

Date Submitted

Quality Rigor Level for Deliverable/Milestone[2]	☒ QRL-4	☐ QRL-3	☐ QRL-2	☐ QRL-1 Nuclear Data

This deliverable was prepared in accordance with Sandia National Laboratories
(Participant/National Laboratory Name)

QA program which meets the requirements of

☒ DOE Order 414.1 ☐ NQA-1-2000 ☐ Other

This Deliverable was subjected to:

☒ Technical Review ☐ Peer Review

Technical Review (TR)
Review Documentation Provided

☐ Signed TR Report or,
☐ Signed TR Concurrence Sheet or,
☐ Signature of TR Reviewer(s) below

Peer Review (PR)
Review Documentation Provided

☐ Signed PR Report or,
☐ Signed PR Concurrence Sheet or,
☐ Signature of PR Reviewer(s) below

Name and Signature of Reviewers

Edward N. Matteo/SNL

September 25th, 2019

Accelerated Testing of Selected Filler Compositions

Spent Fuel and Waste Disposition

Prepared for
US Department of Energy
Spent Fuel and Waste Science and Technology
by
Sandia National Laboratories, Albuquerque, NM

September 27, 2019
M2SF-19SN010305021

DISCLAIMER

This is a technical paper that does not take into account contractual limitations or obligations under the Standard Contract for Disposal of Spent Nuclear Fuel and/or High-Level Radioactive Waste (Standard Contract) (10 CFR Part 961). For example, under the provisions of the Standard Contract, spent nuclear fuel in multi-assembly canisters is not an acceptable waste form, absent a mutually agreed to contract amendment.

To the extent discussions or recommendations in this paper conflict with the provisions of the Standard Contract, the Standard Contract governs the obligations of the parties, and this paper in no manner supersedes, overrides, or amends the Standard Contract.

This paper reflects technical work which could support future decision making by DOE. No inferences should be drawn from this paper regarding future actions by DOE, which are limited both by the terms of the Standard Contract and Congressional appropriations for the Department to fulfill its obligations under the Nuclear Waste Policy Act including licensing and construction of a spent nuclear fuel repository.

Sandia National Laboratories is a multimission laboratory managed and operated by National Technology and Engineering Solutions of Sandia LLC, a wholly owned subsidiary of Honeywell International Inc. for the U.S. Department of Energy's National Nuclear Security Administration under contract DE-NA0003525. Approved for Unclassified, Unlimited Release.

This page is intentionally left blank.

SUMMARY

The fillers R&D program, mostly experimental, is part of a broader R&D program that includes new process modeling and performance assessment of criticality effects and the overall importance of criticality to repository performance (consequence screening).

A literature research and consultation effort with experts by Hardin and Brady (2018) identified several potentially effective and workable filler materials including cements (primarily phosphate based), molten-metal alloys, and low-temperature glasses. Filler attributes were defined and the preliminary lists were compared qualitatively. Further comparative analysis will be done (e.g., cost estimates) after experimental screening has narrowed the list of alternatives.

The following cement filler compositions were selected for experimental development work and accelerated testing in FY19:

- Aluminum phosphate cements (APCs); more specifically aluminum oxide / aluminum phosphate (Al_2O_3 / $AlPO_4$) cements in which Al_2O_3 serves as the filler material bound by an $AlPO_4$ binder formed by the reaction of Al_2O_3 with H_3PO_4;
- Calcium phosphate cements (CPCs); more specifically composed of pure or nearly pure hydroxyapatite ($Ca_5(PO_4)_3(OH)$);
- Magnesium potassium phosphate cements (MKPs) composed of magnesium oxide / magnesium potassium phosphate (MgO / $MgKPO_4$) cements in which MgO serves as the filler and $MgKPO_4$ serves as the binder formed by the reaction of MgO with monopotassium phosphate (KH_2PO_4) and tricalcium phosphate (($Ca_3(PO_4)_2$);

Two additional potential cement materials were explored preliminarily as the result of: (1) continued literature investigations into other filler candidates (wollastonite-based phosphate ceramic) and (2) the experimental discovery of a well-consolidated fly ash phosphate cement during the evaluation of fly ash as a potential filler material with Al_2O_3 in APCs.

- Fly ash phosphate cements, more specifically in which a fly ash material composed primarily of mullite and quartz serves as the filler and is reacted with H_3PO_4 to form amorphous phosphate phase(s) as the binder;
- Wollastonite aluminum phosphate cements (WAPC), specifically wollastonite / aluminum phosphate ($CaSiO_3$ / $AlPO_4$) in which $CaSiO_3$ serves as the filler material and $AlPO_4$ serves as the binder formed by $Al(OH)_3$ or metakaolin as Al sources and H_3PO_4 or ammonium dihydrogen phosphate (ADP) ($NH_4H_2PO_4$) as phosphate sources.

The FY19 effort focused on the optimization of compositions and subsequent processing of these five materials to achieve dense and well-consolidated monolithic samples with relatively low porosity. Once these goals were met basic material properties screening evaluations were performed including an assessment of dissolution resistance in water at elevated temperature (200 °C) and mechanical testing including unconfined compressive strength (UCS) testing.

To date, the aluminum phosphate cements (APCs) appear to show the most promise for continued development. They are easily prepared and form smooth pourable slurries that remain stable for days with relatively low viscosities of several thousand centipoise (cP). They are then set at elevated temperatures (e.g., 170 °C) under ambient (0.1 MPa) or elevated pressure (~1MPa). Overall, they demonstrate the best dissolution resistance in water at elevated temperature (200 °C) and good compressive strengths. However, additional effort is required to optimize the APC slurry formulations and the process used for thermal curing these materials. The calcium phosphate cements (CPCs) can be formed at room temperature to produce a well-consolidated body. However, their slurry viscosities are very high (and difficult to measure) and they

exhibit relatively short cure times of 2 to 3 hours. Also, dissolution resistance is very poor, the poorest of all the cements examined. The same is the case for the small number of MKP cements fabricated; they cure very quickly (10 minutes or less) and disintegrate within a few hours upon immersion in distilled water. Surprisingly, fly ash reacts with phosphoric acid to form dense and well-consolidated cements but the mixture rapidly sets at room temperature (less than 30 minutes) and the subsequent conversion of the binder to an amorphous phosphate phase(s) as a function of temperature is complicated. Finally, the wollastonite aluminum phosphate cements (WAPC) are easily prepared and form smooth pourable slurries that remain stable for several hours. They are then set at 130 °C. A WAPC sample exhibited the highest compressive strengths of all the materials we evaluated but in general their dissolution resistance to water is poor.

ACKNOWLEDGEMENTS

This report was a group effort at Sandia National Laboratories and its subcontractors with contributions from those shown in the table below.

Contributor	Role
Mark Rigali/SNL	Author of Sections 1 and 8; contributing author for Sections 3, 4, 5, 6, 7 and editor (all)
Eric Lindgren/SNL	Author of Section 2
Mark Phillips/ Pleasanton Ridge Research LLC (contractor to Sandia)	Author of Sections 3, 4, and 7
Patrick Burton/SNL	Author of Section 5
Eduardo Basurto/SNL	Author of Section 6 and editor (all)
Edward Matteo/SNL	Technical Reviewer

Compilation, summarization, and production of the document were done by Mark Rigali and Eduardo Basurto of Sandia. Thanks are due to Ed Matteo of Sandia for the technical review as well as to Peter Swift and Ernie Hardin for additional technical and editorial input.

This page is intentionally left blank.

CONTENTS

LIST OF FIGURES

LIST OF TABLES

REVISION HISTORY

Accelerated Testing of Selected Filler Compositions Deliverable: M2SF-19SN010305021 Work Package: SF-19SN01030502 –Direct Disposal of Dual Purpose Canisters-SNL WBS: 1.08.01.03.05	A review draft was first prepared for limited R&A at Sandia, which would lead to submittal to DOE/SFWD for their review prior to publication (internal use only). A technical review was first performed by Edward N. Matteo of Sandia, which resulted in this concurrence draft.

Sandia National Laboratories is a multimission laboratory managed and operated by National Technology and Engineering Solutions of Sandia LLC, a wholly owned subsidiary of Honeywell International Inc. for the U.S. Department of Energy's National Nuclear Security Administration under contract DE-NA0003525.

Approved for Limited Release (Internal Use Only)

ACRONYMS

ACS	American Chemical Society
ADP	ammonium dihydrogen phosphate
APC	Aluminum phosphate cement
BWR	Boiling water reactor
CFR	Code of Federal Regulations
cP	centipoise
CPC	Calcium phosphate cement
DCPA	dibasic calcium phosphate
DDDA	dodecanedioic acid
DI	distilled
DOE	Department of Energy
DPC	Dual-purpose canister
EDAX	energy dispersive analysis x-ray
FEP	Feature, event and/or process
FY	fiscal year
HEPA	high-efficiency particulate air
IC	ion chromatography
ICP MS	inductively coupled plasma mass spectrometry
LLW	low level waste
MKP	Magnesium potassium phosphate
MPa	megapascal
MPC	multi-purpose canister
NRC	Nuclear Regulatory Commission
OPC	ordinary Portland cement
ORNL	Oak Ridge National Laboratory
PA	Performance assessment
psi	pounds per square inch
PTFE	Polytetrafluoroethylene
PWR	Pressurized water reactor
SFWST	Spent Fuel and Waste Science and Technology
SEM	Scanning electron microscope
SNF	Spent nuclear fuel
SNL	Sandia National Laboratories

TAD	Transportation, Aging and Disposal
TGA	Thermogravimetric analysis
TTCP	tetracalcium phosphate
UCS	Unconfined compressive strength
USD	United States Dollars
WAPC	Wollastonite aluminum phosphate cement
Wo-CBPC	Wollastonite-based chemically bonded phosphate ceramic
XRD	x-ray diffraction
XRF	x-ray flourescence

1. INTRODUCTION

Commercial generation of energy by nuclear power plants in the United States (U.S.) has produced thousands of metric tons of spent nuclear fuel (SNF), the disposal of which is the responsibility of the U.S. Department of Energy (DOE). Utilities typically utilize the practice of storing this SNF in dual-purpose canisters (DPCs). And, while DPCs were designed, licensed, and loaded to meet Nuclear Regulatory Commission (NRC) requirements and preclude the possibility of a criticality event during SNF storage and transport, they were not designed or loaded to preclude the possibility of a criticality event during the regulated postclosure period following disposal, which could be up to 1,000,000 years (Price, 2019). As of March 2019, there are over 2,700 DPCs in storage in the United States that contain SNF (StoreFUEL, 2019).

Criticality in a disposed of DPC is not possible unless a moderator, in this case, water is present. This requires that both the DPC disposal overpack and the DPC itself must be breached so that water can enter to facilitate the achievement of critical conditions (Price, 2019). Once water has entered the DPC, the reactivity of the SNF in a DPC is controlled by multiple factors, including fissile mass in the fuel rods; the presence of neutron absorbers in the fuel, in the water, or integral to the basket; the presence of moderator; moderator volume and temperature; basket geometry; and fuel temperature (Price et al., 2019).

There are several options for the disposal of SNF stored in DPCs in a geologic repository (Hardin et al., 2015). One is to repackage the SNF into canisters that are designed to remain subcritical during the regulated postclosure period following disposal. For example, this option was considered for the Yucca Mountain performance assessment (PA) where the SNF was packaged into transportation, aging, and disposal (TAD) canisters. Analyses determined that the probability of a TAD in-package postclosure criticality event was low enough to exclude it from further consideration in the PA (U.S. DOE, 2009, Section 2.1.2.2). However, repackaging presents challenges that include increased disposal cost that has been estimated at approximately $20B in United States dollars (USD) (Alsaed, 2019). Further, repackaging SNF presents increased risk to workers both in terms of dose exposure and a variety of other operational safety and health concerns.

A second option is the direct disposal of DPCs. While DPCs were not designed for ‘as is’ disposal, analyses are currently underway to assess this possibility. These assessments are focused on the post-disposal behavior of SNF in a DPC, particularly the probability and consequences of criticality during a 1,000,000-year postclosure period in several geologic disposal media (Price, 2019).

A third option, and the focus of the current report, is to fill the void space of a DPC with a material before its disposal that significantly limits criticality over the post-closure regulatory period. An estimated cost of filling per DPC is $200K in USD resulting in a total cost of $0.54B to fill all the DPCs currently in storage (Alsaed, 2019).

The effectiveness of a filler material to mitigate criticality will ultimately depend on its ability to reduce moderation effectiveness in a DPC. To do so will require that the filler exhibit several attributes including: (1) neutron moderator displacement by filling more than 60% of the DPC free volume; (2) a minimal intrinsic ability to moderate neutrons and (3) a minimal compaction or volume reduction (10%) after infiltration and solidification. Additional desirable physical, chemical and operational attributes of filler materials are summarized elsewhere (Hardin et al., 2015).

Materials that exhibit these attributes (Hardin et al., 2015) and that are currently under consideration as DPC fillers include low-melting point metals and cements that are primarily phosphate-based. Oak Ridge National Laboratory (ORNL) is currently researching metals while Sandia National Laboratories (SNL) is researching chemically bonded phosphate cements because the encapsulation of radioactive waste in the U.S. and other countries is a potential major application for these materials (Wagh, 2016).

Recently, phosphate-based cement materials have been assessed and recommended for study as potential DPC filler materials (SNL, 2017; Hardin and Brady, 2018). While commonly considered cements, they are

more accurately described as chemically bonded ceramics as they exhibit ionic or covalent bonds instead of the hydrogen bonds and van der Waals bonds that are active in ordinary Portland cements (OPCs) and many of them set at elevated temperatures (Wagh, 2016).

Beyond the desired properties for fillers described above, phosphate-based cements have several properties that make them attractive as potential DPC fillers. They are inorganic, nontoxic, have neutral pH, and are insoluble (at near-neutral pH). They are made from low-cost and often naturally occurring materials, have, or can be modified to have, reasonably long set (working) times of several hours and they are self-bonding, meaning that a second layer will bond to a previously set layer (SNL, 2017).

This progress report describes research conducted for the DOE in FY 2019. It is focused on developing and evaluating a subset of the phosphate-based materials that have been recommended for consideration and include: (1) aluminum oxide / aluminum phosphate (Al_2O_3 / $AlPO_4$) or APC cements; (2) calcium phosphate or CPC cements commonly known as hydroxyapatite ($Ca_5(PO4)_3(OH)$); (3) magnesium potassium phosphate or MKP ($MgKPO_4$) cements (4) wollastonite aluminum phosphate ($CaSiO_3$ / $AlPO_4$) cement or WAPC and (5) a novel Fly ash phosphate cement.

2. ENGINEERING CONSIDERATIONS FOR DPC FILLERS

Globally there are three major dry canister vendors, Holtec International, NAC International and Orano TN (formally Areva). All the vendor's designs are different and proprietary, but all also share many common attributes. All modern multi-purpose canisters (MPCs) are stainless steel cylinders, typically with a 1.59 cm thick wall, a 2.54 cm to 6.35 cm thick bottom and a 20.32 cm to 24.13 cm thick lid that is permanently welded closed after the canister is loaded. Inside the MPC is a basket designed for the type of fuel to be loaded. Figure 2-1 shows a typical basket for 68 BWR assemblies on the left and a typical basket for 37 PWR assemblies on the right. A spent fuel assembly is loaded into each of the basket storage cells.

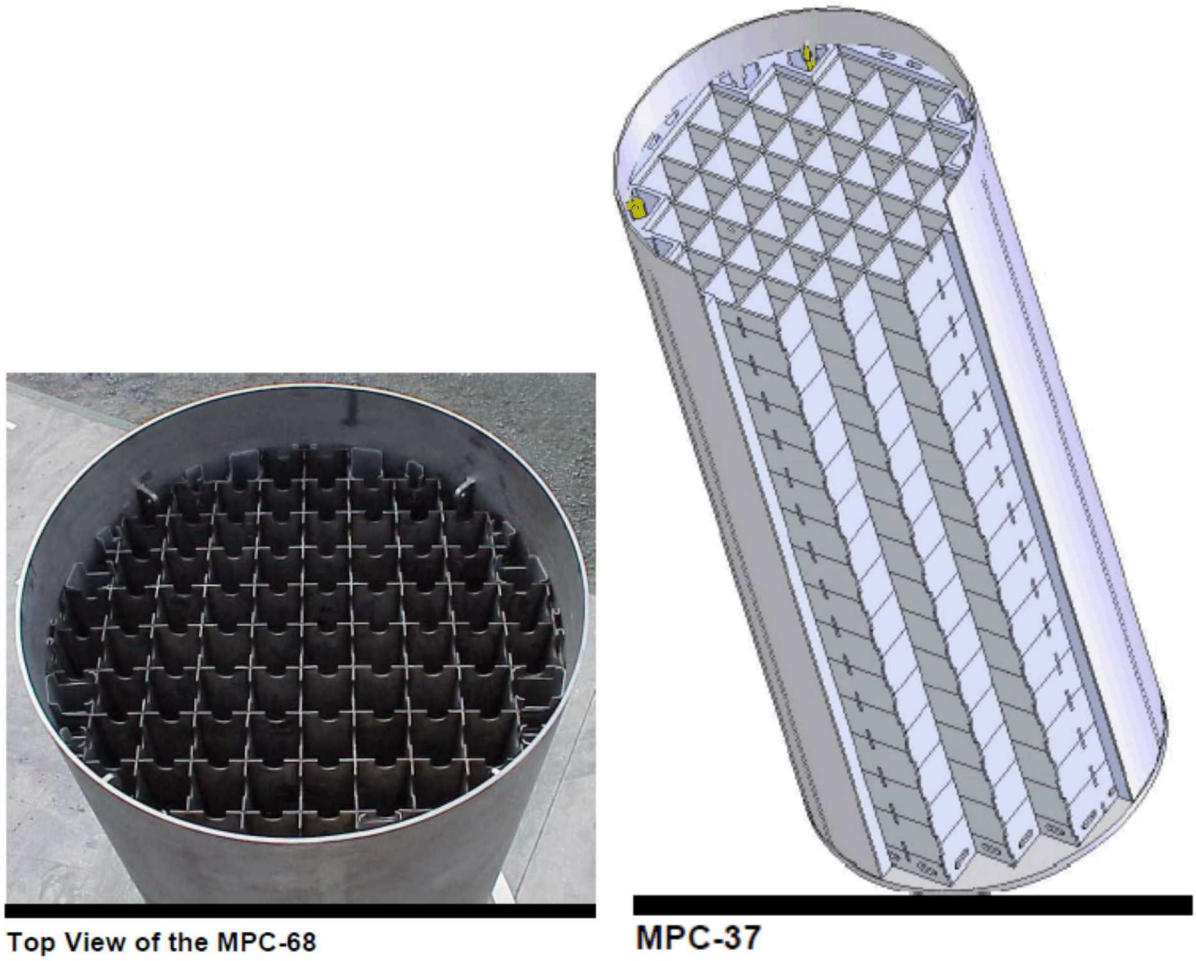

Figure 2-1. MPC with a basket designed for 68 BWR assemblies (left) and 37 PWR assemblies (right) (Green *et al.*, 2012).

Figure 2-2 provides some details comparing a PWR and BWR fuel assembly. Each are basically a grid spacer organized tube bundle. A typical 17 x 17 PWR is 4.1 m tall and eleven grid spacers hold 264 fuel rods in a footprint nominally 21.7 cm on a side. There are 24 control rod guide tubes and one central instrument tube distributed throughout the bundle. The hydraulic diameter of the 17x17 PWR bundle flow area is nominally 1.2 cm. A typical 9x9 BWR is 4.4 m tall and seven grid spacers hold 74 fuel rods and two water rods in a bundle that is positioned inside of a channel box. The footprint of the channel box is 13.9

cm on a side. Eight of the fuel rods in a 9x9 BWR are shorter and absent from the upper third of the fuel bundle. The hydraulic diameter of the 9x9 BWR is nominally 1.2 cm in the lower fully populated bundle and 1.4 cm in the upper partially populated upper bundle.

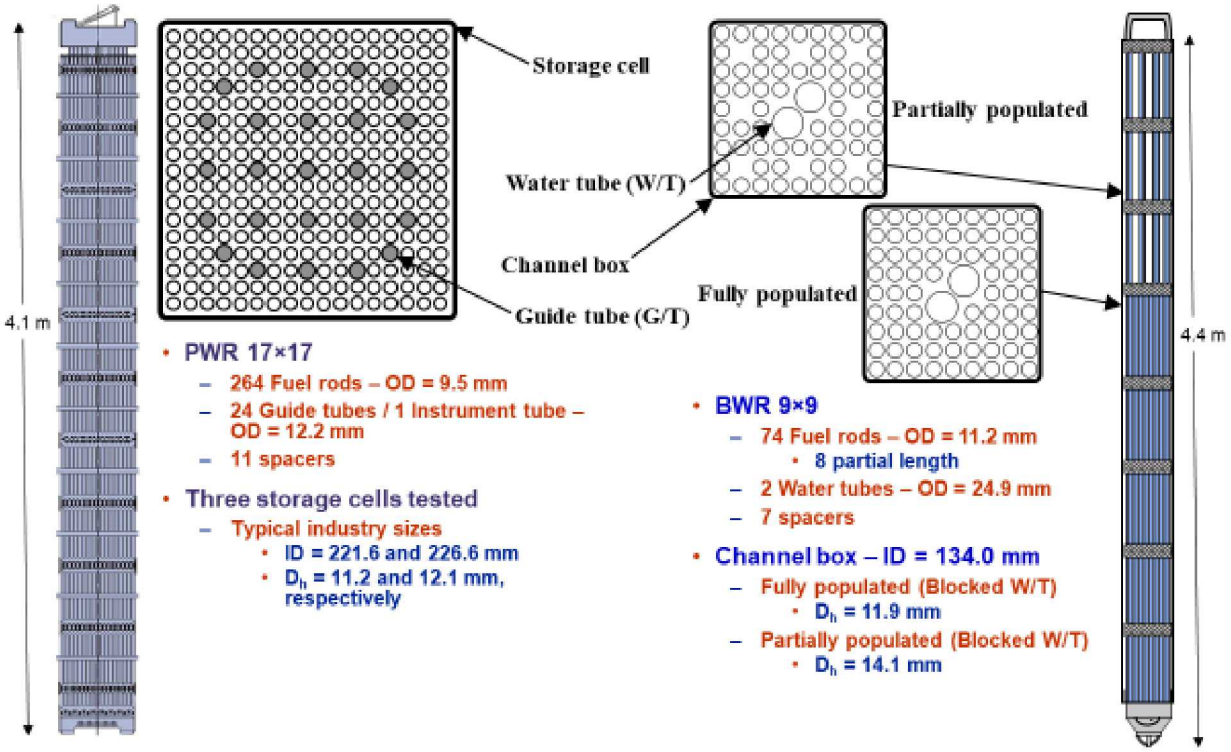

Figure 2-2. Comparison of PWR and BWR assemblies.

Dry storage canisters are loaded while submerged in the spent fuel pool. Once fully loaded, the canister is raised out of the pool and the canister lid is welded in place. The water inside the canister is then removed. All commercial dry storage canisters incorporate some means to remove the water. Typically, there is a drain pipe that runs through the canister lid to the bottom of the canister interior. There is also typically a vent that penetrates the lid. Helium is introduced into the vent port and used to force the water out the drain pipe. Figure 2-3 shows the general arrangement for the Holtec MPC enclosure vessel (Holtec, 2010). There is a smaller diameter port through the lid that connects to a larger diameter drain pipe (via the drain shield block) and runs to the bottom of the canister. The drawing shows that the lid port is not concentric with the drain shield block or the larger diameter drain pipe. Details of the flow path inside the shield block are not known. There are few dimensions provided in this publicly available drawing, but from the stated thickness of the lid and the closure ring the inner diameter of the lid port is nominally 2.5 cm and the outer diameter of the drain pipe is nominally 5.1 cm. The drain pipe is a likely candidate for injecting grout into a canister.

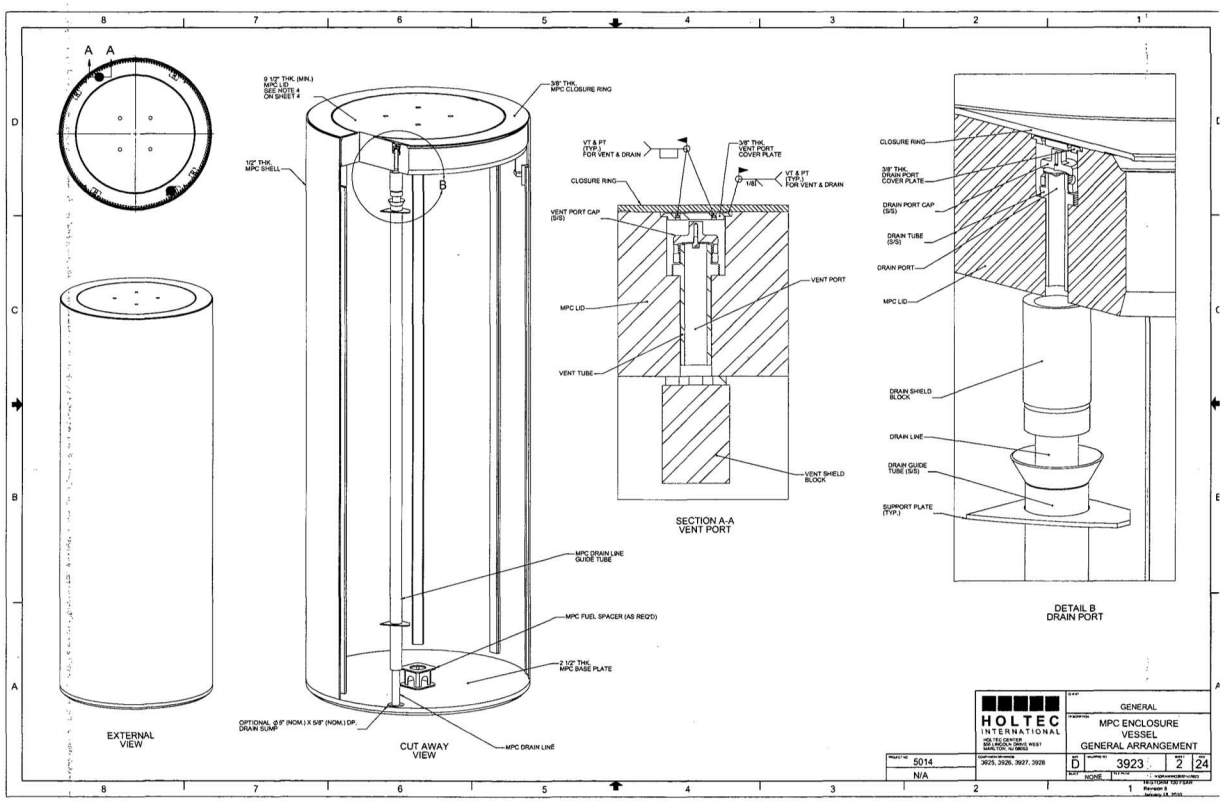

Figure 2-3. Drain pipe and vent arrangement in the Holtec MPC enclosure vessel (Holtec, 2010).

The discussion above highlights some of the geometric complexities found inside of a DPC that present hydraulic issues for filling a canister with grout. Any grout system considered for filling a DPC must fill all the intricate spaces between the fuel rods in each assembly evenly before the grout begins to cure. Since each fuel assemblies will be generating decay heat the fuel cladding will be hot in places. Cladding temperatures will be as high as 200 to 300 ºC in the center and cooler near the walls and the bottom of the canister. The thermal gradients inside the canister will likely influence the cure of the grout inside.

All of the numerous thermal-hydraulic issues need careful consideration to fully evaluate the engineering feasibility of filling a loaded DPC with grout. The most basic of these issues is whether a typical DPC can be filled with grout in a reasonable amount of time using the existing canister drain pipe/vent system. A scoping evaluation was performed that required several assumptions. The free volume inside of a fully loaded canister is nominally 6 m^3 and the drain pipe is nominally 5 m long. A grout flow rate of 100 lpm would fill the canister in one hour. Considering only the flow through the drain pipe and assuming Newtonian flow, the pressure drop needed to deliver the required volume to fill the canister can be calculated by the following equation (Bird et al., 1960):

$$\Delta P = 356 \frac{\mu L Q}{\pi D^4}$$

Where: ΔP is the required pressure drop (bar)
μ is the viscosity (MPa s)
L is the drain pipe length (m)
Q is the grout flow rate (m^3/h)
D is the drain pipe inner diameter (m)

Table 2-1 presents the grout pump pressure required for three grouts with different viscosities delivered through a drain pipe with three different inner diameters. The viscosity of the Portland and Merit 5000 grouts are described in a study by Mohammed et al., 2014 and the APC materials are described in Section 3. The drain pipe inner diameter range considered is based on the estimate of 1.0 cm to 2.0 cm given in Hardin et al., 2017 and 4.0 cm is based on analysis of Figure 2-3.

The pressures calculated ranged from 0.2 bar for the Portland based grout delivered through the 4.0 cm drain pipe to nearly 1700 bar for the APC delivered through the 1.0 cm drain pipe. The pressure results shown in green could be achieved using readily available grout pumps. The pressure results shown in yellow would require larger, less common grout pumps or would require a longer fill time to lower the grout flow rate. The result shown in red is not considered feasible for the 1.0 cm diameter drain pipe.

Table 2-1. Grout pump pressure required to fill a nominal DPC in an hour.

Grout	Portland	Merit 5000	APC
Plastic viscosity, MPa s (or cP)	151	189	5000
Feed rate, m^3/h	6	6	6
Drain pipe length, m	5	5	5
Drain pipe inner diameter, cm	ΔP, bar	ΔP, bar	ΔP, bar
1.0	51.3	64.2	1698
2.0	3.2	4.0	106.1
4.0	0.2	0.3	6.63

It should be noted that the APC, CPC and MKP materials under development in Sections 2 through 7 yield preliminary grout viscosities of between 1,500 and 10,000 cP suggesting that some formulations may be too viscous for use in the DPC filler operation modeled here provided the low-end estimate of drain pipe diameter reported by Hardin et al., 2017 is accurate. Reductions in viscosity of the filler materials under development may be necessary if filling a 1.0 cm drain pipe is required. Such reductions are readily achievable and will be explored if necessary as research continues.

2.1 Summary and Next Steps

The geometry of interstitial spaces inside of a fully loaded canister is highly complex and some of the smallest gaps may be difficult to completely fill. However, if the size of the drain pipe in a Holtec MPC is typical of other commercial canisters then filling a canister with grout in a reasonable time should be feasible. The lower the initial viscosity of the grout the lower the required grout pump pressure. A lower viscosity grout will also fill the complex interstitial space better.

Next steps will include establishing nondisclosure agreements with all the dry cask vendors to obtain detailed drawings of the drain pipe so that more detailed pressure calculations can be made. More detailed viscosity measurements will be performed with the grout systems under study to establish the shear stress versus shear rate relationship. There are also plans to solicit partnerships with grout vendors who may have expertise in tailoring grout properties to better suite our needs.

3. ALUMINUM PHOSPATE CEMENT (APC) FILLER MATERIALS

3.1 Aluminum Phosphate Cement (APC) Overview

Metal oxide-phosphoric acid reactions to form refractory materials at low temperature were investigated in the early 1950's by Kingery who observed that unlike a number of other metal oxides (e.g. ZnO, CaO, CuO, SnO, etc.) heating was required to promote the reaction between aluminum oxide and phosphoric acid (Kingery, 1950). More recent work by Wagh (2003) describes the formation of aluminum oxide (or corundum) chemically bonded to anhydrous berlinite ($AlPO_4$).

The basic formula utilizes an excess of Al_2O_3 reacted with phosphoric acid (H_3PO_4). Water is added as necessary to adjust reactant viscosity and form a smooth pourable slurry. The reaction between phosphoric acid and alumina may be written as:

$$Al_2O_3 + H_3PO_4 \rightarrow 2AlPO_4 + 3H_2O \text{ (EQ 1)}$$

The $AlPO_4$ product is expected to be berlinite and is thought to be the binder phase. The remaining unreacted Al_2O_3 effectively serves as the filler. From EQ 1, it is clear that water is generated by the reaction. The pH of the final product is expected to be neutral unless the reaction does not go to completion and excess H_3PO_4 remains.

Subsequent production of a densified cementitious APC (Al_2O_3 / $AlPO_4$ body) requires heating of the slurry in excess of 130 °C at ambient pressure (Wagh et al., 2003). However, the preliminary work by Wagh in 2003 on this system produced well-consolidated but porous bodies. Alternatively, a hydrothermal process may be necessary - a pressure vessel under a hydrothermal or pressurized steam atmosphere in order to produce less porous bodies (Wagh, personal communication, 2018). Both processes were explored preliminarily (and subsequent research resulted in the development of each process independently (Sections 3.2 and 3.3) to generate well consolidated bodies with reduced porosity.

We also recognized early in the development and optimization of APC materials that using different starting reagents may provide some control over the acid-base reaction. In turn, controlling the acid-base reaction may help in gaining control of the formation of $AlPO_4$ in terms of the subsequent consolidation and porosity of the final APC product. For example, the replacement of Al_2O_3 with $Al(OH)_3$ as a starting reagent with phosphoric acid (the phosphate source for APC fabrication based on Wagh, 2016). Alternatively, the phosphate reagent may be replaced by a phosphonic acid. Different aluminum and phosphate materials were also explored as additives with goal of fine tuning the reaction while enabling consolidation and reduced porosity Sections 3.2.3 and 3.3.3).

Because of the relatively small openings (1.0-4.0 cm) through which a DPC can be filled (for more details, see Section 2 above), slurry viscosities of below 5,000 cP are recommended. A preliminary investigation on the possibility of reducing the fluid viscosity by using plasticizers was conducted. The results showed that the additives explored proved largely unsuccessful as these additives tended to have a marked effect on raising viscosity as compared to water by itself (Section 3.3.4).

Neutron absorber additives should also be considered for APCs (Hardin and Brady, 2018). H_3BO_3 was initially deemed compatible with the reagents used for APC fabrication. Unfortunately, its effect on consolidation is ambiguous at best and in some experiments, it led to poor consolidation (Section 3.2.3.2). Meanwhile, the use of B_4C has, at present, been deferred over concerns that it may inhibit APC formation similar to what was observed in experiments with its use as an additive in the $MgKPO_4$ cements described in Section 6 of this report below.

3.1.1 Composition Space Studied

Initial work focused on identifying an alumina source that reacted at moderately elevated temperatures (150-250 °C) and did not strongly react at room temperature. An equally high priority was identifying the

role of water in the Al_2O_3 + H_3PO_4 reaction; specifically, we wanted to know if water should be removed during the reaction to minimize large void formation.

A simple set of exploratory experiments were conducted to evaluate the reaction products of H_3PO_4 with various aluminum oxides in addition to aluminum oxide. Three aluminum oxides were reacted with H_3PO_4 at a mole ratio of Al/P = 11.24. These sources were $Al(OH)_3$ (gibbsite), Sasol Catapal B (nominally AlO(OH), amorphous) and Aluchem AC19RG reactive aluminum oxide (corundum). Reaction conditions were for 5 days at 150 °C.

The results of these experiments are described below:

Sample No. 1025a: The reaction of Aluchem AC19RG with H_3PO_4 in a closed polytetrafluoroethylene (PTFE) cup in a Parr reactor produced a well-consolidated porous monolith. XRD analyses revealed the monolith's composition as predominately the reactive alumina starting material with some berlinite.

Sample No. 1025b: The reaction of gibbsite with H_3PO_4 in closed PTFE cup produced a crumbly powder. XRD analyses revealed the monolith's composition as predominately the gibbsite starting material with some boehmite (γAlO(OH)).

Sample No. 1025c: The reaction of Catapal B, with H_3PO_4 in closed PTFE cup appeared to produce no reactants only starting materials were observed at the completion of the experiment.

Sample No. 1025d: The reaction of Aluchem AC19RG with H_3PO_4 in closed PTFE cup produced a porous monolith XRD analyses revealed the monolith's composition as predominately the reactive alumina starting material with some berlinite.

Sample No. 1025e: The reaction of gibbsite with H_3PO_4 in closed PTFE cup loaded inside of a sealed Parr reactor resulted in a thick paste. XRD analyses revealed the paste's composition as predominately the gibbsite starting material.

Sample No. 1025f: The reaction of Catapal B, with H_3PO_4 in closed PTFE cup loaded inside of a sealed Parr reactor appeared to produce no products only starting materials were observed at the completion of the experiment. Attempts to remove the monoliths from the PTFE cups as intact bodies proved difficult (Figure 3-1), requiring them to be broken up in order to remove them from the cups. It was decided to switch to glass vials and subsequently Teflon centrifuge tubes to facilitate sample extraction and avoid damaging the expensive PTFE Parr reactor cups.

The results of the preliminary exploratory experiments suggested some changes in direction for further investigations in response to the observations that: (1) the reaction mixture dries out in some cases, i.e., water is lost at a lower temperature before the reaction can occur between H_3PO_4 and Al_2O_3; (2) when the reaction does occur, the H_3PO_4 reagent has likely oligomerized into polyphosphates and formed a sticky, viscous reaction medium; and (3) one of the reaction products of H_3PO_4 and Al_2O_3 is steam, which then forms voids in the reacting H_3PO_4 and Al_2O_3 mixture.

Figure 3-1. Photograph of Sample Nos. 1025a, 1025d and 1025e.

3.1.2 Phosphonic acids as Alternative Starting Reagents

One of the reasons that Al_2O_3 slurries experience expansion upon heating is because the H_3PO_4 becomes increasingly viscous as it loses water. We considered the possibility that removing a hydroxyl group from H_3PO_4 would reduce viscosity and prevent large void formation. This could be done by replacing H_3PO_4 with H_3PO_3, or by using an alkyl- or aryl-substituted H_3PO_4. It is unlikely that H_3PO_3 would be desirable in the use case, because H_3PO_3 disproportionates to H_3PO_4 and phosphine gas (PH_3) a colorless, flammable, toxic gas when heated above approximately 200 °C. Thus, H_3PO_3 was eliminated as a potential phosphate reagent. Alternatives to phosphoric acid such as methylphosphonic and phenylphosphonic acids do not produce phosphine and were tested as H_3PO_4 substitutes. Both of these are solids at room temperature, and rather than slurrying with water, they were dry-mixed with alumina as powders, loaded into glass vials, and degassed under vacuum while being lightly compacted with a glass rod.

The pressed powders were heated for 36 hr at 200 °C in air. They both sintered into monoliths with no obvious pores (Figure 3-1). XRD shows corundum plus peaks at low angle, suggesting the presence of microporous or layered phases containing CH_3-$AlPO_4$ and C_6H_5-$AlPO_4$. $AlPO_4$ phases are not observed in the XRD pattern (Figure 3-2).

Figure 3-2. APC sintered monolith Sample Nos. 1123b sand 1123c using organo-phosphonic acids. Samples are 2.5 cm in diameter and 1.3 cm tall.

Unfortunately, these materials may be difficult to use in a DPC application due to a number of factors, including: (1) the potential challenges with filling a DPC and its complex inner void space with a dry

powder; (2) the expense of procuring methylphosphonic acid (a specialty chemical); and (3) the high organic content of phenylphosphonic acid which may produce gas upon gamma irradiation. That said, these were the first relatively nonporous aluminophosphate monoliths we were able to make at ambient pressure.

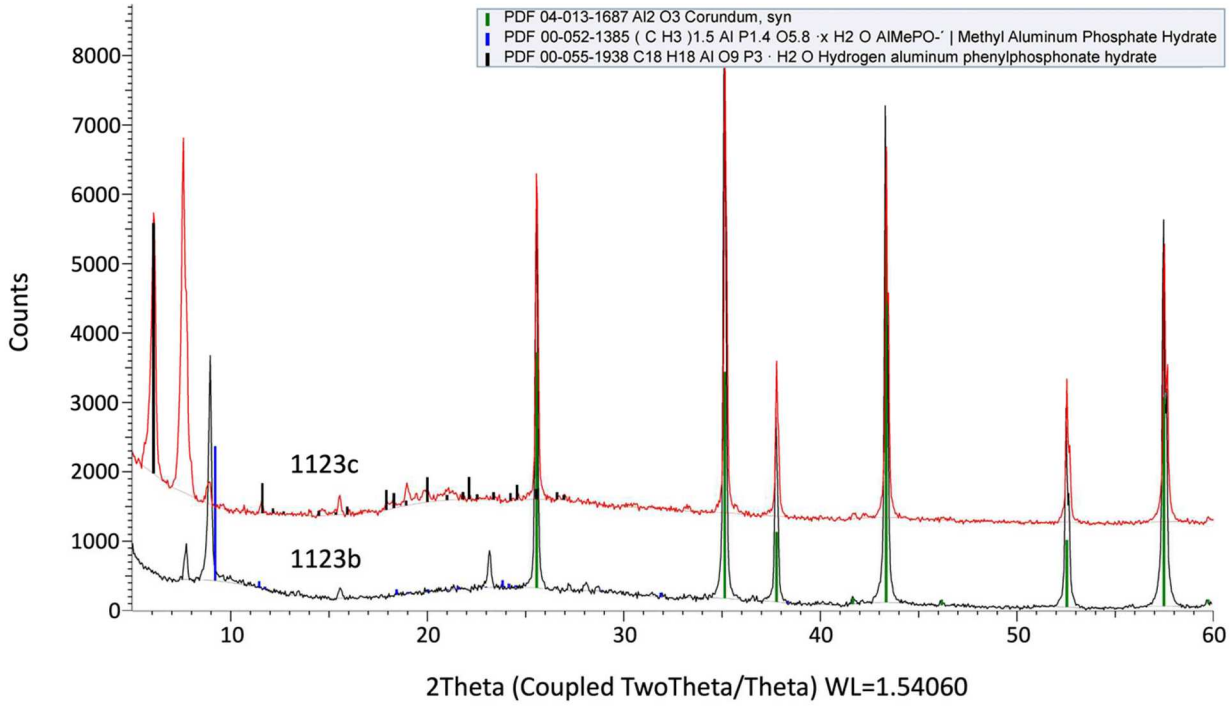

Figure 3-3. Powder XRD patterns of aluminophosphate ceramics prepared with methylphosphonic (1123b) and phenylphosphonic (1123c) acids.

3.1.3 $NH_4H_2PO_4$ as an Alternative Starting Reagent

Ammonium dihydrogen phosphate ($NH_4H_2PO_4$ or ADP) is a solid that may enable the production of APC materials by heating the alumina and phosphate reactants in the absence of water. The material is considerably less acidic than H_3PO_4 and would potentially minimize corrosion reactions with steel. ADP begins to lose ammonia at relatively low temperature (approx. 200 °C) and thus can be considered a H_3PO_4 source. ADP was dry blended with alumina and pressed into a glass vial under vacuum, then heated at 250 °C for 16 hr. This formed a porous but reasonably well-consolidated granular monolith (Figure 3-4).

Figure 3-4. Photograph of Sample No. 1124a. The sample is 2 cm long and 1.2 cm in diameter.

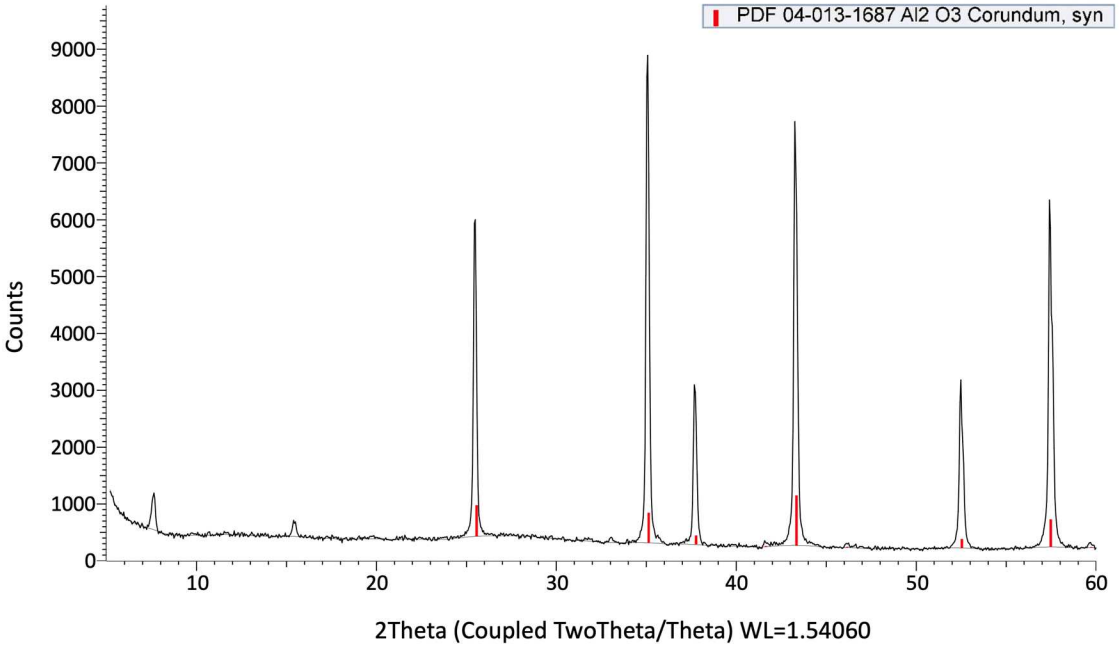

Figure 3-5. XRD pattern of Sample No. 1124a showing Al_2O_3 starting material.

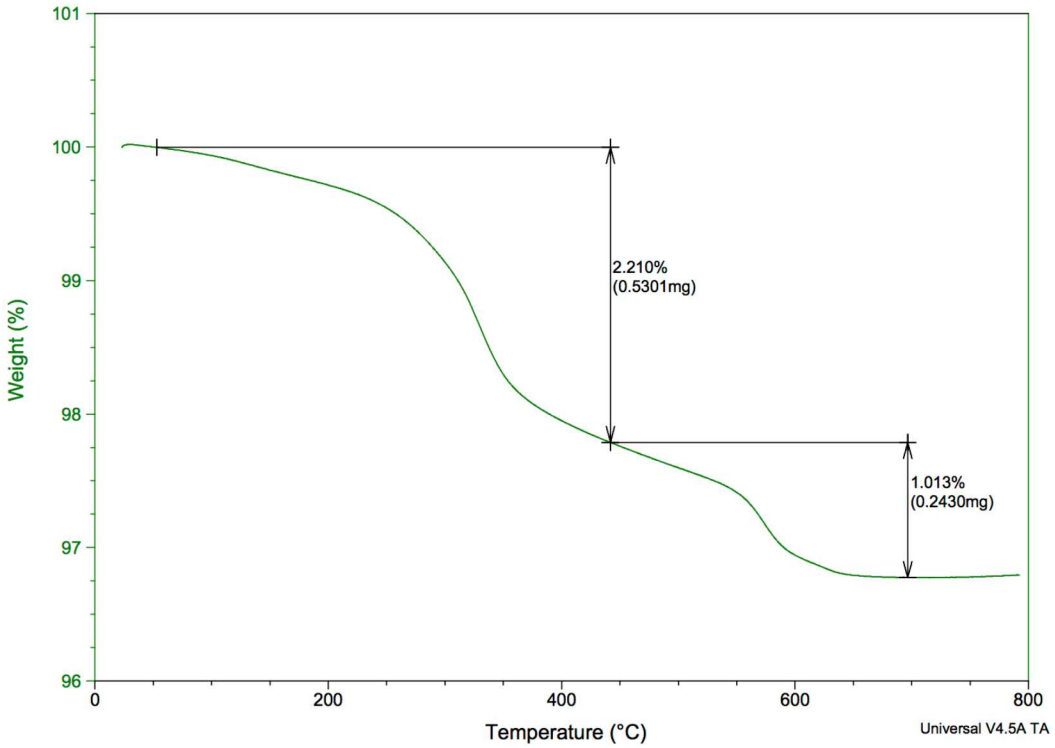

Figure 3-6. TGA of Sample No. 1124a.

The powder XRD pattern of Sample No. 1124a indicates Al_2O_3 starting material (Figure 3-5). The TGA plot for 1124a is more complex than those from the other aluminophosphates tested in this work, with two apparent decompositions occurring between approximately 250 and 350 °C, and from 550 to 600 °C (Figure 3-6).

While the results of this experiment produced a monolith of modest quality additional experimental work with ADP was deferred given the expected challenges with emplacing and assuring the thorough distribution of a dry powder at scale within the complex internal porosity of a DPC.

It should be noted that aluminophosphates were later made as aqueous slurries (Section 3.3 below) using ADP and a 1:1 mole ratio combination of ADP and H_3PO_4 to produce $NH_4H_5(PO_4)_2$. These were heated from 82 to 130 °C at 2 °C/hr, followed by 8 hr at 130 °C. ADP and alumina produced a fragile monolith with no large pores, while $NH_4H_5(PO_4)_2$ yielded a stronger monolith with numerous 1-2 mm pores. Remarkably, neither monolith exhibited significant expansion.

3.1.4 Nonaqueous Solvents as Alternatives to Water

Nonaqueous solvents may potentially entrain water as a positive pressure azeotrope and remove it from the aluminophosphate slurry before the it becomes highly viscous. Alternatively, a solvent that boils at a temperature higher than 130 °C ("high boiling solvent") would allow the H_3PO_4 to react with the alumina in a less viscous reaction medium, thereby allowing steam to escape without forming voids.

The azeotropic entraining hypothesis was tested with a series of aluminophosphate slurries was made with an Al/P ratio of 10. The slurries varied only in the solvent used; these solvents were water, isopropanol, acetonitrile, isobutanol, toluene, 1-methoxy-2-propanol, and nitromethane, all of which (excepting water) form positive pressure (negative temperature) azeotropes with water. The slurries were ramped at ambient pressure from 15 to 170 °C at 5 °C/hr. Heating continued at 170 °C for 24 hr.

The aqueous slurry formed an expanded monolith (Sample No. 0102a) containing corundum and berlinite (Figure 3-7). None of the other solvents yielded monoliths or berlinite, but all contained what has been identified by XRD as $AlPO_4$–cristobalite type that is distinct from berlinite. Similar to SiO_2, the compound $AlPO_4$ has two crystal structures, a quartz type structure is known as berlinite and an unnamed cristobalite type structure that will be referred to in this report as '$AlPO_4$–cristobalite type' (Figure 3-7).

The "high-boiling" solvent idea was tested by first evaluating compatibility of candidate solvents (i.e., solvents that are miscible with water and H_3PO_4) with H_3PO_4 at temperatures exceeding 150 °C. Three solvents were tested: propylene carbonate (240 °C) dipropylene glycol (230 °C), and 1,2-bis (2-methoxyethoxy) ethane ("triglyme") (216 °C). Upon mixing with 85% H_3PO_4 and heating to 150 °C for 90 min, the propylene carbonate turned black and started to fizz (possibly from decomposition to CO_2), the dipropylene glycol became amber and viscous, and the triglyme turned brown but was still a mobile liquid.

Triglyme and H_3PO_4 were mixed and heated at 150 °C for 2 hr in order to dewater the H_3PO_4. To this was added Al_2O_3 to produce an Al/P ratio of 10. This slurry was heated at 150 °C for 2 days. The result was a powder containing berlinite and $AlPO_4 \bullet H_2O$ in addition to starting material.

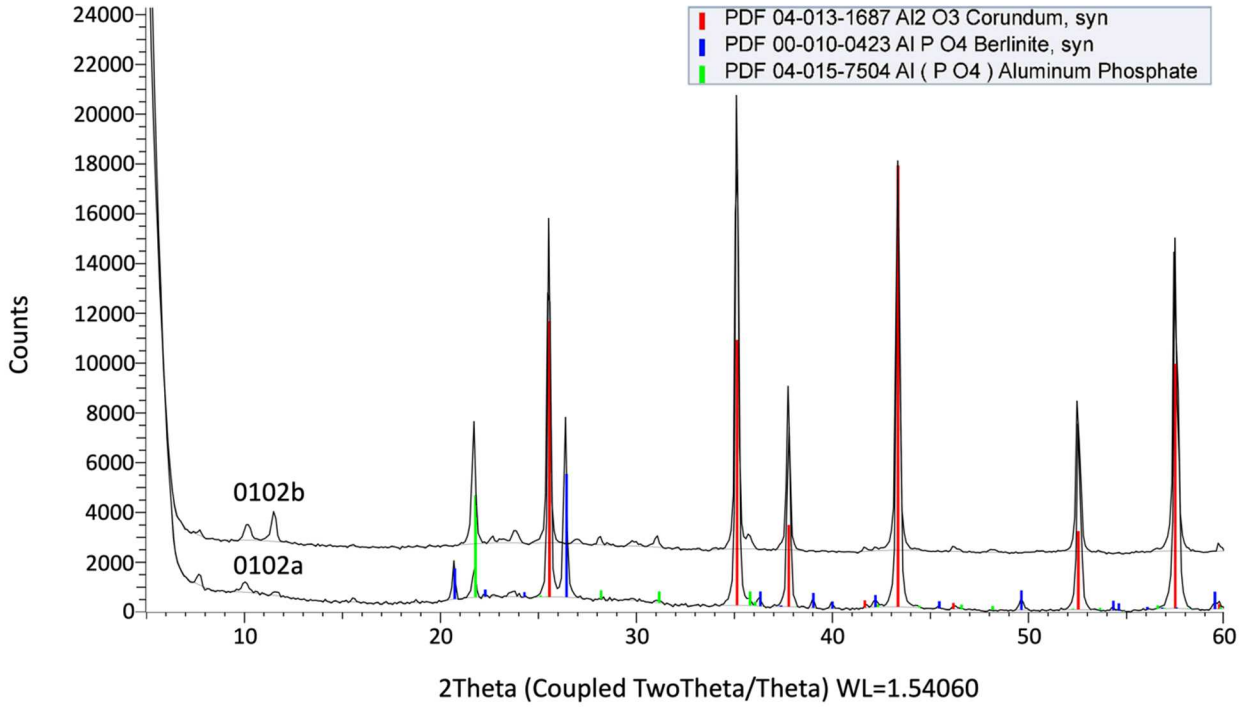

Figure 3-7. XRD pattern of Sample Nos. 0102a and 0102b.

3.2 Hydrothermal Process

The hydrothermal process, i.e., heating the APC aqueous slurries in a sealed pressure vessel, was investigated in response to the hypothesis that expansion and large voids form because the H_3PO_4 / Al_2O_3 reaction occurs at ~130 °C. Since the slurry water has evaporated by this point the mixture of the two reactants is a very thick paste because the H_3PO_4 has oligomerized into polyphosphates. Recall from EQ 1 above that one of the reaction products is water in the form of steam, which then creates voids as it escapes from the reacting H_3PO_4 and Al_2O_3 mixture. By adding excess water to the reaction vessel (see description

of procedure below) a steam overpressure is created. Because excess water and steam remain in equilibrium, the thick H_3PO_4 and Al_2O_3 mixture does not boil or yield foam. The monolith that forms is then expected to have significantly lower porosity than a similar monolith synthesized at ambient pressure.

3.2.1 Description of Procedure

Starting materials for the initial phase of hydrothermal process development were Aluchem AC19RG reactive aluminum oxide (corundum), ACS reagent grade 85% phosphoric acid, and deionized water. The H_3PO_4, H_2O and Al_2O_3 starting materials were thoroughly slurried by mixing. The mixture was then degassed to remove air entrained as a result of mixing by loading the material into a reactor jar, which caused the mixture to expand, then collapse (see Figure 3-8). Evacuation continued for a few minutes after foam collapse.

Figure 3-8. Photographs of the Al_2O_3 / H_3PO_4 / H_2O slurry before (left), during (center), and after (right) degas.

The reaction mixtures were loaded into glass or PTFE vials or tubes and degassed once more. The vessels were then loosely capped with Al foil in order to prevent condensate from dripping into the tubes, but not hinder transport of steam to and from the samples. The vials or tubes are placed in a stainless-steel reactor containing sufficient water to keep from boiling dry during the reaction but less than 32% of the volume of the vessel. (Figure 3-9) (32% is the critical fill volume of water, above which the water volume will expand as the vessel is heated.) The reactor is heated externally to the desired temperature for anywhere from a few hours to several days. In all experiments autogenous steam pressure was used, i.e., the reactor was not pressurized with any additional gas. The pressure in the reactor was thus approximately the same as the vapor pressure of water at the reaction temperature.

Figure 3-9. Parr reactor with glass tubes containing Al_2O_3 / H_3PO_4 / H_2O slurries.

For small samples, 23 mL PTFE-lined Parr vessels or a 1.5 L unlined Parr reactor was used. For larger or more numerous samples, a 4 L Autoclave Engineers reactor was used.

3.2.2 Phase evolution

In an exploratory experiment (Sample No. 1108a), 5.10 g Al_2O_3 was mixed with 1.02 g H_3PO_4 (this corresponds to an Al/P mole ratio of 11.24 a recommended starting ratio of reactants by Wagh, 2018, personal communication) and loaded into a glass vial, which was placed in a 23 mL Parr vessel containing 10 mL H_2O. The vessel was sealed and placed in a 170 °C oven for 4 days. XRD analysis of the resulting product indicated the presence of corundum, a hydrous aluminum phosphate ($AlPO_4 \bullet H_2O$), and a trace of berlinite (Figure 3-10).

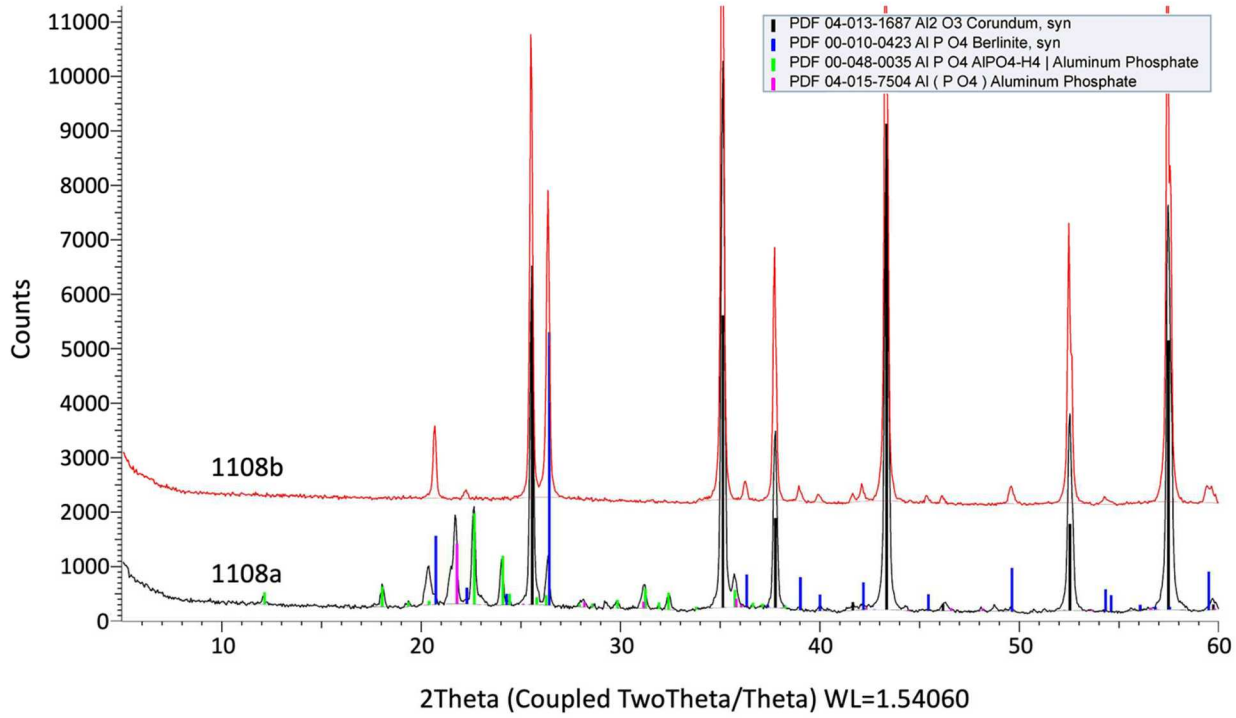

Figure 3-10. XRD pattern of Sample Nos. 1108a and 1108b. Note the primary berlinite peak (red line) at 26.3° 2θ. The comparatively larger intensity of the peak at 26.3° 2θ in the pattern of 1108b suggests more berlinite is present as compared to 1108a.

A second sample (Sample No. 1108b) was made with 5.10 g Al_2O_3 and 1.44 g H_3PO_4, (Al/P = 8.0) sealed in a Parr reactor with 10 mL H_2O and heated alongside the previous vial. The product contained corundum, a significant amount of berlinite, and little, if any $AlPO_4 \bullet H_2O$ (Figure 3-10 above). This result suggests that an Al/P ratio that is lower than 11.24 may be required to follow the production of berlinite, i.e., the 11.24 ratio may not produce sufficient berlinite to be detected via XRD even if the reaction is complete.

A scale-up experiment was conducted by mixing 153.0 g Al_2O_3, 30.7 g H_3PO_4 (85% aq. soln.), and 20 mL H_2O. This was loaded into a 100 mL Pyrex beaker, loosely covered with Al foil, and placed in a 1.5 L Parr reactor containing 400 mL H_2O. This was heated at 155 °C for 5 days, then baked at 170 °C for 33 hr. The product (Sample No.1123a) contained corundum and $AlPO_4 \bullet H_2O$, but no berlinite. The product was a hard monolith with minor isolated pores that weighed 164.54 g with a density of 2.30 g/cm^3 (Figure 3-11).

Thermogravimetric analysis (TGA) data were acquired from a sample of the product. Between 250 °C and 900 °C, the sample lost 2.5% of its weight, and all of that loss occurred below 250 °C (Figure 3-12) subsequently the monolith was annealed at 250 °C for 9 hr, after which it weighed 160.04 g for a weight loss of 2.7%. It should be noted that the percent weight loss measured by TGA and that measured after annealing are fairly similar. Meanwhile, XRD analyses (Figure 3-13) were performed on samples taken from the monolith before and after the annealing process at 250 °C. These analyses show $AlPO_4 \bullet H_2O$ is present before annealing (1123a 155 °C) while the sample collected after annealing (1123a 250 °C) shows that $AlPO_4 \bullet H_2O$ is absent and $AlPO_4$–cristobalite is now present. This indicates that $AlPO_4 \bullet H_2O$ was likely replaced by $AlPO_4$–cristobalite and that the weight loss observed by TGA and post-annealing can be attributed to water loss due to the decomposition of $AlPO_4 \bullet H_2O$.

Figure 3-11. Photograph of Sample No. 1123a, a large APC monolith 4.5 cm in diameter and 4.5 cm long. Sample was sectioned in half lengthwise to reveal the presence of small isolated pores ~1mm or less in diameter.

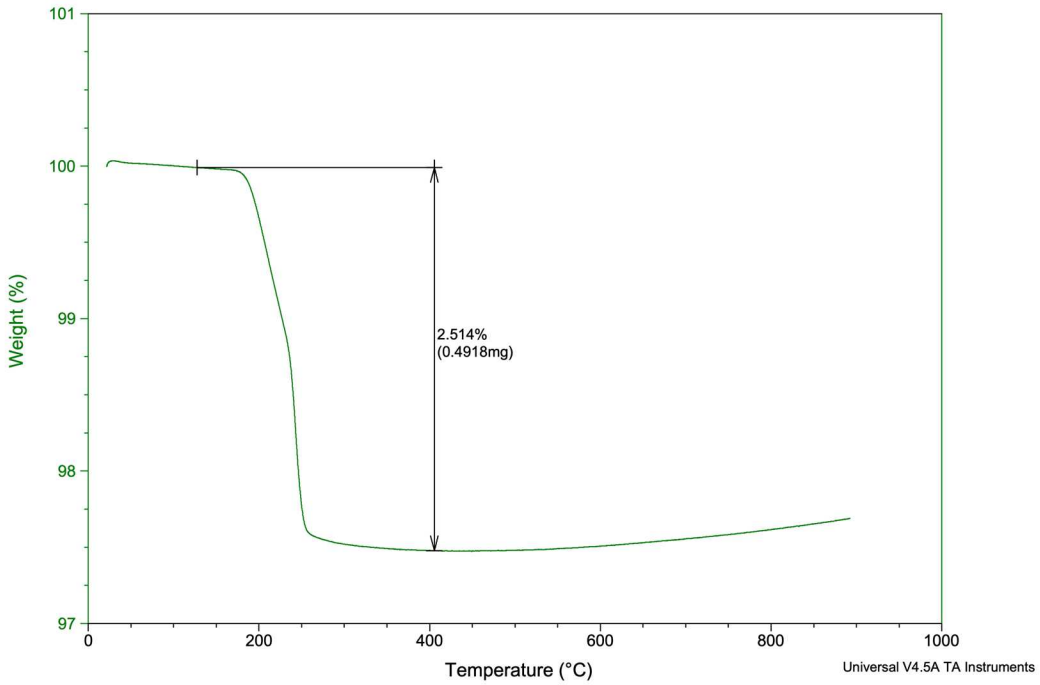

Figure 3-12. TGA of Sample No. 1123a indicating a small sample weight loss of 2.5%.

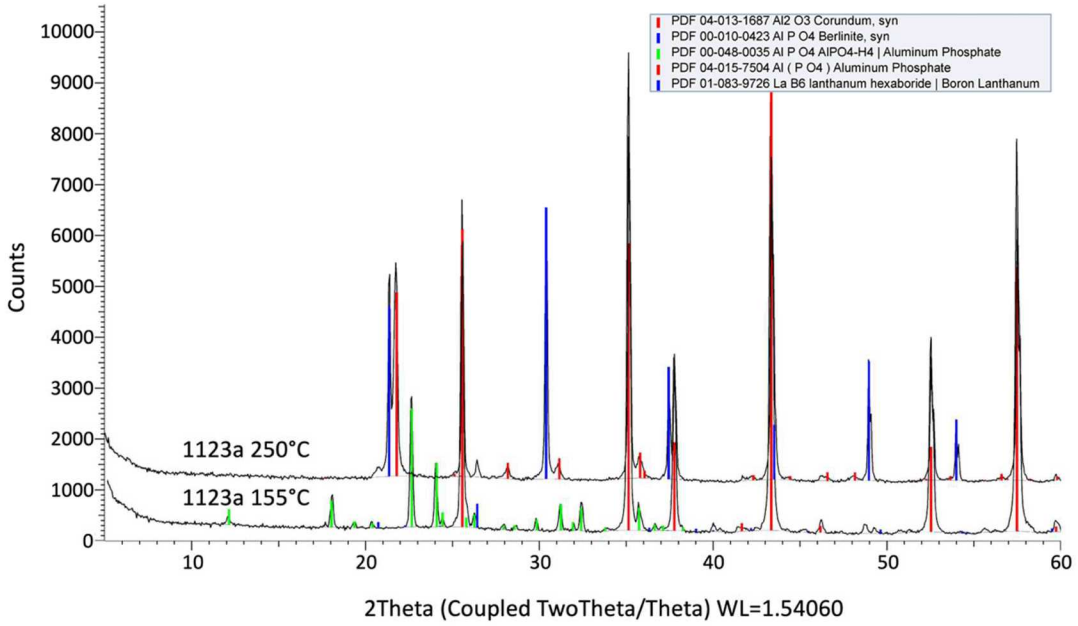

Figure 3-13. Powder XRD patterns of Sample No. 1123a before and after the 250 °C anneal. The green lines represent to the XRD pattern of $AlPO_4 \bullet H_2O$. Note these green lines correspond to peaks in the pattern of 1123a 155 °C indicating the presence of $AlPO_4 \bullet H_2O$. However, the peaks corresponding to $AlPO_4 \bullet H_2O$ are absent in the pattern of 1123b 250 °C but the magenta lines corresponding to $AlPO_4$–cristobalite type are present. This is indicative of the replacement of $AlPO_4 \bullet H_2O$ by $AlPO_4$–cristobalite type as a result of thermal annealing at 250 °C. Note that LaB6 (lanthanum hexaboride) was added to this sample as a calibration standard.

3.2.3 Role of additives

An investigation to ascertain the effects of additives in APC synthesis was undertaken. It has been suggested by Wagh (2016) that there are other Al sources such as gibbsite ($Al(OH)_3$) that can potentially release Al ions into solution more quickly than aluminum oxide without changing the desired cement bonding. Boric acid (H_3BO_3) could serve as a reaction retarder and may actually increase strength of the APC monoliths (Hardin and Brady, 2017). Further, the addition of boron to the system provides some neutron attenuation to further reduce the potential for criticality.

3.2.3.1 Alternative Al Sources

A simple experimental test matrix was designed to evaluate the effects of alternative Al ion sources (Table 3-1).

Table 3-1. Sample formulations for the evaluation of alternative Al ion sources.

Sample No.	Al_2O_3 (g)	H_2O(g)	H_3PO_4 (g)	Fumed Al_2O_3 (g)	$Al(OH)_3$ (g)
0123a	51.0	11.5	11.5	-	-
0123b	45.9	13.5	11.5	5.1	-
0123c	45.9	23.5	11.5	-	7.8

Mixtures of Al_2O_3, H_3PO_4 and H_2O with and one sample without (Sample No. 0123a) the alternative Al ion source additives were prepared. Sample No. 0123c reacted vigorously upon addition of H_3PO_4 and required extra water to make a free-flowing slurry. Following sample preparation, they were loaded in 20 mm glass tubes degassed, placed in individual Parr reactors and then heated at 170 °C for 79 hr under hydrothermal conditions. Following the 79 hr reaction, the reactor was cooled, the tubes removed and heated at 170 °C at ambient pressure for 24 hr.

Sample No. 0123a was retrieved as a monolith with a set of crystals on the top of the body (Figure 3-14). This was the first appearance of observable crystals in any of the APC hydrothermal experiments. After collection and XRD analyses it was determined that these crystals were nearly pure berlinite (Figure 3-15). The remainder of the monolith is composed of corundum with $AlPO_4 \bullet H_2O$ and no detectable berlinite.

Figure 3-14. Photograph of Sample Nos. 0123a and 0123b. Note the top surface of the monolith (left) is covered with small crystals.

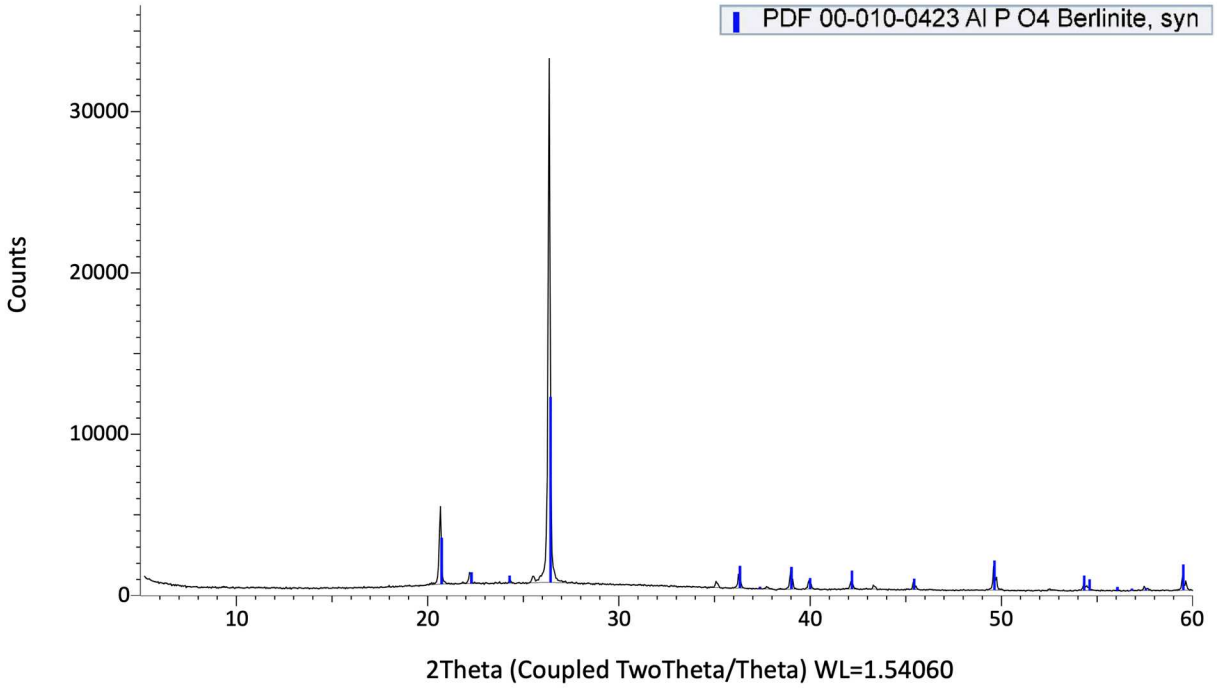

Figure 3-15. XRD pattern of small berlinite crystals on the top surface of 0123a.

Sample No. 0123b which contained fumed alumina as an additive was also retrieved as a monolith with a few isolated pores evident on its surface (Figure 3-14). Subsequent XRD analyses revealed the composition is corundum with $AlPO_4 \bullet H_2O$ and no detectable berlinite. Meanwhile, Sample No. 0123c which contained $Al(OH)_3$ is composed of corundum with $AlPO_4$–cristobalite type with no detectable berlinite.

The use of fumed Al_2O_3 as an additive in the APC starting material appears to favor the formation of $AlPO_4 \bullet H_2O$ at the expense of berlinite. Meanwhile, use of $Al(OH)_3$ seems to favor formation of $AlPO_4$–cristobalite at the expense of berlinite. These experiments suggest that the phosphate product can be controlled at least to some extent by the starting Al ion source additive. It remains unclear as to the relative or ultimate effectiveness of the 3 phosphate phases $AlPO_4$–cristobalite, $AlPO_4 \bullet H_2O$, or $AlPO_4$–berlinite as binders in the APC material system.

3.2.3.2 Boric Acid

A simple experimental test matrix was designed to evaluate the effects of H_3BO_3 on the properties of APC materials (Table 3-2).

Table 3-2. Sample formulations for the evaluation of H_3BO_3 as an additive.

Sample ID	Al_2O_3 (g)	H_3PO_4 (g)	H_3BO_3 (g)	H_2O (g)
0328a	51.0	11.5 g	-	12 g
0328b	50.5	11.5	0.62 g	12
0328c	50.0	11.5	1.24 g	12
0328d	48.45	11.5	3.09 g	12
0328e	45.9	1.5	6.18 g	12

Mixtures of Al_2O_3, H_3PO_4 and H_2O with varying amounts of H_3BO_3 were prepared. These samples were degassed, poured into 20 mm glass tubes, capped with Al foil, and placed in a 1.5 L Parr reactor containing 400 mL H_2O. This was placed in a 170 °C oven for 5 days. After cooling, the tubes were recovered and then sampled for XRD analyses. The remaining material was then thermally annealed heated at 170 °C for 16 hr at ambient pressure and sampled again for XRD analyses. Overall, the recovered monoliths are observed to be poorly consolidated making them fragile and chalky when handled (Figure 3-16).

Figure 3-16. Photograph of the 0328 series of samples with the H_3BO_3 additive.

Table 3-3. Summary of XRD analyses of the 0328-sample series containing varying amounts of H_3BO_3.

Sample ID	Product after 170 °C hydrothermal
0328a	Corundum with $AlPO_4 \bullet H_2O$, minor berlinite
0328b	Corundum with $AlPO_4 \bullet H_2O$, minor berlinite
0328c	Corundum with $AlPO_4 \bullet H_2O$, berlinite
0328d	Corundum with big berlinite peaks
0328e	Corundum with $AlPO_4$–cristobalite,

The results of this 170 °C hydrothermal experiment again show a clear trend in the formation of $AlPO_4$ products as a function of heating time. Aluminum phosphate hydrate ($AlPO_4 \bullet H_2O$) appears first followed by berlinite and finally $AlPO_4$–cristobalite. From these data it is tempting to think of H_3BO_3 as a reaction accelerant, assuming that at high temperature and/or longer timescale the phase evolution of Al_2O_3 and H_3PO_4 progresses from $AlPO_4 \bullet H_2O$ to berlinite and ultimately $AlPO_4$–cristobalite. However, its effect on consolidation is disappointing as it appears to result in low strength monoliths.

3.2.3.3 Fly Ash

Fly ash has been recommended for use as a mildly reactive aggregate or conditioner, to control slurry consistency and to impart more strength to the final product (Hardin and Brady, 2017). Specifically, Class F is favored because it contains less Ca (which could react rapidly with phosphate in the mix) than Class C, and contains only moderate amounts of carbon (inert, graphitic, dark in color). APC setting behavior should be tested without fly ash addition, and interaction of 50% H_3PO_4 and fly ash, without alumina, should also be tested to understand the potential effects on pH, setting behavior, and slurry thickening at T < 150°C.

An initial set of experiments performed using Class F fly ash reveal fly ash to be a non-contributor to the structural integrity of the APC cement in the hydrothermal process, and an important contributor in the ambient pressure process (0223 Series, Section 4.2 below). In addition, it is evident that even small quantities of fly ash relative to Al_2O_3 promote the formation of near net-shape monoliths. By near net-shape we mean that the volume of the final consolidated product is close to the starting slurry volume. Also noteworthy is the fact that fly ash and H_3PO_4 form hard and pore-free monoliths (even in the absence of Al_2O_3 and without any special thermal treatment such as a slow ramp to final bake temperature. These observations led to the decision to examine fly ash phosphates as an alternative filler composition. For this reason, further discussion on fly ash is deferred to Section 4 Fly Ash-Based Fillers.

3.2.4 Role of Time

An investigation of the effect of time on the formation of the reaction products of Al_2O_3 and H_3PO_4 was undertaken to evaluate the evolution of reaction products as the APC monoliths consolidate. Previous work on APC (Wagh 2003) suggests that the $AlPO_4$ binder forms slowly as a result of the slow dissolution of alumina in the presence of phosphate. A series of experiments was performed to evaluate the effect of shorter heating times on APC product formation.

A mixture of 51.0 g Al_2O_3, 11.5 g H_3PO_4 (85%), and 12 g H_2O was degassed and loaded into 5 glass vials. These samples, called the 0406 series, were each capped with Al foil and placed into separate 23 mL Parr cups containing 10 mL H_2O. The cups were installed in Parr vessels and loaded into a 170 °C oven. The vessels were withdrawn from the oven after 1, 2, 4, 8, and 16 hr. The vials were sampled and placed in a 200 °C oven at ambient pressure for 16 hr.

Table 3-4. Time effects on $AlPO_4$ binder formation.

Sample ID	Product after 170 °C hydrothermal	Product after 200 °C dry bake
0406_1	Corundum with $AlPO_4 \bullet H_2O$	Corundum with $AlPO_4$–cristobalite, berlinite
0406_2	Corundum with $AlPO_4 \bullet H_2O$, minor berlinite	Corundum with $AlPO_4$–cristobalite, small berlinite peaks
0406_4	Corundum with $AlPO_4 \bullet H_2O$, big berlinite peaks	Corundum with berlinite, some $AlPO_4$–cristobalite
0406_8	Corundum with $AlPO_4$–cristobalite, small berlinite peaks	Corundum with $AlPO_4 \bullet H_2O$, berlinite, $AlPO_4$–cristobalite
0406_16	Corundum with $AlPO_4$–cristobalite, big berlinite peaks	Corundum with $AlPO_4 \bullet H_2O$, large berlinite, $AlPO_4$–cristobalite

The results of the 170 °C hydrothermal experiment show a clear trend in the formation of $AlPO_4$ products as a function of heating time (Table 3-4). Aluminum phosphate hydrate ($AlPO_4 \bullet H_2O$) appears first followed by berlinite and finally $AlPO_4$–cristobalite. The appearance of $AlPO_4 \bullet H_2O$ after dry bake at 200 °C in two of the samples (those heated for 8 and 16 hours respectively) is unexpected. It is conceivable that in 0406_1, 0406_2, and 0406_4, $AlPO_4 \bullet H_2O$ thermally decomposes to both berlinite and $AlPO_4$–cristobalite in a certain temperature range. (Note that we had previously observed in Sample No. 1123a that nearly all of the $AlPO_4 \bullet H_2O$ present after 155 °C became cristobalite upon anneal at 250 °C.) Another possibility is that free H_3PO_4 is still present in these sample after hydrothermal treatment at 170 °C, and this reacts with the excess alumina to form $AlPO_4$–cristobalite. However, it is still unclear why $AlPO_4 \bullet H_2O$ would have formed from free H_3PO_4 and alumina in the 200 °C 0406_8 and 0406_16 samples, and not in 0406_1, 0406_2, and 0406_4.

The fact that H_3PO_4 reacts with alumina at 170 °C in hydrothermal conditions on the scale of hours rather than days was unknown to us before this experiment. The effects of size scaling on reaction time are not yet known, so it is not clear how this result will impact the use case.

3.2.5 APC Viscosity Data

Candidate filler materials must be injected into a DPC through one or more ports with relatively small inner diameters of 4.0 cm or less. Thus, fillers must be pumpable so that ~6,000 liters can be pumped into a canister and flow into all interstices, before setting as a monolithic pour. Further they need to be self-leveling, and readily penetrating DPC interstices with apertures as small as ~1mm.

Both the chemical stability of the filler and its viscosity over time are important for a DPC filling operation. Viscosity measurements of the baseline APC filler slurry as a function of time were collected and are presented below (Figure 3-17). This slurry is identical in composition to that used for 1123b above and composed of 102 g Al_2O_3, stirred into 23 g each of H_3PO_4 and DI H_2O and subsequently degassed.

Samples were stored in a location with a diurnal temperature variation from 21.6 to 23.3 °C. Viscosity data were collected by shaking the samples for 2-3 seconds to reverse settling of the alumina, inserting the viscometer spindle, and recoding the viscosity indicated after 5 sec of measurement (longer acquisition times can result in lower viscosity values due to thixotropy of the cement).

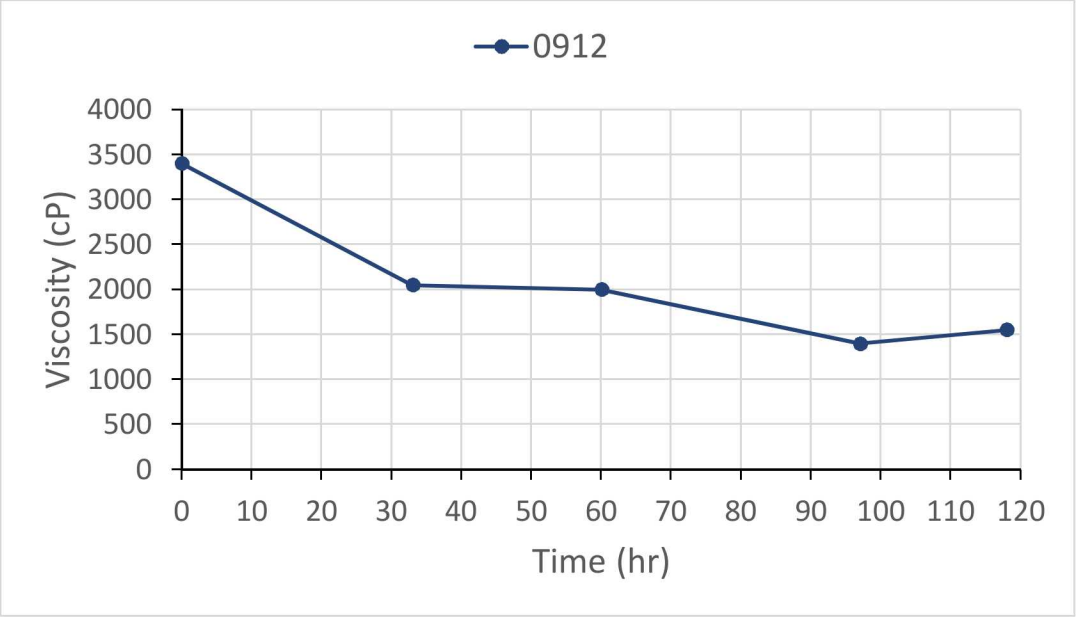

Figure 3-17. Viscosity measurements as a function of time for a typical Al_2O_3 / H_3PO_4 / H_2O slurry.

The measured viscosity data of the slurry drops initially and then remains relatively stabile between ~1,500 and 2,000 cP over a period of nearly 118 hours. Under reasonable assumptions of DPC filling times, on the order of several hours, these slurries can be expected to remain stable. In fact, it may be possible to prepare and store this APC slurry in advance of filling operations.

3.2.6 APC Mechanical Properties

If disposed of directly, DPC filler materials will require, at a minimum, modest mechanical strengths for the purpose of maintaining their configuration within the canister in the post-disposal environment. A minimum compressive strength target of ≥ 500 psi has been recommended (Ernest Hardin, personal communication, 2019) based on the unconfined compressive strength (UCS) of a calcium aluminate-phosphate cement used in high temperature geothermal wells (Sugama, 2007).

A scaled-up version (1.5 x) of the Sample No.1123a formulation (described in Section 3.2 above) was prepared hydrothermally. This scaled-up formulation known as Sample No. 0914b is composed of 204.0 g Al_2O_3, 46.0 g H_3PO_4, and 23.0 g H_2O. The reactants were mixed and degassed, then poured into a 1.25" diameter x 5" long glass mold. This was loosely capped with Al foil and placed in a 1.5 L stainless steel reactor along with 400 mL H_2O and heated at 170 °C for 17 hr, then cooled. This curing and annealing profile was adjusted (higher temperature shorter time) based on the observation that berlinite forms fairly rapidly under hydrothermal conditions (Section 3.2.5). The sample was then annealed at 250 °C for 8 hr while still in the glass mold (Figure 3-18). The resulting product upon removal from the mold and subsequent machining (Figure 3-19) is very similar in appearance to Sample No. 1123a (Figure 3-11 above) with small isolated pores ~1 mm or less in diameter.

A basic unconfined compressive strength (UCS) test was performed on two hydrothermal APC samples. The APC samples were provided as small cast/molded samples and required machining of the outer diameter, and length to develop the desired right circular cylinders for strength testing. The finished dimensions, density, unconfined compressive strength (UCS), and Young's modulus are given in Table 3-5.

The UCS test consists of measurements of axial and lateral deformations of right circular cylinder samples loaded in the axial direction to failure. The UCS test is a triaxial test with zero confining pressure. The UCS is the maximum axial stress level measured during the test. The strain to UCS is about 0.01 (1%) for all samples except 230 which is closer to 0.02 (2%). The Young's Modulus is the ratio of axial stress difference to axial strain difference in the linear portion of the stress strain curve; Poisson's ratio is the ratio of (-) lateral strain to axial strain.

Table 3-5. Physical and Mechanical Property Data for Sample No. 0914b.

Sample ID	Dimension				Weight grams	Density	UCS	Young's Modulus	Poisson's ratio
	Diameter (in)	Diameter (cm)	Length (in)	Length (cm)		g/cc	psi	psi	
0914b	1.278	3.246	2.83	7.188	130.46	2.19	798	164138	1.278

Figure 3-18. Photograph of Sample No. 0914b after annealing.

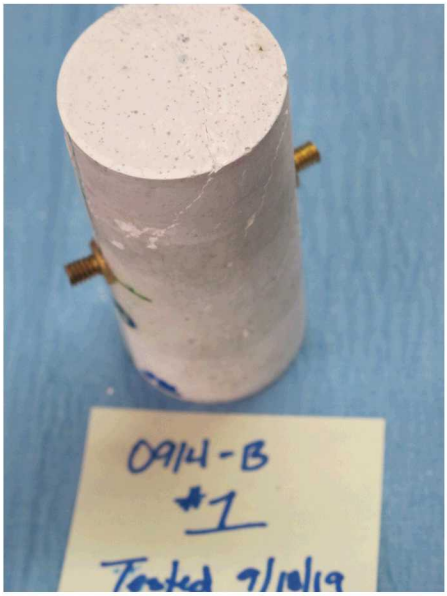

Figure 3-19. Photographs of Sample No. 0194b after completion of the UCS test. Isolated millimeter to submillimeter pores (dark specks) are evident on the top of the sample.

Results of the test reveal a UCS of 798 psi for this baseline APC recipe. Although the results are preliminary, and additional testing on multiple samples is required to establish reliability and reproducibility, this material exceeds the recommended strength target of 500 psi set by Hardin.

3.2.7 APC Water Resistance Testing of Hydrothermal APCs

Representative APC samples (Sample Nos. 1025a and 0914b) were fabricated using the hydrothermal process and selected for water resistance testing. Pieces from these broken monoliths were selected then placed in a sleeve made from folding a sheet of PTFE in half, sealing the edge, then sealing one end to create an envelope. After adding each piece, 40 g water was added and sealed along with the sample piece. The sleeve was then placed in an Autoclave Engineers 4-liter reactor, into which was poured 2 liters of DI water, then sealed. The reactor was heated to 200 °C for 48 hr, after which the reactor was cooled, and the sleeves were recovered. The pH of the water was tested, and if intact, the disc was recovered and dried at 130 °C, then weighed. Low weight loss is reasonably anticipated to be indicative of water resistance. Only the sample was recovered and weighed; any sediment that fell off the sample during the test was considered lost weight. The results of the test are presented in Table 3-6.

Sample No. 1025a was prepared with10.0 g Al_2O_3 and 2.85 g of 60% H_3PO_4 (Al:P ratio of 11.24). This was heated under pressure (hydrothermally) without excess water in a sealed Parr reactor for 96 hr at 150 C.

Sample No. 0914b was prepared with 204.0 g Al_2O_3, 46.0 g H_3PO_4 (Al:P ratio of 10.0) and 23.0 g H_2O that were mixed and degassed, then poured into a 1.25” diameter x 5” long glass mold. This was loosely capped with Al foil and placed in a 1.5 L stainless steel reactor along with 400 mL of excess water and heated at 170 °C for 17 hr, then cooled. The sample was then annealed at 250 °C for 8 hr while still in the glass mold.

Table 3-6. Results of water resistance testing of selected 1025 series hydrothermal APC samples.

Sample No.	Starting wt. (g)	pH after test	Wt. after test (g)	Pct. wt. loss
1025a	3.26	7	3.15	3.4%
0914b	22.52	5.5	22.4	0.53%

The results of the test indicate that weight loss is fairly low for Sample No. 1025a. Meanwhile with respect to 914a we see very little weight loss. Note that this sample has been processed at a higher pressure (1 MPa) and temperature (250 °C) and it also has a lower Al:P ratio. Under hydrothermal conditions, the application of both pressure and temperature are likely to drive the synthesis of $AlPO_4$ further towards completion which may explain the reduction in weight loss with Sample No. 0914b.

3.2.8 Summary

We found that the reaction of Al_2O_3 and H_3PO_4 at 170 °C in the presence of liquid water in equilibrium with steam at a pressure of approximately 1 MPa is fairly rapid, and at the scales we tested may be substantially complete in less than 24 hr. This reaction produces well-consolidated, dense monoliths with adequate mechanical strength. The reaction products are principally berlinite, $AlPO_4$–cristobalite, and $AlPO_4 \bullet H_2O$. The data suggest that $AlPO_4$–cristobalite is the decomposition product of $AlPO_4 \bullet H_2O$. It is not clear whether either berlinite or $AlPO_4$–cristobalite function as binder phases in the monoliths. Once we learn this we may be able to alter the reaction conditions to favor one phase over the other.

Boric acid and fly ash were tested as additives to the Al_2O_3 and H_3PO_4 starting materials. Neither contributed to the mechanical stability of the resulting products.

The viscosity of the Al_2O_3 and H_3PO_4 mixture in water is stable over at least several days. While the viscosities of the reaction mixtures tested were on the order of 2,000 cP, it is likely that higher starting water concentrations and thus lower viscosities are available, since the water in the starting material rapidly comes into equilibrium with steam as the reaction starts.

3.3 APC Ambient Pressure Overview

There may be significant engineering utility in using DPC fillers that cure under conditions of ambient pressure (0.1 MPa), rather than requiring 1 MPa of steam pressure during the hydrothermal cure cycle. Our initial investigation of the ambient pressure process studied the reaction of H_3PO_4 with various forms of corundum, alumina hydrates, and alumina precursors at different values of Al/P and different heating rates and final temperatures. For most systems the combination of the alumina source and H_3PO_4 determines whether it is excessively or insufficiently reactive or whether it produces near net-shape monoliths. This changed when we reduced the acidity of the phosphate by replacing some of the H_3PO_4 with monobasic sodium and ammonium phosphates. Ultimately, we showed that a combination of reduced phosphate acidity with reactive corundum mixed with reactive additives produces well consolidated monoliths with low porosity in near net-shape forms after heating at DPC-realistic temperatures (130 to 250 °C).

3.3.1 Description of Procedure

Starting reagents for the APC materials were identical to those used in hydrothermal process development. This investigation began with the use of Aluchem AC19RG reactive aluminum oxide (corundum), ACS reagent grade 85% phosphoric acid, and deionized water. The H_3PO_4, H_2O and Al_2O_3 starting materials were thoroughly mixed with a silicone spatula. The mixture was then degassed as described in Section 3.2.1 above to remove air entrained as a result of mixing.

Mixtures were loaded into glass or PTFE vials or plastic centrifuge tubes and degassed once more. The vials or tubes were placed in an oven to cure. After removal and inspection, the samples were removed from their molds and then placed in the oven again for annealing. A representative curing and annealing

process is to heat the sample from 82 to 130 °C at 2°C/hr, then hold the temperature at 130 °C for 8 hr. Subsequently, the sample were removed from their molds and again placed in an oven for annealing at 250 °C for 8 hr. The curing and annealing steps are varied in temperature and time to explore the effects of these process variables on the consolidation of APC materials.

3.3.2 Phase Evolution

Early results with Al_2O_3 / H_3PO_4 mixtures in water and subsequent heating at ambient pressure did not yield near net-shape monoliths. An example of this is Sample No. 1108d which was prepared by adding 5.1 g of alumina to a solution of 1.44 g of H_3PO_4 in 1.5 g of DI water. The Al:P ratio was 8.0. The mixture was heated in an open Teflon beaker for 4 days at 170 °C. The resulting highly porous monolith is shown in Figure 3-20. XRD analyses indicates the presence of Al_2O_3 along with $AlPO_4$–cristobalite and minor berlinite.

Figure 3-20. Sample 1108d is a small APC monolith 3 cm in diameter and 1 cm thick. Note numerous large and irregular pores as large as 1 cm in diameter.

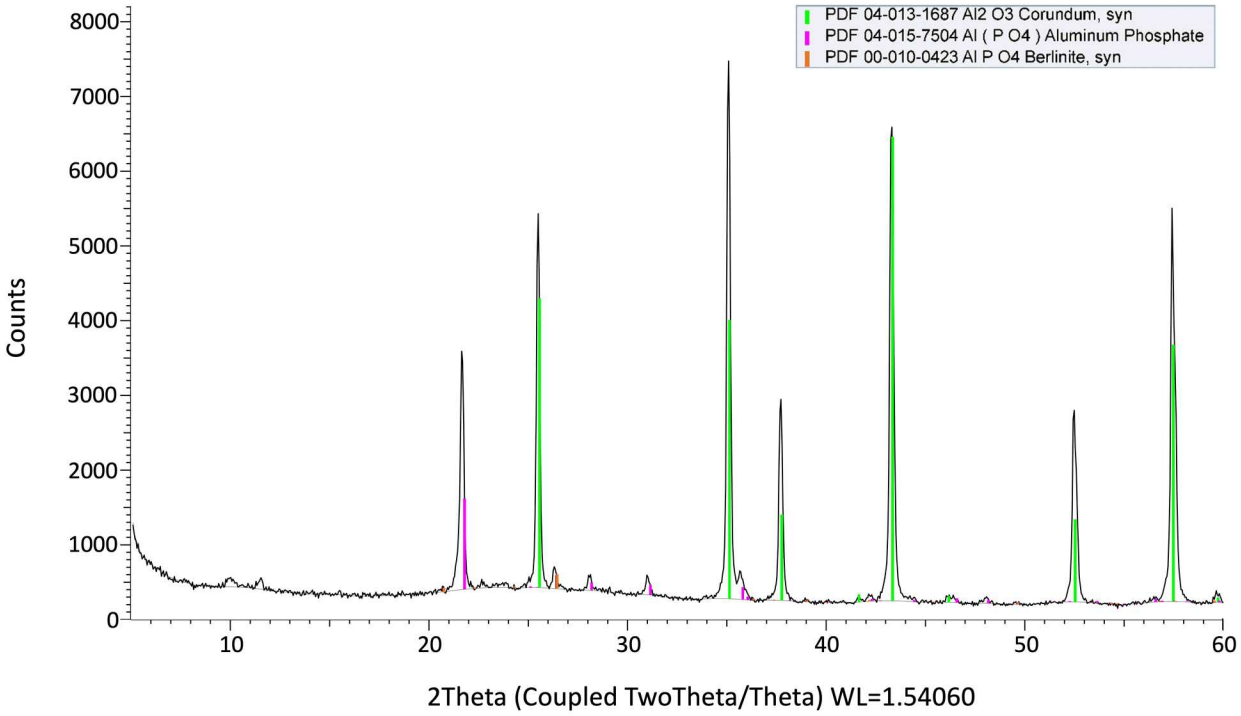

Figure 3-21. XRD pattern of the Sample No. 1108d showing Al_2O_3 along with $AlPO_4$–cristobalite and very minor berlinite.

In another early attempt, Sample No. 1206 was prepared by mixing 200 g alumina with water until a slurry formed, adding 40.0 g H_3PO_4, and mixing. The mixture was dried at 70 °C until the slurry was viscous, whereupon it was re-mixed and degassed under vacuum. This was loaded into a beaker, degassed again, and placed in a dry 1500 mL Parr reactor. The reactor was installed in a forced draft oven set to 165 °C (actual reactor temp: 168 °C) for 4 days.

The resulting monolith (Figure 3-22) is hard and very well-consolidated. However, it contains substantial pore space. XRD analyses indicate that it is composed of Al_2O_3 and berlinite.

Figure 3-22. Photograph of Sample No. 1206 that is 4.5 cm in diameter and 4.5 cm long. Sample was sectioned in half lengthwise to reveal the numerous large pores up to 8 mm in diameter.

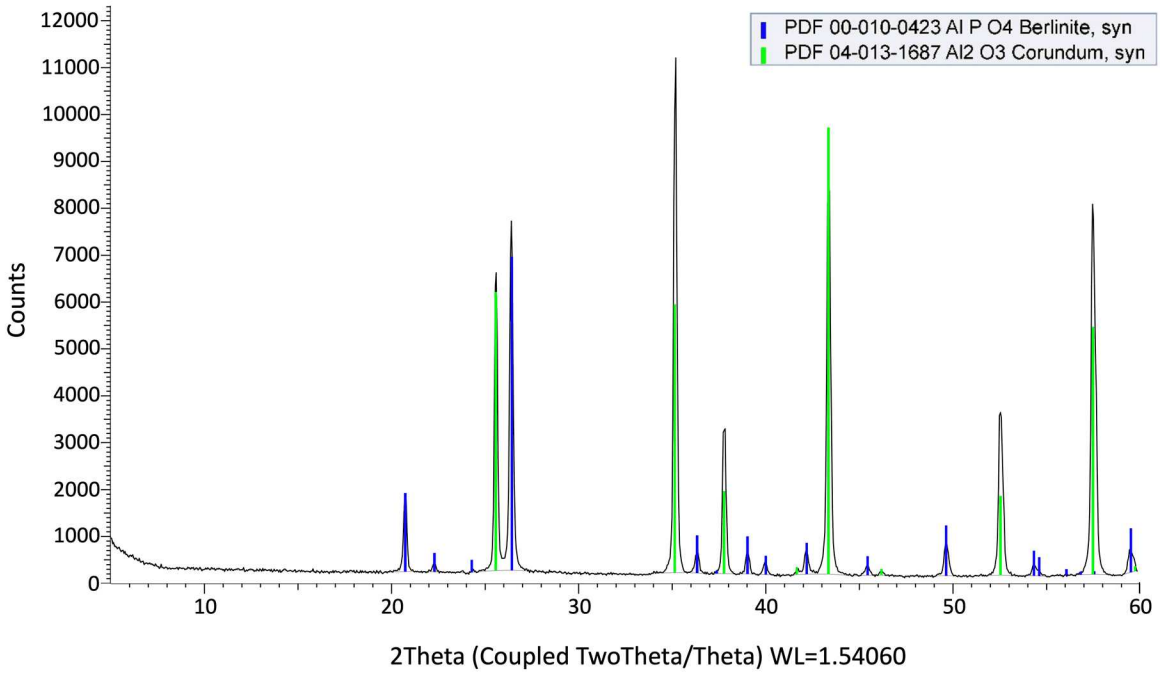

Figure 3-23. XRD pattern of Sample No. 1206 showing Al_2O_3 (corundum) and $AlPO_4$ (berlinite).

3.3.3 Role of Additives

Based upon the results of the preliminary experiments described above, with we undertook exploratory experiments to determine whether there are other suitable aluminum and phosphate sources to facilitate the formation of the $AlPO_4$ binder and produce a dense and well-consolidated APC monolith.

Amorphous AlOOH (Catapal B) was deferred because of its lack of reactivity as observed in the hydrothermal experiments described above. Meanwhile, both gibbsite ($AlOH_3$), and a new potential additive, metakaolin (an anhydrous calcined form of the clay mineral kaolinite) were examined. The latter is rich in alumina and silica and because it is considered a reactive pozzolan (it has twice the reactivity of most other pozzolans) metakaolin is a valuable additive for concrete/cement applications.

The first aluminum additive tried was metakaolin, which was initially investigated by itself as a possible replacement for Al_2O_3. In this experiment, 51 g Sika M100 metakaolin was mixed with 11.5 g H_3PO_4 and 36 g H_2O; this slurry was degassed and poured into two 20 mm glass tubes. One tube was left at room temperature (Sample No. 0407a) while the other was ramped from 80 to 140 °C at 1.5 °C/hr (Sample No. 0407b). The room temperature mixture eventually fully cured to a brittle solid. The heated sample experienced substantial shrinkage and became a monolith with breaking strength similar to a stick of chalk (Figure 3-24).

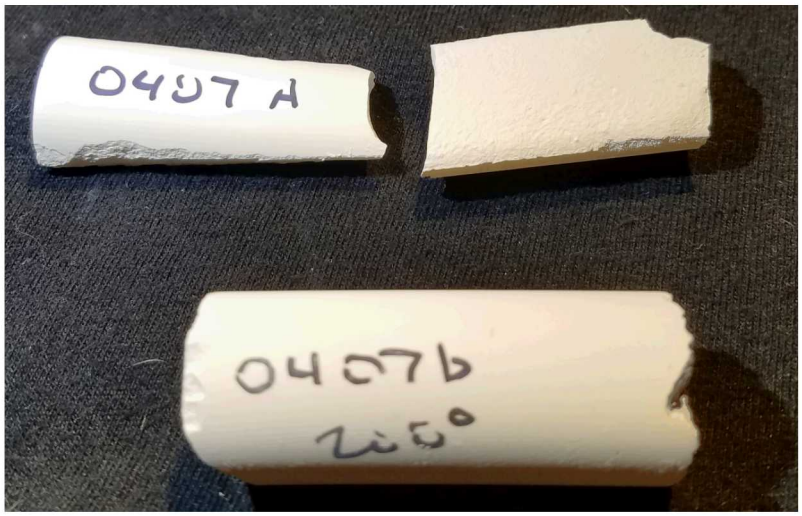

Figure 3-24. Photograph of Sample Nos. 0407a and 0407b. Both the room temperature (0407a) and the heated sample (0407b) yielded smooth monoliths that appear to be pore free, but both proved easy to break upon handling.

Both the shrinkage and the poor strength may be due to the fact that metakaolin by itself requires 3 times the amount of water vs. the same amount of alumina. We attribute this to higher surface area and porosity, which causes metakaolin to require more water to make a fluid slurry.

While the experiment with pure metakaolin produced weak monoliths we also examined the inclusion of metakaolin as an additive (aluminum source) in a baseline Al_2O_3 / H_3PO_4 mixture. Slurries were made according to Table 3-7. These were mixed, degassed, and poured into 50 mL Teflon centrifuge tubes. The samples were ramped from 84 to 130 °C at 2 °C/hr, removed from the tubes, then ramped from 130 to 165 °C at 2 °C/hr.

Table 3-7. Al_2O_3 and Al_2O_3 / Metakaolin with H_3PO_4.

Sample No.	0606b	0606c
Al_2O_3, g	51.0	45.9
metakaolin, g	-	5.1
H_3PO_4, g	11.5	11.5
H_2O, g	11.5	11.5

Sample No. 0606b is a hard but broken monolith that appears to have expanded during synthesis while Sample No. 0606c has some crack-like surface defects but appears to be a hard monolith also, but unlike 0606b it showed no signs of expansion (or shrinkage) appearing as a near-net-shape monolith when removed from the centrifuge tube (Figure 3-25).

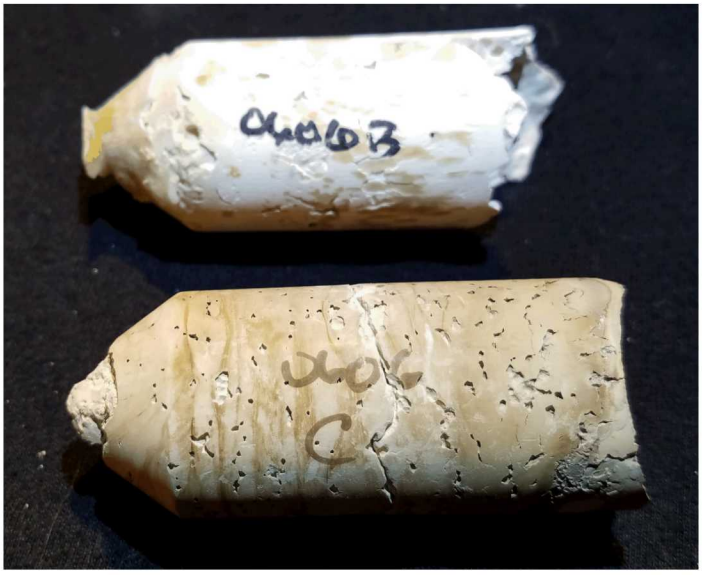

Figure 3-25. Photographs of Sample Nos. 0606b (top) and 0606c (bottom). Note the pores (1-2 mm across) and crack-like features in 0606c.

Two additional phosphate sources were identified and explored with Al_2O_3. These include ammonium pentahydrogen diphosphate ($NH_4H_5(PO_4)_2$) a salt of ADP and phosphoric acid, and ammonium dihydrogen phosphate ($NH_4H_2PO_4$). Slurries using these additives were made according to Table 3-8. These were mixed, degassed, and poured into 50 mL centrifuge tubes. The samples were ramped from 84 to 130 °C at 2 °C/hr, removed from the tubes, then ramped from 130 to 165 °C at 2 °C/hr.

Table 3-8. Al_2O_3 with $NH_4H_5(PO_4)_2$ and $NH_4H_2PO_4$.

Sample No.	0606d	0606e
Al_2O_3 (g)	51.0	51.0
$NH_4H_5(PO_4)_2$ (g)	11.5	-
$NH_4H_2PO_4$ (g)	-	11.5
H_2O (g)	11.5	18.0

Both were recovered as somewhat fragile monoliths. Sample No. 0606d but has many millimeter-sized pores on the surface and interior, while Sample No. 0606e is a cracked but well-consolidated monolith that shrank away from the wall of the centrifuge tube during consolidation indicating net negative expansion of the sample (Figure 3-26).

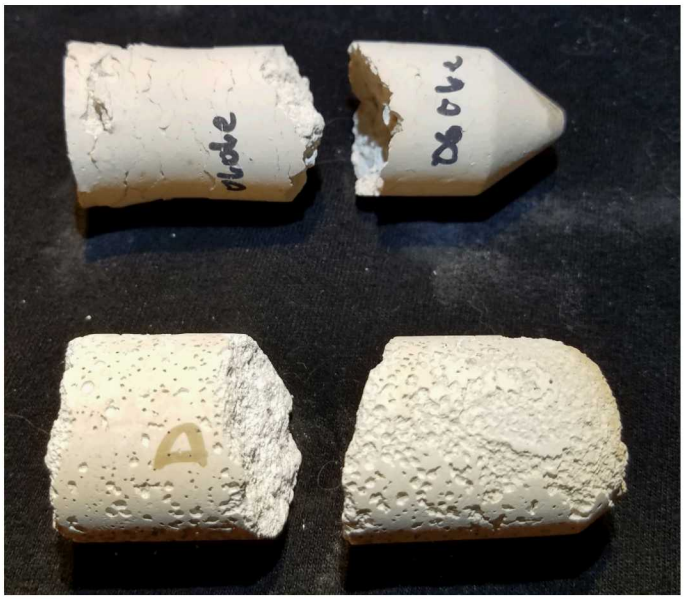

Figure 3-26. Photograph of Sample Nos. 0606d and 0606e. Note that 0606e (top) is slightly smaller in diameter than 0606d (bottom).

The results of these exploratory experiments indicate metakaolin is promising as an additive although more experiments are needed to determine its optimal loading into the APC system. Also, it appears that some buffering with the ammonium phosphate may be helpful.

Based on the encouraging results of the 0606 experimental series, a text matrix was designed to further explore the composition space (Table 3-9). In addition to the examination of metakaolin and $NH_4H_5(PO_4)_2$ as additives, several experiments were also attempted to evaluate the effects of boric acid (H_3BO_3) as an additive. It is desirable to have boron present as a neutron getter and it has been hypothesized that the boric acid may serve to strengthen the resulting products (Hardin and Brady, 2017).

Table 3-9. Recipes to examine Al_2O_3 with metakaolin along with $NH_4H_5(PO_4)_2$ and H_3BO_3 additives.

Sample No.	Al_2O_3 (g)	Metakaolin (g)	$NH_4H_5(PO_4)_2$ (g)	H_3PO_4 (g)	H_2O (g)	H_3BO_3 (g)
0610a	48.45	2.55	-	11.5	11.5	-
0610b	45.90	5.1	-	11.5	11.5	-
0610c	45.90	5.1	11.5	-	11.5	-
0614a	45.90	2.55	-	20.13	8.0	-
0614c	48.45	2.55	-	11.5	12.5	3.09
0614d	48.45	2.55	11.5	-	11.5	3.09
0614e	48.45	2.55	11.5	-	12.5	-
0617b	45.90	5.1	11.5	-	11.5	-
0617c	48.45	2.55	11.5	-	11.5	3.09
0621b	45.90	5.1	11.5	-	11.5	-
0621c	48.45	2.55	11.5	-	11.5	3.09

The sample recipes in Table 3-9 were mixed, degassed, and poured into 50 mL centrifuge tubes. The 0610 samples were ramped from 80 to 160 °C at 2 °C/hr, and the 0614 samples were ramped from 80 to 155 °C

at 2 °C/hr. The 0617 samples were ramped from 80 to 130 °C at 2 °C /hr, then held at 130 °C for 16 hr. The 0621 samples were ramped from 80 to 110 °C at 2 °C /hr, then held at 110 °C for 16 hr.

In the 0610 series we examined the effects of lowering the ratio of metakaolin to alumina by half while using H_3PO_4 as the phosphate source (0610a and 0610b), and of replacing H_3PO_4 with $NH_4H_5P_2O_8$ (0610c vs. 0610b).

Sample No. 0610a was expanded, with large voids.

Sample No. 0610b was slightly expanded, fragile, and had surface cracks.

Sample No. 0610c in which $NH_4H_5(PO_4)_2$ completely replaced phosphoric acid as the phosphate source produced a strong and near net-shaped monolith with no obvious surface cracks and minimal voids (Figure 3-27). However, the monolith was very easily broken by hand.

Figure 3-27. Photograph of Sample No. 0610c. Sample is 2.5 cm in diameter and ~ 6 cm long. Isolated pores that are evident are 1 mm or less in diameter.

The results of the 0610 series indicate that reducing the metakaolin / alumina ratio below 0.1 appears unhelpful in producing a dense and well-consolidated APC sample. Using $NH_4H_5(PO_4)_2$ as a replacement for H_3PO_4 while maintaining the metakaolin / alumina ratio at approximately 0.1 yielded a much better result (Sample No. 0610c). Never-the-less, the relatively low strength of these APC formulations upon handling is unfavorable for the use case.

In the 0614 series, we formulated Sample No. 0614a to examine the effect of lowering the Al/P ratio to 5 in what is otherwise the same recipe as Sample No. 0610a. Sample No. 0614c was formulated to examine the addition of H_3BO_3 to the same recipe as Sample No. 0610a In Sample No. 0614d we halved the amount of metakaolin as in the Sample No. 0610c recipe and added H_3BO_3. Finally, in the Sample No. 0614e formulation we again halved the amount of metakaolin as in the Sample No. 0610c recipe but did not add H_3BO_3.

Figure 3-28. Photograph of Sample Nos. 0614a and 0614d.

Sample No. 0614a and 0614c were highly expanded, with 0614a exhibiting numerous large voids. (Figure 3-28, left) and 0614c appearing hollow with a very large internal void open to the sample surface. In stark contrast, Sample No. 0614d was smooth, near net-shape, with slight scaling on the surface. (Figure 3-28, right). Meanwhile, Sample No. 0614e was a very well consolidated monolith with no surface cracks or voids but which shrank away from the tube wall during consolidation demonstrating a small amount of negative expansion.

The results of the 0614 experimental series indicate that while the H_3BO_3 additive may impart some increased strength, it is ineffective at controlling the expansion and formation of porous APC monoliths.

Sample Nos. 0617b and 0617c are repeats of 0610c and 0614d, respectively. Recall that both of these samples (Figures 3-27 and 3-28) were recovered as well-consolidated, relatively pore-free and fracture-free near net-shape samples. When reproduced as Sample No. 0617b and Sample No. 0617c both were again recovered as smooth, near net-shape monoliths with no surface cracks or voids. These were then cut into 1" diameter x 0.5" thick discs and were used for water resistance testing. On average, there was more weight lost from 0617c, which contains borate, than from 0617b which contains no borate.

Sample Nos. 0621b and 0621c were made identically to 0617b and 0617c, respectively, except that they were ramped to a lower cure temperature of 110 °C instead of 130 °C. They are smooth, near net-shape, with no surface cracks or voids. These were surprisingly well-consolidated considering their cure temperature.

The significance of this result is that: 1) the aluminophosphate recipes studied here can be cured at lower temperatures than we had previously thought, and 2) it may be possible to shorten the cure cycle by ramping only to 110 °C, reserving the option of annealing at a desired temperature immediately after ramp or at a later date.

The next series of exploratory experiments was conducted in order to examine $Al(OH)_3$ (gibbsite) as a reactive alumina source. We anticipated that gibbsite will be more reactive than metakaolin due to its higher basicity, and thus may be more compatible with a phosphate source that is less acidic than $NH_4H_5(PO_4)_2$, such as $NaH_5(PO_4)_2$. The latter is generated *in situ* through reaction of equimolar quantities of H_3PO_4 and $NaH_2PO_4 \bullet H_2O$.

Table 3-10. Recipes to examine Al_2O_3 with gibbsite as the aluminum source and H_3PO_4, $NH_4H_5(PO_4)_2$ and $NaH_5(PO_4)_2$ as alternative phosphate sources.

Sample No.	0630a	0703a
Al_2O_3 (g)	48.45	48.45
$Al(OH)_3$ (g)	2.55	2.55
$NH_9P_2O_8$ (g)	11.5	-
$NaH_2PO_4 \bullet H_2O$ (g)	-	6.9
H_3PO_4, 85% (g)	-	5.75
H_2O (g)	12.5	12.5

Sample Nos. 0630a and 0703a in Table 3-10 were mixed, degassed, and poured into 50 mL centrifuge tubes and then placed in an oven that was ramped from 84 to 130 °C at 2 °C /hr, then held at 130 °C for 7 hr.

Sample No. 0630a was recovered as a well consolidated and near net-shape monolith with surface cracks. In contrast, Sample No. 0703a was strong, smooth with faint cracks evident on its surface (near the top of the sample) and just a few bubbles on the side of the sample (Figure 3-29). The sample exhibits a density of 1.9 g/cm^3. Finally, Sample No. 0705e produced a very crumbly and fragile monolith.

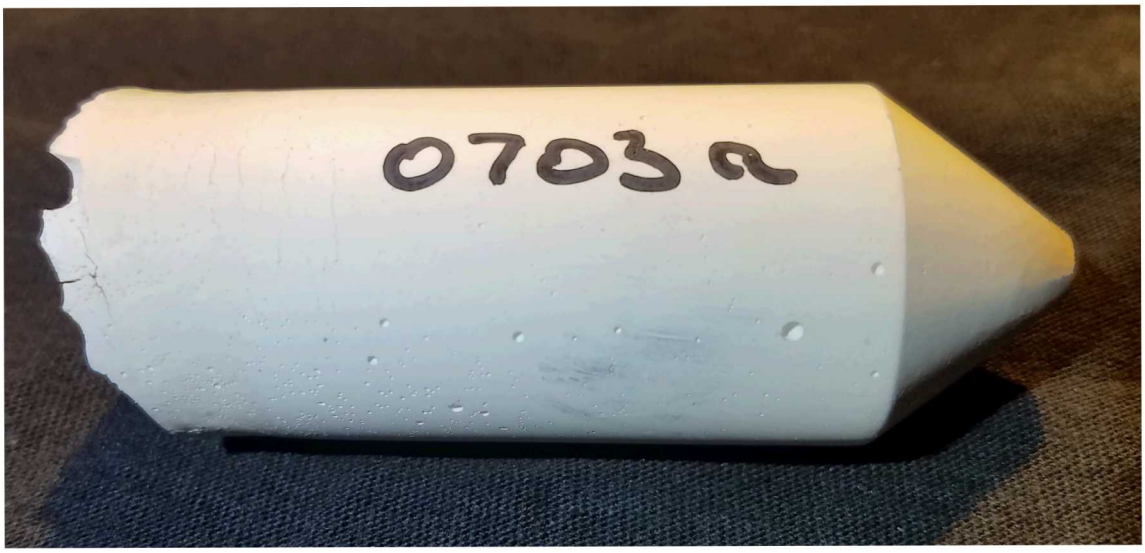

Figure 3-29. $Al_2O_3/Al(OH)_3$ with the $NaH_5(PO_4)_2$ phosphate source. Small cracks are evident near the top (left side of photo). Isolated pores are on the order of 2 mm or less in diameter.

The use of $Al(OH)_3$ as an alternative aluminum source with H_3PO_4 produced a very poorly consolidated monolith. Use of $Al(OH)_3$ with $NH_4H_5(PO_4)_2$ and $NaH_5(PO_4)_2$ phosphate sources produced better results, with the $Al(OH)_3$ and $NaH_5(PO_4)_2$ combination producing the best results, a well consolidated APC monolith. However, the effects of this sodium phosphate salt as compared to the ammonium phosphate salt on APC strength and solubility will require additional evaluation. This is because Na remains in the APC it doesn't evaporate from the slurry during cure as does ammonium (NH_3) to leave behind free phosphate which subsequently reacts to form the $AlPO_4$ binder.

In the 0723 series, the 0630a and 0703a recipes were repeated at 2x scale to verify that $NaH_2PO_4 \bullet H_2O$ is more appropriate to use with $Al(OH)_3$ than $NH_4H_5(PO_4)_2$. In addition, the larger scale affords samples with

an aspect ratio of 3 rather than 2, which was used in 0630a and 0703a. As a further benefit, the longer monoliths are of sufficient length for mechanical testing.

The samples were mixed, degassed, and poured into 50 mL centrifuge tubes and then placed in an oven that was ramped from 84 to 130 °C at 2 °C/hr, then held at 130 °C for 8 hr.

Table 3-11. Al_2O_3 with $Al(OH)_3$ and $NH_4H_5(PO_4)_2$ or $NaH_5(PO_4)_2$ as phosphate sources.

Sample No.	0723a	0723b
Al_2O_3 (g)	96.9	96.9
$Al(OH)_3$ (g)	5.1	5.1
$NH_9P_2O_8$ (g)	23	-
$NaH_2PO_4 \bullet H_2O$ (g)	-	13.8
H_3PO_4, 85% (g)		11.5
H_2O (g)	23	23

Upon recovery, Sample No. 0723a was an expanded monolith with numerous pores and cracks while Sample No. 0723b was smooth, with slight expansion and cracking near the top (Figure 3-30).

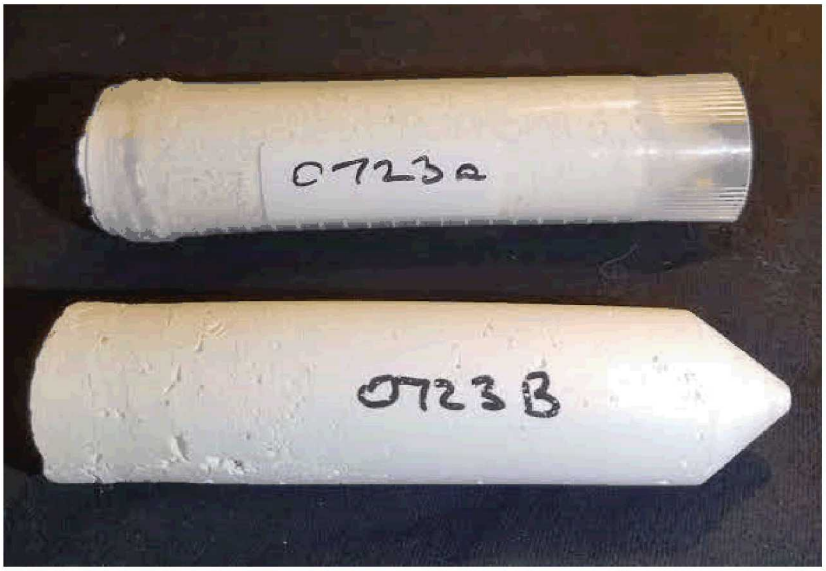

Figure 3-30. Photograph of Al_2O_3 with $Al(OH)_3$ and $NH_4H_5(PO_4)_2$ (top) and $NaH_5(PO_4)_2$ (bottom) as phosphate sources.

$NaH_5(PO_4)_2$ appears to be a more appropriate phosphate source for Al_2O_3 / $Al(OH)_3$ slurries than $NH_4H_5(PO_4)_2$. This may be due to the fact that $Al(OH)_3$ is a stronger base than metakaolin and hence the $Al(OH)_3$ may require a less acidic (higher pH) phosphate source than $NH_4H_5(PO_4)_2$. That said, it is possible that $NaH_5(PO_4)_2$ is more effective with Al_2O_3 / metakaolin mixtures as well.

In 0705b we tested the effect of replacing $NH_4H_5P_2O_8$ in the metakaolin-containing 0614e recipe with the less acidic $NaH_5P_2O_8$ (made in situ as a 1:1 molar combination of H_3PO_4 and $NaH_2PO_4 \bullet H_2O$). In 0705c and 0705d we investigated whether H_3BO_3 can reduce expansion and large pore formation without any reactive alumina sources present. In 0705c we tested whether boric acid can replace metakaolin as an additive in the 0705b recipe, and in 0705d we repeated the 0614d experiment but removed metakaolin.

Table 3-12. Effects H_3BO_3 expansion and pore formation.

Sample No.	0705b	0705c	0705d
Al_2O_3 (g)	48.45	48.45	48.45
Metakaolin (g)	2.55	-	-
H_3BO_3 (g)	-	2.55	2.55
H_3PO_4, 85% (g)	5.75	5.75	-
$NH_4H_5(PO_4)_2$ (g)	-	-	11.5
$NaH_2PO_4•H_2O$ (g)	6.9	6.9	-
H_2O, g	12	12	12.5

These samples were ramped from 84 to 130 °C at 2 °C/hr, then held at 130 °C for 8 hr.

The resulting monoliths were recovered for examination. Sample No. 0705b is smooth and near net-shape, with small cracks at the top and bottom while Sample No. 0705c was expanded and porous and 0705d was very expanded, and not a monolithic.

These results demonstrate that H_3BO_3 is not useful as an additive to mitigating expansion and/or large pore formation at ambient pressure. Only metakaolin and $Al(OH)_3$ have proven successful at mitigating expansion and/or large pore formation. The influence of choosing $NH_4H_5(PO_4)_2$ vs. $NaH_5(PO_4)_2$ as the phosphate source is unclear as a result of these experiments.

To further explore the influence of $NH_4H_5(PO_4)_2$ vs. $NaH_5(PO_4)_2$ as the phosphate source a test matrix was set up for the purpose of directly comparing Al_2O_3 / $Al(OH)_3$ and Al_2O_3 / metakaolin slurries with both $NH_4H_5(PO_4)_2$ and $NaH_5(PO_4)_2$ as phosphate sources (Table 3-13). Additionally, aspect ratio was tested as a variable by filling tubes to 2 different volumes with the same slurry. The aspect ratio values tested were 2.3 and 3.0; the aspect ratio of a DPC is approximately 2.3. (Most of the previously made samples have aspect ratios closer to 2.0.) Slurries were prepared as described previously in this section.

Table 3-13. Test matrix to evaluate Al_2O_3 / $Al(OH)_3$ and Al_2O_3 / metakaolin slurries with both $NH_4H_5(PO_4)_2$ and $NaH_5(PO_4)_2$ as phosphate sources.

Sample No.	0830a	0830b	0830c	0830d
Al_2O_3 (g)	145.35	145.35	145.35	145.35
metakaolin (g)	7.65	-	7.65	-
$Al(OH)_3$ (g)	-	7.65	-	7.65
85% H_3PO_4 (g)	17.25	17.25	17.25	17.25
$NH_4H_2PO_4$ (g)	17.25	17.25	-	-
$NaH_2PO_4•H_2O$ (g)	-	-	20.71	20.71
H_2O (g)	36.0	34.0	34.0	36.0

Each slurry was poured into two 50 mL centrifuge tubes, one to the 45 mL mark and the other to the 35 mL line. This was done in order to quantify the amount of volume expansion of the monoliths during curing. These were all loaded into an oven and ramped from 82 to 130 °C at 2 °C/hr, then held at 130 °C for 8 hr.

Upon recovery, Sample Nos. 0830a-35mL and 0830a-50mL exhibited significant expansion (Figure 3-31). Calculated expansion ratios were 14% for the 35 mL tube and 22% for the 45 mL tube, meaning that the monolith total volumes were 114% and 122% those of the original slurry volumes, respectively.

Figure 3-31. Photograph of Sample No. 0830a-50mL. Note the monolith has expanded above the top of the 50 mL centrifuge tubes.

The expansion ratios for Sample Nos. 0830b-35mL and 0830b-50mL were measured at 9% for both tubes. The monoliths were both chalky and cracked.

The expansion ratios for Sample Nos. 0830c-35mL and 0830c-50mL were measured at 7%. Both monoliths were smooth with few visible pores. There were some surface cracks at the top and bottom of each (Figure 3-32).

The expansion ratios for Sample Nos. 0830d-35mL and 0830d-50mL were measured at 3% for the 35 mL tube and 5% for the 45 mL tube. While little expansion was observed both monoliths were cracked through.

Figure 3-32. Photograph of Sample No. 0830c-50mL Al_2O_3/Metakaolin combined with H_3PO_4/NaH_2PO_4•H_2O.

Figure 3-33 shows XRD data for 0830a, 0830b, 0830c and 0830d. Many of these samples' data resemble 0830d, with only lines from the Al_2O_3 starting material present. Some have small peaks such as those in 0830a and 0830b, but these had no obvious match to phases containing Al, P, O, or Si (note that silicon-containing phases are a possibility in samples synthesized from metakaolin, which contains considerable amounts of silicon).

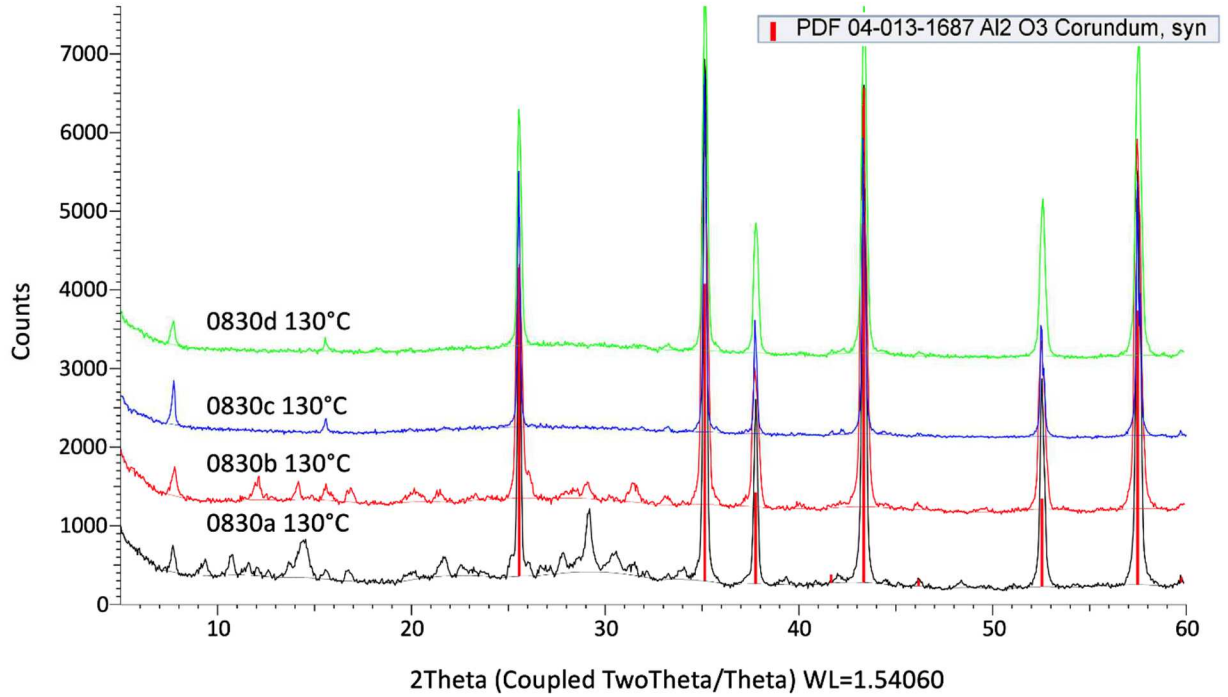

Figure 3-33. XRD data for Sample Nos. 0830a, 0830b,0830c and 0830d.

This preliminary assessment comparing Al_2O_3 / $Al(OH)_3$ and Al_2O_3 / metakaolin slurries with both $NH_4H_5(PO_4)_2$ and $NaH_5(PO_4)_2$ as phosphate sources revealed that the combination of $NaH_5(PO_4)_2$ as the phosphate source and metakaolin as the Al source produced higher quality monoliths at the scale tested than the other three combinations tested.

Weight losses (as measured by TGA) from ambient pressure samples that did not contain borate ranged between 3-6% as measured from the maximum synthesis temperature. It appears that the samples containing borate reversibly absorb water from ambient humidity.

3.3.4 Viscosity Data

A set of experiments to measure viscosity over time was conducted on a very promising APC system developed for thermal processing at ambient pressure. A baseline composition was fabricated to measure viscosity change upon slurry aging. In addition, we tested the effects of three commercial water reducers on the slurry's viscosity and aging behavior.

A large sample of the Al_2O_3 / metakaolin / $NaH_5(PO_4)_2$ slurry, compositionally identical to Sample No. 0830c (Section 3.3.3 above), was made by dry blending 969.0 g Al_2O_3 (Aluchem AC19RG) and 51.0 g Sika M100 metakaolin. Separately, 115 g of 85% H_3PO_4 and 138.1 g $NaH_2PO_4 \bullet H_2O$ were dissolved in 180 g deionized H_2O. This was stirred into the alumina / metakaolin mixture thoroughly and the mixture was degassed. Five 120 g portions were taken from this batch. Another 20.0 g H_2O was then stirred into the main batch. Of the five 120 g portions, one had nothing added (0905), one had 4.0 g H_2O added (0905-w), one had 4.0 g of a 10% solution of sodium ligninsulfonate in water added (0905-l), one had 0.4 g Sika Viscocrete plus 3.6 g H_2O added (0905-v), and one had 0.4 g Arkema Ethacryl SR plus 3.6 g H_2O added (0905-e). Sample 0905-w was considered the control for this experiment.

Samples were stored in a location with a diurnal temperature variation from 21.6 to 23.3 °C. Viscosity data were collected by shaking the samples for 2-3 seconds to reverse settling of the alumina, inserting the

viscometer spindle, and recoding the viscosity indicated after 5 sec of measurement (longer acquisition times can result in lower viscosity values due to thixotropy of the cement).

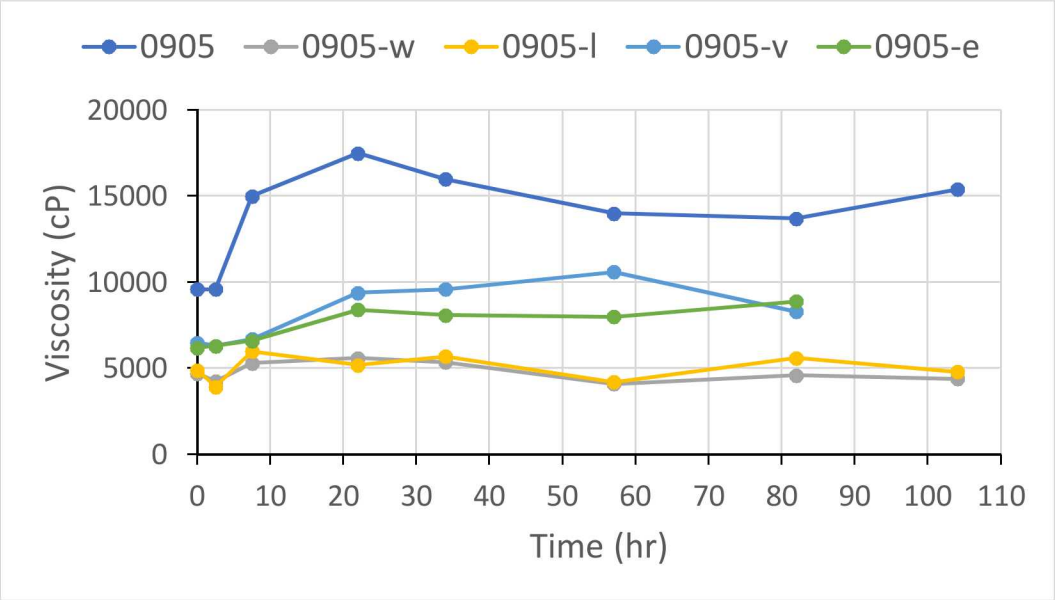

Figure 3-34. Plot of viscosity versus time for various APC slurries.

After 3 days, the base batch 0905 had increased in viscosity and plateaued at around 5,000 cP. The 0905-v, and 0905-e samples showed similar behavior but with greater viscosities in the range of 8,000-10,000 cP. The 0905-w and 0905-l batches did not exhibit the early increase and plateau behavior of the other samples. They have also maintained very similar viscosities and are the lowest viscosities measured (~5,000 cP).

This experiment showed the addition of a 4 g aliquot sodium ligninsulfonate solution was as effective as a 4 g aliquot of pure water at maintaining viscosity of the 0905 slurry. The others, Viscocrete and Ethacryl SR, was considerably less effective than the addition of pure water. Meanwhile the control sample with no additives proved to have the highest viscosity. To date it appears the simple addition of water is most effective at maintaining a low and consistent viscosity over time. The experiment remains ongoing to continue the evaluation of viscosity over time and assess if any of the additives behave as a retarder, i.e., if they attenuate increase of viscosity with time.

3.3.5 Ambient Pressure APC Mechanical Properties

Two of the experiments described above resulted in the production of well consolidated, low porosity samples, and were then selected for preliminary mechanical testing. Again, measurements of unconfined compressive strength were used as a preliminary screening test for mechanical the properties evaluation.

Sample 0830c was prepared as described in Section 3.3.3 above. The resulting slurry was poured into two 50 mL centrifuge tubes, which were used as molds. These were heated from 82 to 130 °C at 2°C/hr, then held at 130 °C for 8 hr. After removing the cured samples from their molds, one sample was selected for anneal at 250 °C for 8 hr and subsequent mechanical testing.

Sample 914a was prepared by mixing dry 193.8 g Al_2O_3 and 10.2 g $Al(OH)_3$ to form a starting material with 23.0 g H_3PO_4, 27.62 g $NaH_2PO_4 \bullet H_2O$, and 45.0 H_2O This slurry was poured then poured into a 1.25” ID x 5” long Pyrex mold. This was heated from 82 to 130 °C at 2°C /hr, held at 130 °C for 8 hr, cooled and inspected, then annealed at 250 °C for 8 hr.

These samples then required machining of the outer diameter, and length to develop the desired right circular cylinders for compressive strength testing. In addition, the ends were trimmed to retain enough material for thermal property measurements. The finished dimensions, density, unconfined compressive strength (UCS), and Young's modulus are given in Table 3-14.

Table 3-14. Sample dimensions and acquired mechanical property data for ambient pressure APCs.

Sample ID	Dimension				Weight grams	Density	UCS	Young's Modulus	Poisson's ratio
	Diameter (in)	Diameter (cm)	Length (in)	Length (cm)		g/cc	psi	psi	
0830c	0.9421	2.393	2.098	5.329	43.92	1.83	1382	129242	0.9421
0914a	0.848	2.154	1.988	5.050	32.14	1.75	817	124842	0.848

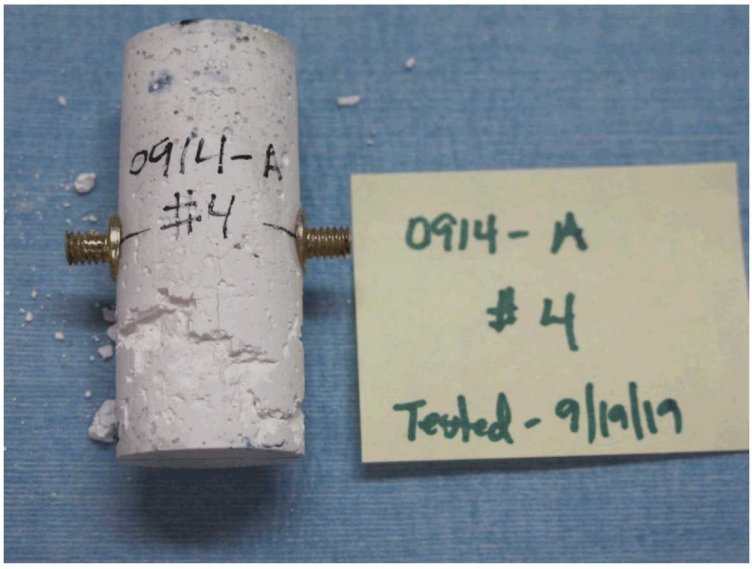

Figure 3-35. Photograph of Sample No. 0914a post-test.

The UCS test consists of measurements of axial and lateral deformations of right circular cylinder samples loaded in the axial direction to failure. The UCS test is a triaxial test with zero confining pressure. The UCS is the maximum axial stress level measured during the test. The strain to UCS was about 0.01 (1%) for all samples except 230 which was closer to 0.02 (2%). The Young's Modulus is the ratio of axial stress difference to axial strain difference in the linear portion of the stress strain curve, and the Poisson's ratio is the ratio of (-) lateral strain to axial strain. The Poisson's ratio is presented for just one sample, as the lateral displacement measurements were challenging and quite small on these very small diameter samples.

Sample No. 0830c, composed of Al_2O_3 / metakaolin with a buffered H_3PO_4 / $NaH_2PO_4 \bullet H_2O$ phosphate source yielded the second highest compressive strength of 1,382 psi. Whereas Sample No. 0914a was composed of an Al_2O_3 / $Al(OH)_3$ aluminum source with the buffered H_3PO_4, / $NaH_2PO_4 \bullet H_2O$ phosphate source, it yielded a notably lower UCS of 817 psi. These sample compositions vary only in the choice of Al source ($Al(OH)_3$ vs metakaolin) which may have a potentially significant effect on compressive strength that warrants further exploration going forward. However, it should be noted that both are exhibiting UCS above the target value of 500 psi (Hardin, 2019 personal communication).

3.3.6 Water Resistance Testing of Ambient Pressure APCs

APC samples fabricated for mechanical testing in Section 3.3.5 above were also subjected to water resistance testing.

Table 3-15 Results of water resistance testing of selected APCs thermally cured at ambient pressure.

Sample No.	Starting wt. (g)	pH after test	Wt. after test (g)	Pct. wt. loss
1025d	4.90	6	4.73	3.5%
0830c	19.76	5.5	19.19	2.88%
0914a	11.36	5.5	11.06	2.64%

All of the samples lost a small amount of weight. The resulting pHs of the supernatant measured post-test decreased, suggesting that the weight loss was from excess H_3PO_4 that did not react with the aluminum sources. This will be evaluated in FY20 by inductively coupled plasma mass spectrometry (ICP-MS) and ion chromatography (IC).

3.3.7 Summary

After a detailed exploration of the composition space and additive effects it appears that well-consolidated APC monoliths lacking large voids can be made by thermal treatment at ambient pressure. The best results were obtained by adding small amounts of metakaolin or $Al(OH)_3$ to the Al_2O_3 starting material. We believe these additives both function by reacting with a portion of the phosphate source at a lower temperature than that at which the phosphate reacts with Al_2O_3 alone. This causes the cement to partially consolidate and enables it to retain shape while allowing the water to escape as steam from the reacting Al_2O_3 and phosphate.

The phosphate sources that are most effective with these additives are $NaH_5(PO_4)_2$ and $NH_4H_5(PO_4)_2$. Of these, $NaH_5(PO_4)_2$ yielded high-quality monoliths more consistently than did $NH_4H_5(PO_4)_2$ and thus the $NaH_5(PO_4)_2$ based APCs with metakaolin and $Al(OH)_3$ additives were subsequently selected for mechanical testing. Of the two additives, metakaolin and $NaH_5(PO_4)_2$ produced monoliths with fewer cracks than did $Al(OH)_3$ and $NaH_5(PO_4)_2$.

We have started to investigate the relative compressive strengths of Al_2O_3 / metakaolin and Al_2O_3 / $Al(OH)_3$ monoliths made with the same alumina / additive ratios but do not have sufficient data to draw conclusions favoring one additive over the other.

This page is intentionally left blank.

4. FLY ASH PHOSPHATE FILLERS

4.1 Fly Ash Overview

Fly ash was originally recommended for use as a mildly reactive aggregate or conditioner, to control slurry consistency and to impart more strength to the final product in aluminum phosphate cements (Hardin and Brady, 2017). Based on discussions with Arun Wagh in 2017, Hardin and Brady recommended the following as a baseline formulation for the evaluation.

- Calcined alumina, 49 wt.%
- Aluminum hydroxide, 1 wt.%
- Class F fly ash, 50 wt.%
- 50% H_3PO_4 solution, ca. 45 mL per 100 g dry alumina
- Water: sufficient for slurry; no more than ca. 50 mL per 100 g fly ash

Exploratory experiments based upon this recommended formulation were initiated as described below. However, as mentioned above, the observation that fly ash and H_3PO_4 form hard and pore-free monoliths (even in the absence of Al_2O_3 and without any special thermal treatment such as a slow ramp to final bake temperature led us to examine fly ash phosphates as an alternative filler composition.

4.2 Composition Space Studied

Class F fly ash originates from the burning of anthracite and bituminous coals and is composed primarily of silicon, aluminum and iron oxide phases. Class F fly ash obtained from Salt River Materials Group was used in these experiments and analyzed using both powder XRD and x-ray fluorescence (XRF). XRD indicates the presence of quartz (SiO_2) and mullite (nominally $3Al_2O_32SiO_2$ or $2Al_2O_3$ SiO_2) (Figure 4-1). There were no iron phases definitively identified by XRD. However, there was significant fluorescence background in the XRD pattern, which we attributed to the presence of first-row transition metals. This was later confirmed by XRF, which identified significant amounts of iron in the sample. (Figure 4-2). It is possible that amorphous material(s) of unknown composition is also present.

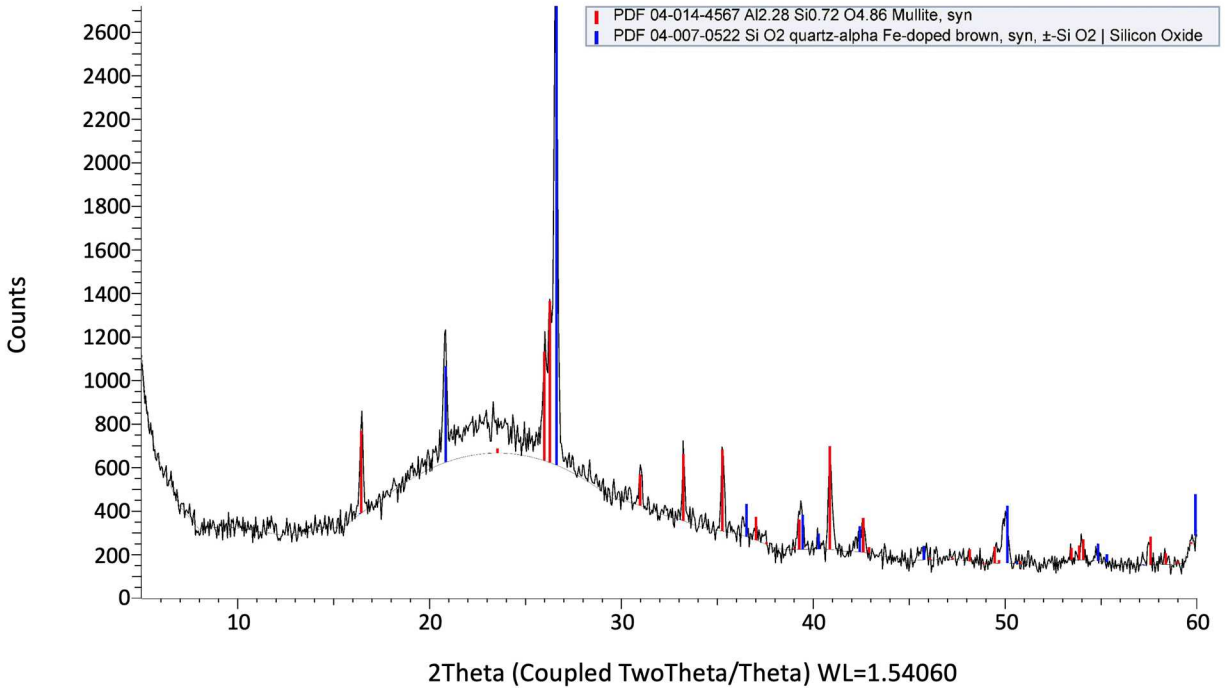

Figure 4-1. XRD pattern of Class F fly ash starting material.

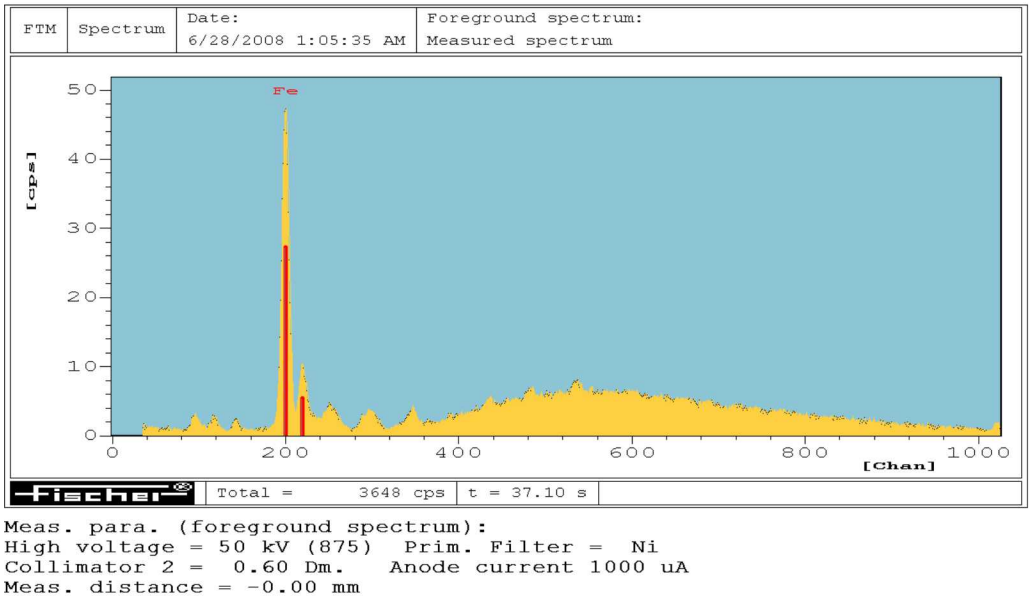

Figure 4-2. XRF spectrum of Class F fly ash.

0223 Series – Fly Ash Phosphate under Ambient Pressure and Hydrothermal Conditions

A series of slurries to assess fly ash phosphate consolidation in the presence and absence of Al_2O_3 were made and heated to 170 °C under both ambient pressure and hydrothermal conditions.

Table 4-1. Al_2O_3 / Class F fly ash samples.

Sample No.	Al_2O_3(g)	Fly ash (g)	H_3PO_4 (g)	H_2O (g)
0223a	51.0	-	11.5	11.5
0223b	38.25	12.75	11.5	13.5
0223c	25.5	25.5	11.5	23.5
0223d	-	51.0	11.5	30.0

Each slurry was degassed and poured into two 20 mm glass molds. These sat at room temperature overnight. One set of slurry tubes (Sample Nos. 0223a-H to 0223d-H) were loosely capped with Al foil and placed in a 1.5 L Parr reactor 1/3 full of DI water, which was then sealed and placed in a 170 °C oven for 90 hr. After cooling, the tubes were removed and heated at ambient pressure at 170 °C for 15 hr. The other set of slurry tubes (Sample Nos. 0223a-A to 0223d-A) were heated at 170 °C at ambient pressure alongside the reactor.

In general, the hydrothermal experiment (Sample Nos. 0223a-H to 0223d-H) yielded poor results by producing poorly consolidated products as either fragile monoliths or unconsolidated powders (Figure 4-3 Sample Nos. 0223b-H and 0223d-H). XRD analyses of the baseline APC recipe (Sample No. 0223a-H with no fly ash) revealed Al_2O_3 and $AlPO_4 \bullet H_2O$ as the phosphate binder present (Figure 4-4). In samples with Al_2O_3 and fly ash (Sample No.s 0223b-H and 0223c-H) we observe no evidence of aluminum phosphate phases. However, quartz was evident. As expected, Sample No. 0223d-H, which was pure fly ash, yielded no obvious $AlPO_4$ phases.

Figure 4-3. Photograph of Sample Nos. 0223b-H and 0223d-H. 0223b-H (top) is a crumbly powder that did not survive removal from the tube while 0223d-H is a wet unconsolidated powder. The sample tubes are 7.5 cm long and 2 cm OD.

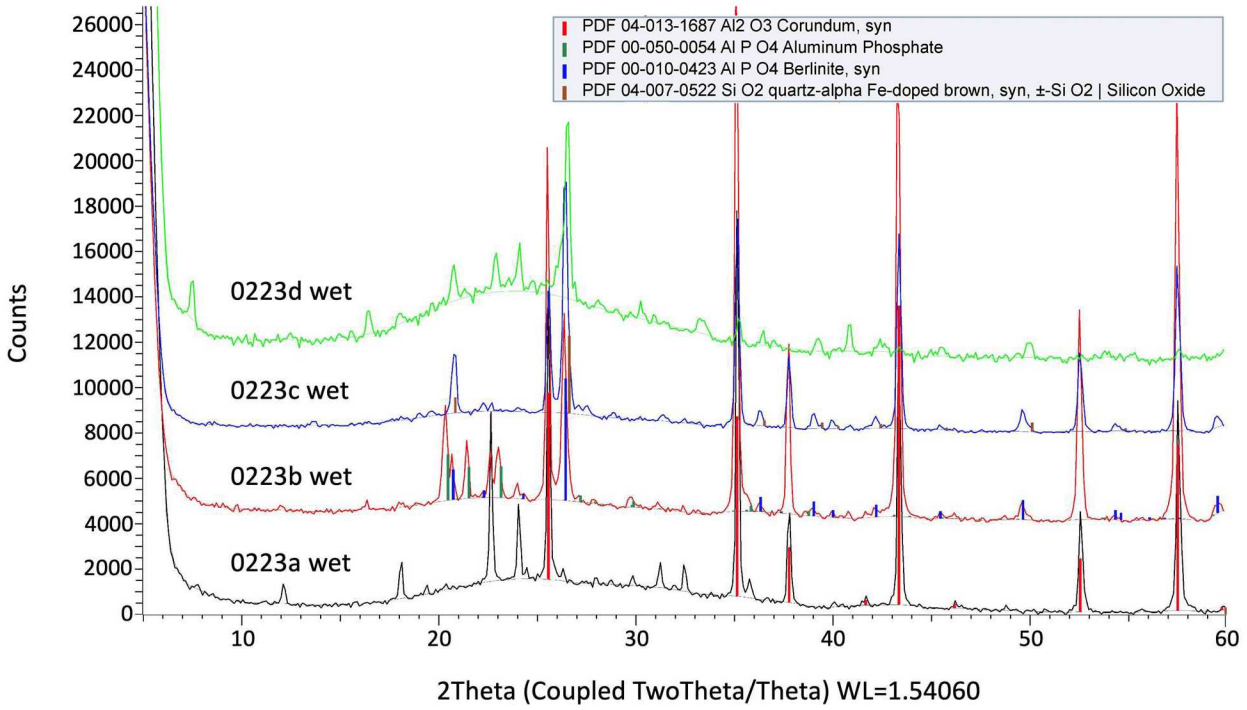

Figure 4-4. XRD patterns of Sample Nos. O223a, 0223b, 0223c and 0223d.

In contrast to the hydrothermal experiment, the samples processed at ambient pressure were better consolidated (Figure 4-5). Nevertheless, Sample Nos. 0223a-A, 0223b-A and 0223c-A were all highly porous and broke up upon removal from their tubes. XRD analyses (Figure 4-4) were indeterminant regarding the presence of aluminum phosphate phases because quartz which is present in the fly ash cannot easily be resolved from berlinite using the available XRD equipment; the two minerals are isostructural and have very similar cell constants. However, it should be noted that Sample No. 0223a contains no quartz or source of Si yet there is evidence for a minor amount of berlinite.

Surprisingly, Sample 0223d-A, appears as a well-consolidated monolith with no obvious porosity and a density of 1.5 g/cm^3. It is particularly noteworthy because this is the 100% fly ash sample which is well-consolidated in the absence of an obvious phosphate or other binder phase as indicated by XRD (Figure 4-7). As can be seen in Figure 4-7 the only crystalline phase evident is quartz. In fact, the pattern matches best with a Fe-doped quartz of unspecified composition. This is a reasonable interpretation given the substantial presence of Fe in the fly ash as indicated by XRF (Figure 4-2). These observations also raise the possibility that a poorly crystalline or amorphous phase is present and acting as the binder.

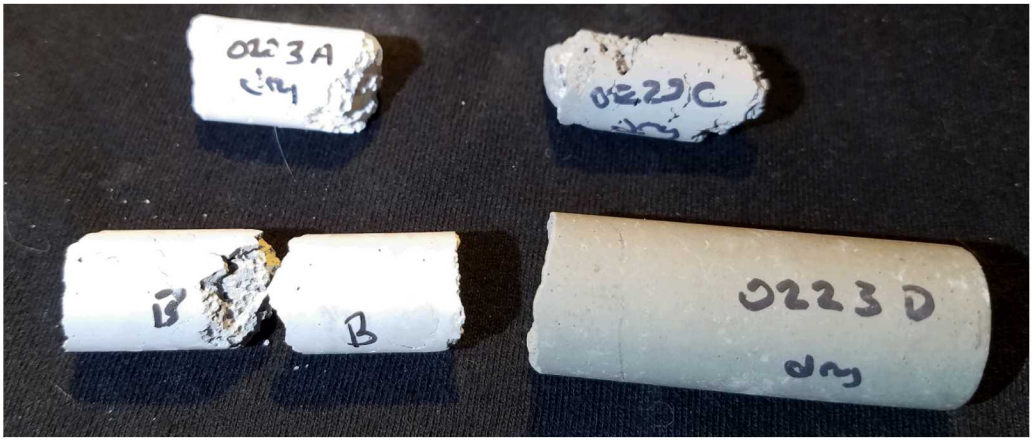

Figure 4-5. Photograph of Sample Nos 0223a-A, 0223b-A 0223c-A and 0223d-A. Sample No. 0223d-A (lower right) is a well-consolidated monolith with no obvious evidence of pores.

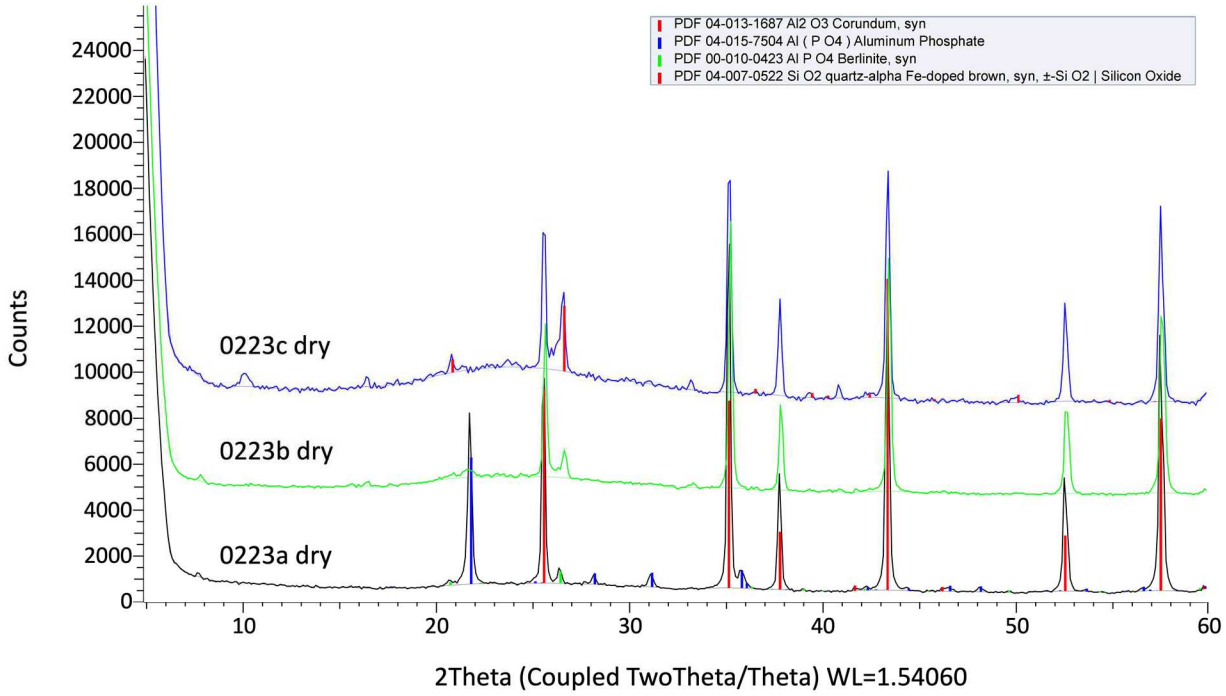

Figure 4-6. XRD patterns of Sample Nos. 0223a-A, 0223b-A and 0223c.

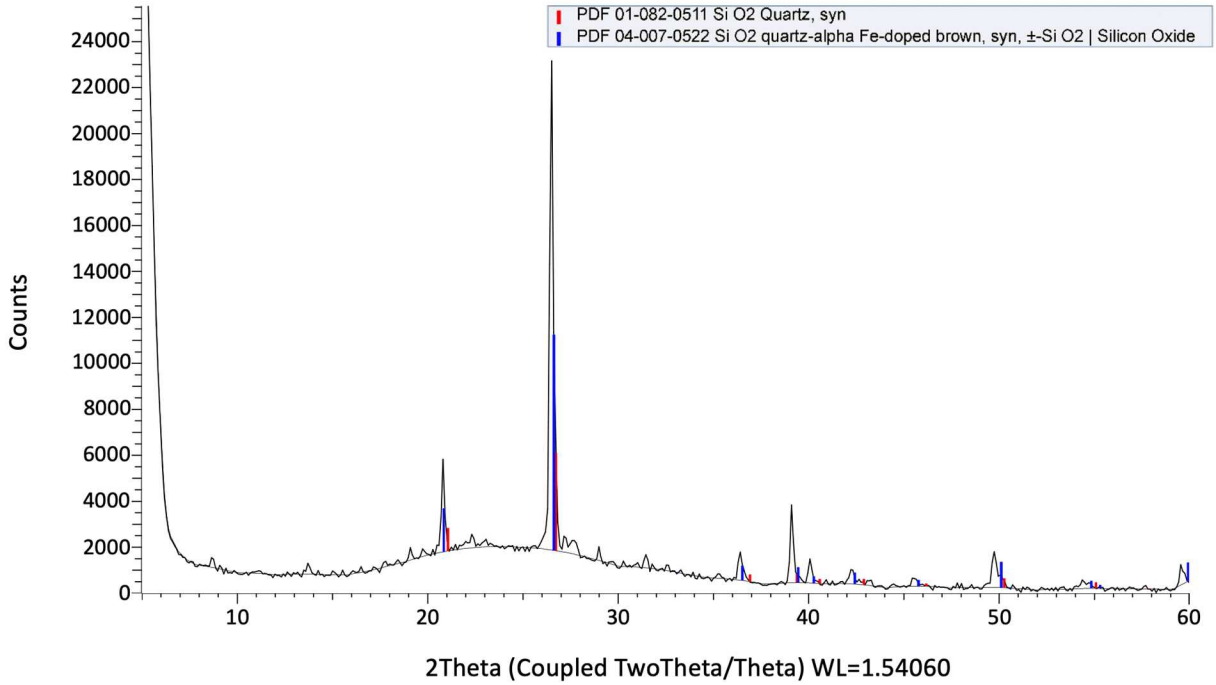

Figure 4-7. XRD pattern of Sample No 0223d indicating the presence of Fe doped quartz.

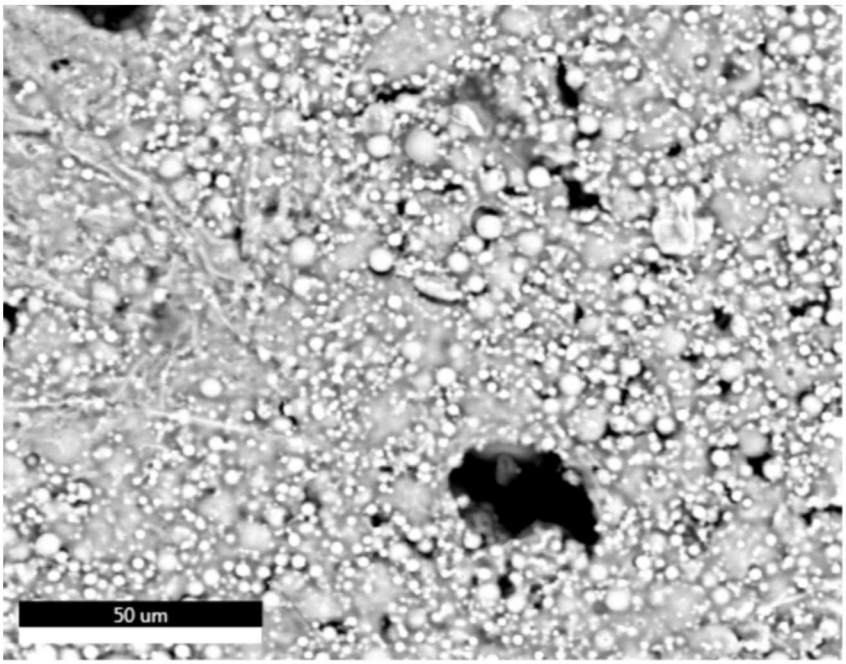

Figure 4-8. SEM image of 0223d-A in secondary electron mode showing numerous spherical and other shaped particles in a diffuse matrix. Scale bar is 50 microns.

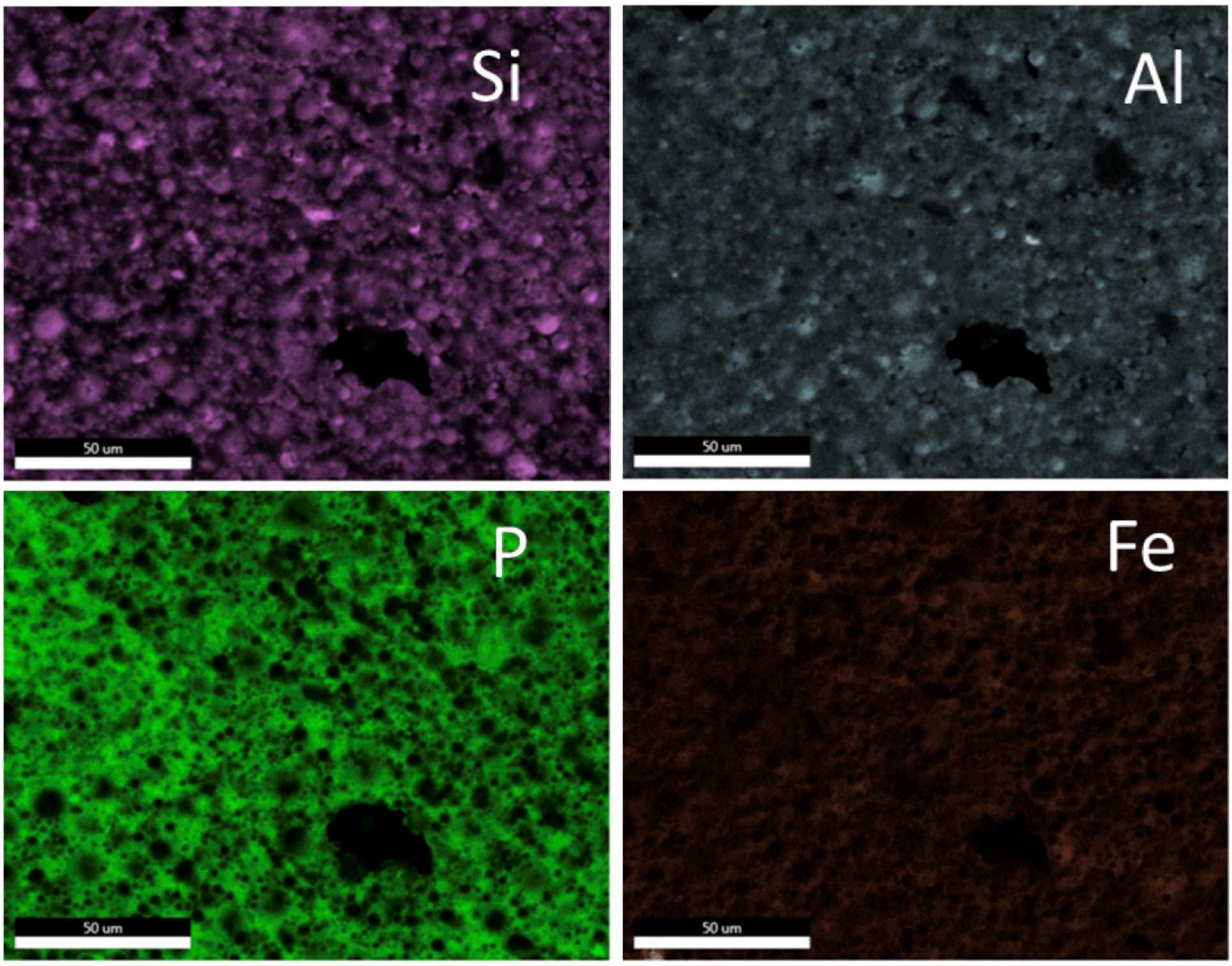

Figure 4-9. Element maps from the same location as Figure 4-8 showing the distribution of Si, Al, P and Fe.

Analyses by scanning electron microscopy (SEM) were performed to examine the morphology of 0223d-A as well as the distribution of elements in the material using energy dispersive analysis x-ray (EDAX) mapping. It is clear from the elemental mapping (Figure 4-9) that both Al and P are abundant and well distributed in the sample despite the absence of Al and/or P phases in the XRD pattern. The presence of significant quantities of the two elements suggest one or more Al and/or P phases are present in the sample but are likely poorly crystalline or amorphous.

The results of the 0223 experimental series are significant in that they reveal fly ash to be a non-contributor to the structural integrity of the cement in the hydrothermal process, and an important contributor in the ambient pressure process. Also noteworthy is the fact that fly ash and H_3PO_4 form a monolith without any special thermal treatment such as a slow ramp to final bake temperature.

0413 Series – Thermal Behavior of Refined Fly Ash Compositions at Ambient Pressure

A second series of samples (0413) was made to further investigate possible fly ash-based compositions where the ratio of fly ash to alumina by weight exceeds unity (Table 4-2). In this series, fly ash and alumina were reacted with H_3PO_4 in the weight ratios of 100% fly ash, 9:1 fly ash: Al_2O_3, and 3:1 fly ash: Al_2O_3. In order to observe the stability of these slurries over time, they were allowed to sit for 16 hours at room temperature prior to heating. After this sit time the samples had all set up into soft solids indicating that the

fly ash-based materials begin to react at room temperature. This observation then led to a decision to ramp the processing temperature in stages to better understand the structural evolution with temperature. Thus, the soft solid samples were then ramped from 80 to 130 °C at 1 °C/hr, sampled, ramped again from 130 to 150 °C at 1 °C/hr, then annealed at 200 °C. Samples were acquired from the monoliths for XRD characterization at 130, 150, and 200 °C.

Table 4-2. Samples with high fly ash loadings.

Sample No.	Al_2O_3 (g)	Fly ash (g)	H_3PO_4 (g)	H_2O (g)
0413a	-	100.0	23.0	19.0
0413b	10.0	90.0	23.0	17.0
0413c	20.0	60.0	18.4	14.0

All of the slurries formed well consolidated monoliths with minor and isolated pores as exhibited by Sample No. 0413a (Figure 4-10). Of significant note was the presence of two unusual phases as indicated by XRD (in addition to quartz and mullite) in Sample No. 0413a after it was cured at 130 °C but before it was annealed at 200 °C. The first matches the standard for hydrogen calcium phosphate hydrate ($H_4Ca(PO_4)_2 \bullet H_20$) and the second matches the standard for a triclinic $AlPO_4$ phase with a distorted tridymite structure (Figure 4-10). After the 200 °C anneal, 0413a was sampled again for XRD analyses which revealed that only the quartz and mullite peaks remained (Figure 4-11).

When considering the XRD data from both the 0223 series and the 0413 series and the formation of aluminum phosphate phases, it appears that triclinic $AlPO_4$ may be the favored binder phase at lower temperatures (130 °C), berlinite at intermediate temperatures (170 °C) and finally the appearance of an amorphous phase at higher temperatures (200 °C). The presence of an amorphous phosphate phase (or phases) at elevated temperatures in the absence of $AlPO_4$ – cristobalite is intriguing. Further research is required to understand phosphate phase evolution and the nature of the amprphous phase(s) that appear to be forming at higher temperatures.

Figure 4-10. Photograph of Sample No. 0413a (after mechanical testing). Sub-millimeter pores can be observed appearing as very dark specks.

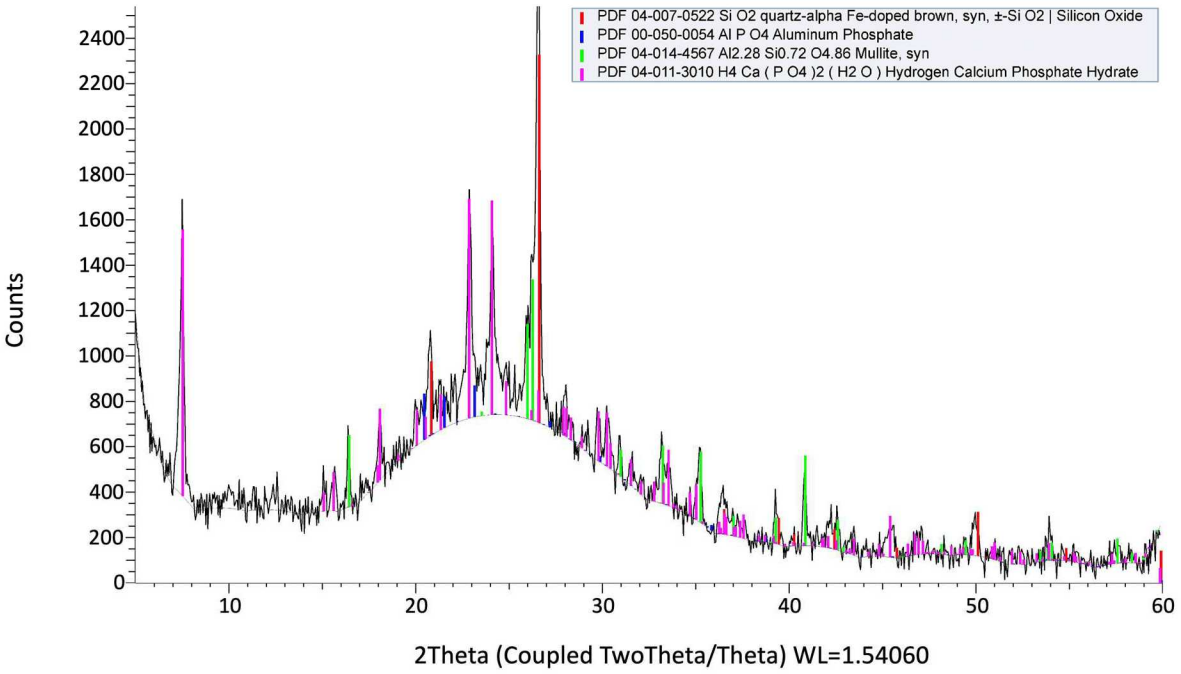

Figure 4-11. XRD pattern of Sample No. 0413a. Four crystalline phases have been identified including quartz, mullite, hydrogen calcium phosphate hydrate ($H_4Ca(PO_4)_2\ H_2O$) and a triclinic $AlPO_4$ phase.

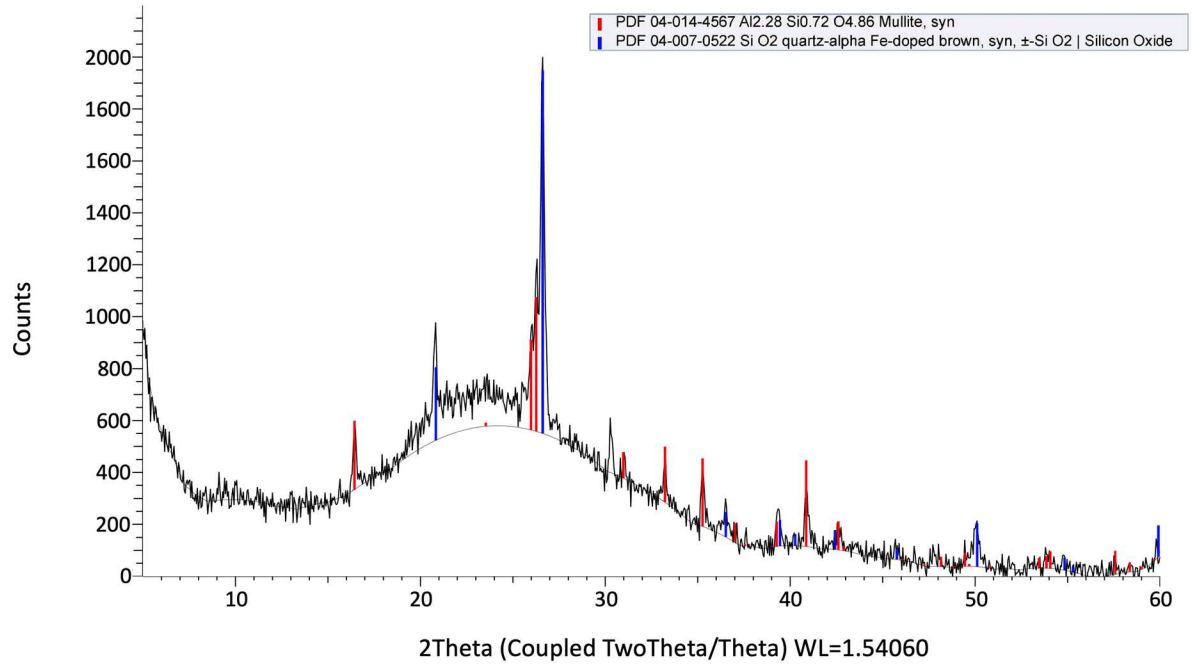

Figure 4-12. XRD pattern for Sample 0413a annealed at 200 °C showing only the presence of quartz and mullite.

These results suggest that the samples containing both Al_2O_3 and fly ash in the 0223 series (described above) may have produced monoliths had they been ramped to temperature rather than simply baked at 170 °C. This is highly significant in that it suggests that fly ash is acting as a reactive binder that maintains structural integrity of the cement as it cures and does so by hardening before the Al_2O_3 / H_3PO_4 reaction starts.

0823 Series – Effects of Boric Acid on Fly Ash Phosphate Formation

Samples were also made of fly ash with and without boric acid. Both of these resulted in fairly strong monoliths (Figure 4-13). Two samples were made for potential mechanical, thermal and water resistance testing as shown in Table 4-3.

Table 4-3. Fly Ash samples for mechanical, thermal and water resistance testing.

Sample No.	Fly ash (g)	H_3BO_3 (g)	H_3PO_4 (g)	H_2O (g)
0823h	200.0	-	46.0	40.0
0823hB	200.0	10.0	46.0	50.0

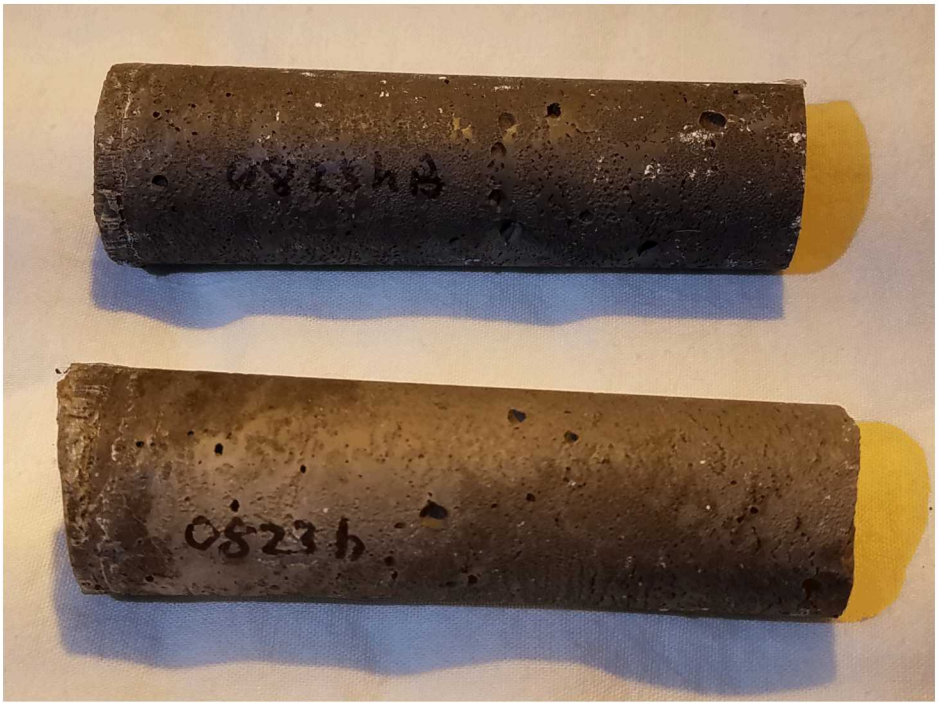

Figure 4-13. Photograph of Sample Nos. 0823h and 0823hB. Samples are 2.5 cm in diameter and 10 cm in length.

Both slurries were degassed and poured into 50 mL centrifuge tubes. These were placed in an oven and ramped from 82 to 130 °C at 2 °C/hr, then ramped to 150 °C at 20 °C/hr and held at 150 °C for 7 hr. The resulting monoliths (Figure 4-13) were mechanically robust but had significant pores on their sides, likely from air trapped during slurry pouring and therefore they were excluded from mechanical and thermal testing due to these surface irregularities.

XRD data indicate the presence of mullite, quartz and an unexpected SiO_2 zeolite phase (Figure 4-14). TGA data were collected from Sample No. 0823h (Figure 4-15). Approximately half of the weight loss happens before 150 °C is reached, suggesting that the sample had absorbed water from the air after synthesis. The remaining weight loss from 130 to 800 °C is more likely to represent residual volatiles that are relevant to the use case as a DPC filler.

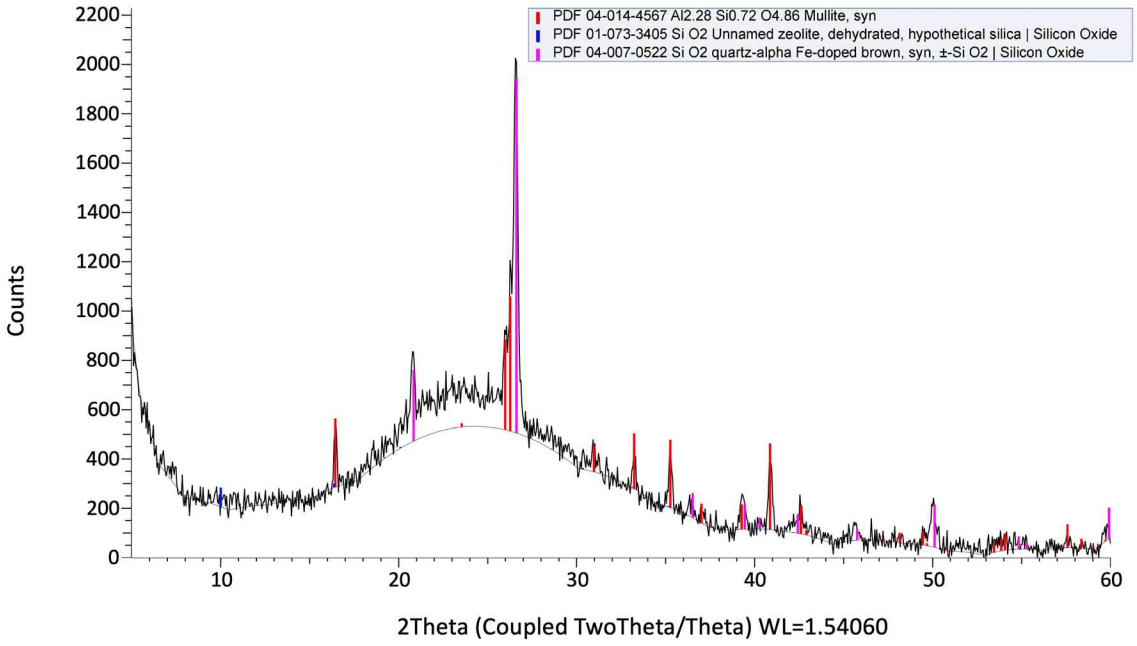

Figure 4-14. XRD pattern for Sample No. 0823h.

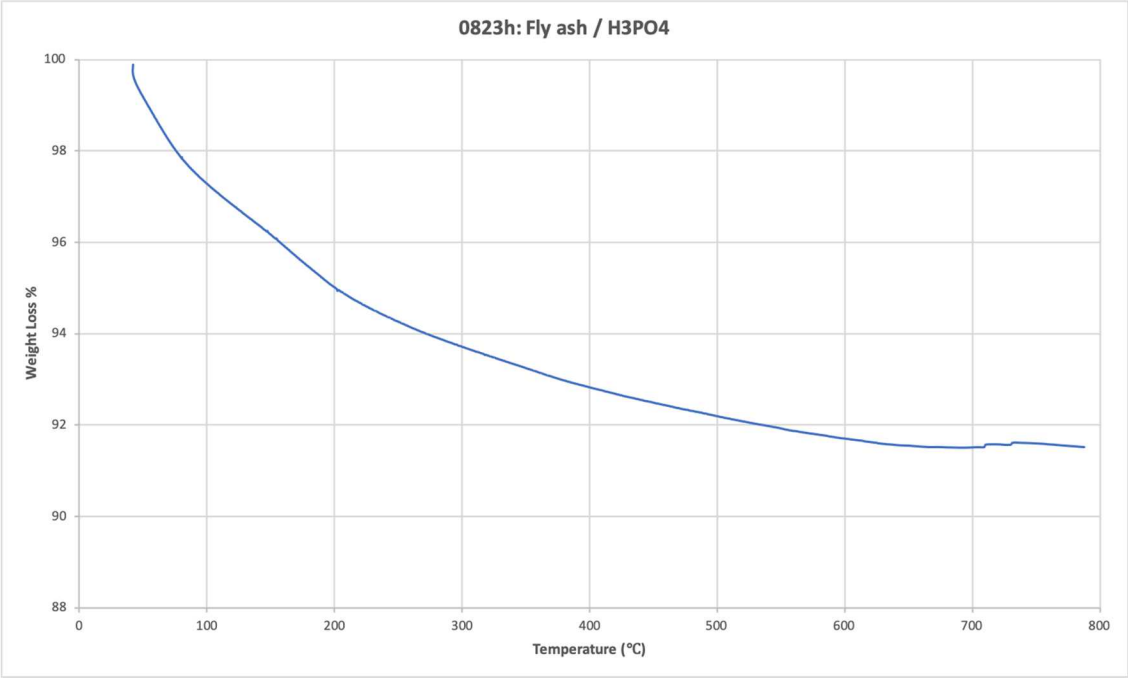

Figure 4-15. TGA data for Sample No. 0823h.

4.3 Viscosity Measurements on Fly Ash Fillers

The change in viscosity of fly ash filler slurries is rapid resulting in very short working time and becoming demonstrably thicker on the order of a few minutes. One half hour after mixing the slurry has begun to set and accurate measurements of viscosity are not possible. Note the indentation from the viscometer spindle in the slurry after an attempt to measure viscosity 30 minutes after mixing indicating the slurry is well on its way to setting at room temperature (Figure 4-16).

Figure 4-16. Photograph of Fly Ash Phosphate Slurry at t=30 minutes.

4.4 Mechanical Properties of Fly Ash Fillers

Given its overall appearance as a well-consolidated monolith, density, and lack of obvious voids or surface irregularities Sample No. 0413a was selected for basic mechanical and thermal properties testing (Figure 4-17).

The sample monolith required machining of the outer diameter, and length as reported in Table 4-4 below to create the right circular cylinders required for compressive strength testing. In addition, the ends were trimmed to retain enough material for thermal property measurements. The measured mechanical properties data including density, unconfined compressive strength (UCS), and Young's modulus is given in Table 4-4.

Table 4-4. Physical and Mechanical Property Data for Sample No. 0413a.

Sample ID	Dimension				Weight grams	Density	UCS	Young's Modulus	Poisson's ratio
	Diameter (in)	Diameter (cm)	Length (in)	Length (cm)		g/cc	psi	psi	
0413-A	0.9045	2.297	1.971	5.006	31.07	1.50	825	121809	n/a

Figure 4-17. Instrumented Sample No. 0413a. Left (pretest) and Right: posttest with fractures.

4.5 Water Resistance Testing

A representative set of fly ash samples were selected for water resistance testing. This process (described previously) involves sealing sample discs with DI water in individual pouches in PTFE sleeves and then heating them to 200 °C for 48 hr. After heating the reactor was cooled and the sleeves were recovered. Sample discs were weighed before and after testing except in cases where the sample disc had disintegrated. Also note that any sediment that fell off the disc during the test was considered lost weight. Finally, the pH of the water was also measured after the test was complete (Table 4-5).

Two more monoliths (0823h and 0823hB) were prepared by mixing 100 g fly ash, 23 g H_3PO_4, and 30 g H_2O (0823h), and 100 g fly ash, 23 g H_3PO_4, 10 g H_3BO_3, and 40 g H_2O (0823hB). These were heated under the same conditions as the previous monolith, however, just the ends were cut off and annealed at 250 °C for 16 hr.

Table 4-5. Results of Water Resistance Testing of Fly Ash Phosphates.

Sample No.	Starting wt. (g)	pH after test	Wt. after test (g)	Pct. wt. loss
0617a 250 C	5.29	5.67	4.99	5.7%
0823h 250 °C	8.43	3	8.20	2.7%
0823hB 250 °C	8.21	3	8.00	2.6%

The low pH (3) of the water of these fly ash phosphate samples tested likely indicates the presence of unreacted H_3PO_4. There wasn't much sediment lost from the samples so the lost weight may be soluble components, such as alkali metal phosphates. This will be evaluated in FY20 by inductively coupled plasma mass spectrometry (ICP-MS) and ion chromatography (IC). In addition, higher temperature ranges and longer anneal times would have to be tested to establish meaningful trends.

4.6 Summary

The observation that fly ash and H_3PO_4 form hard and pore-free monoliths led us to perform a small set of screening experiments to assess fly ash phosphates as a potential candidates for filling DPCs. The evaluations completed to date reveal it is possible to produce well-consolidated fly ash phosphate fillers at the bench top scale. These materials can also exhibit acceptable compressive strengths for the use case.

However, very rapid set times are problematic. Further, the low pH observed for all samples after the water resistance test is counter to the use case. Finally, the thermochemistry of the system, specifically the evolution of unexpected phosphate phases (hydrogen calcium phosphate hydrate and triclinic $AlPO_4$) and their subsequent conversion to amorphous phosphate phases as a function of temperature is complicated; likely the most complicated of all the systems examined in this report. Continued study of the fly ash phosphate system for DPC filler applications is not recommended at this time.

This page is intentionally left blank.

5. CALCIUM PHOSPHATE (CPC) FILLERS ($Ca_5(PO_4)_3(OH)$)

5.1 CPC $Ca_5(PO_4)_3(OH)$ Overview

Calcium phosphate cement or CPC, commonly known as hydroxyapatite, has the chemical formula $Ca_5(PO4)_3(OH)$. Hydroxyapatite minerals (natural analogs) are very are stable in sedimentary rock formations. Additional natural analog support for the use of CPCs comes from buried vertebrate bones and teeth that are made of hydroxyapatite and can remain intact for thousands of years. Hydroxyapatites have the added benefit in that they are a very effective sorbent for a variety of radionuclides including uranium, other actinides, strontium, and radium (e.g. Moore and Rigali 2015; Rigali et al. 2016). Hydroxyapatites have demonstrated high-temperature stability as components of sealants for geothermal wells (Sugama 2006).

CPCs specifically hydroxyapatite are widely studied and used as a biocompatible bone repair cements (Achelhi et al., 2010; Bohner, Gbureck, & Barralet, 2005; Habraken, Habibovic, Epple, & Bohner, 2016; Krogstad, Wang, & Lin-Gibson, 2017; Owuor et al., 2018), as media for drug or gene delivery medium (Habraken et al., 2016; Zeng et al., 2009), and as filters for water purification filter. While these disparate applications have a variety of system-specific requirements, common themes do exist. Specifically, control over the composition, nucleation, growth rate, and system compatibility are achieved by modifying a relatively consistent set of parameters among these diverse fields. The composition is controlled by using specific ratios of calcium to potassium, ideally as close to a Ca/P stoichiometric ratio of 1.67 as possible.

While there are well-established routes to prepare CPC primarily based on its use for clinical applications these synthesis routes typically have the disadvantage of fast set times and because the starting materials are produced in small industrial volumes there is the added disadvantage of relatively high cost.

5.2 CPC Composition Space Studied

CPC synthesis work was initiated using a well-established method of producing CPC from the medical literature with tetracalcium phosphate or TTCP ($Ca_4(PO_4)_2O$) and dibasic calcium phosphate or DCPA ($CaHPO_4$) powders mixed in water with a 73:27 weight ratio to assure a Ca/P stoichiometric ratio of 1.67 which is typical of hydroxyapatite (EQ 2). Our efforts focused on developing synthesis routes based on these well-established clinical applications and then optimizing these formulations for increased set times and robust chemical and mechanical properties.

$$Ca\square(PO\square)\square O + CaHPO_4 \rightarrow Ca\square(PO\square)\square(OH) \text{ (EQ 2)}$$

To address the relatively high cost of TTCP and DCPA from sources used by medical and dental practices, we also explored the production of CPCs by reacting inexpensive and commonly available salts of calcium including calcium carbonate, ($CaCO_3$) calcium nitrate ($Ca(NO_3)_2$) and calcium hypochlorite ($Ca(OCl)_2$), with phosphate salts in water and with the presence of a metal chelator to control set times.

5.3 CPC Fabrication Process

Mixing TTCP and DCPA in water produces a thick paste which subsequently approaches solidification in approximately 25 minutes (Figure 5-1). However, this relatively rapid cure time is considered too fast for use as a DPC filler where a minimum set time of at least two hours is desired in order to assure there is sufficient time to complete the filling process for a full-scale DPC. Increased set times are possible through the addition of calcium chelators that inhibit the rapid reaction of calcium with phosphate to form CPCs.

After setting was complete, x-ray diffraction analysis of the resulting CPC revealed that it was composed of hydroxyapatite (Figure 5-2). In addition. peaks at approximately 30° 2θ, corresponding to unreacted TTCP, were also be seen in the pattern.

The rapid thickening of the CPC paste, which begins just a few minutes after mixing the reactants in water is an undesirable characteristic when considering process scale-up and the filling of a DPCs. However thickening rate and set time can be increased through the use of modifying additives as described below.

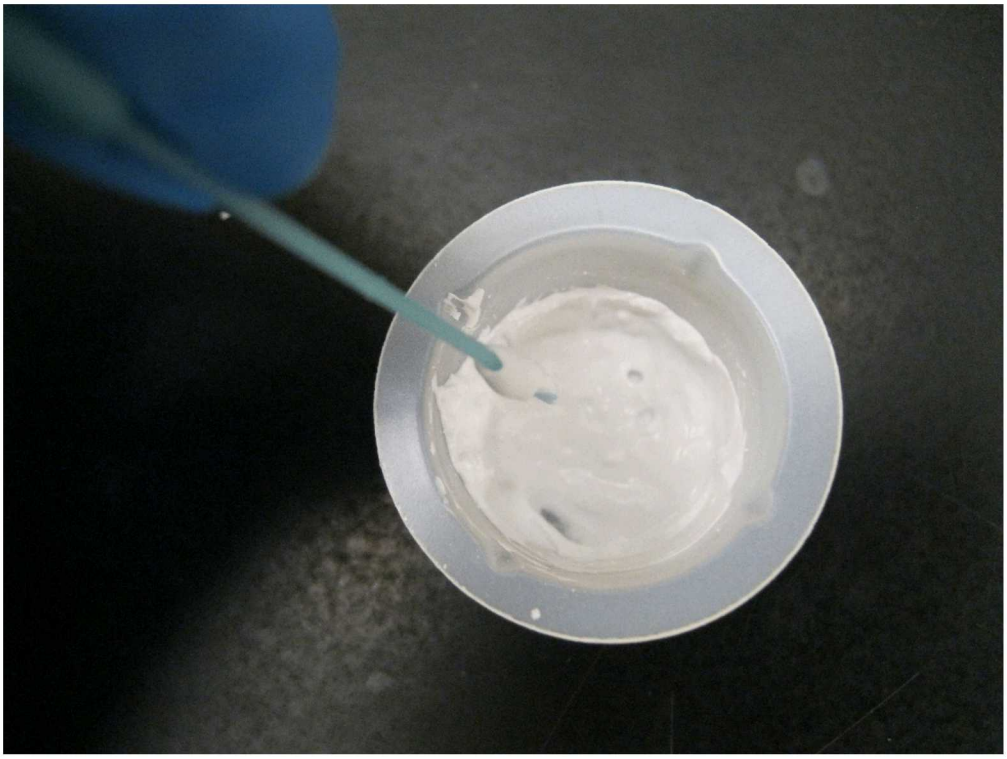

Figure 5-1. CPC synthesized from TTCP and DCPA in a 25 ml beaker. After 25 minutes the cement is effectively set.

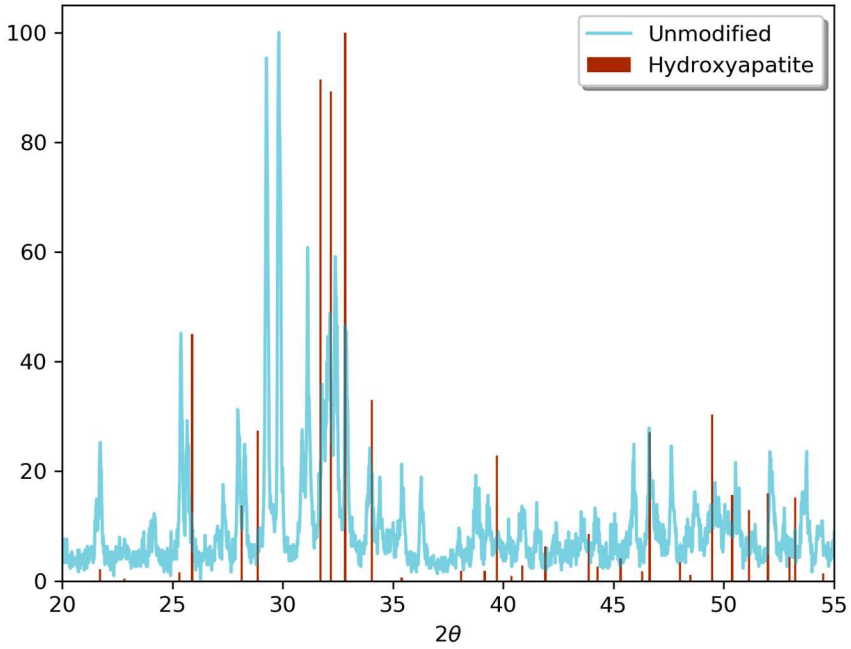

Figure 5-2. XRD pattern of the TTCP/DCPA based CPC cement (blue). The red lines indicate the position of characteristic peaks for hydroxyapatite. The unidentified blue peaks such as those observed at ~30° 2θ correspond to unreacted TTCP.

5.4 CPC Additives Examined

A variety of potential chelating agents were examined in order to improve the TTCP/DCPA based CPC cement workability and setting time. In some cases, the natural setting time of CPC is too fast even for biomedical use (Santa Cruz Chavez, Alge, & Chu, 2011). In these cases, organic or mineral acids, including citric acid, have been used to increase setting time.to evaluate their effects such as citric acid (Santa Cruz Chavez et al., 2011; J. Zhang, Liu, Schnitzler, Tancret, & Bouler, 2014).

5.4.1 CPCs with Carboxylic Acid Modifiers

Several carboxylic acids including malonic acid and citric acid were studied to increase CPC setting time. Formic acid, the smallest possible carboxylic acid, was intentionally excluded from this study as an impractical candidate. While it is a low molecular weight organic acid, and only possesses two hydrogen atoms per formula unit, it is highly volatile (44 mmHg at 20 °C), flammable, and toxic. Other small molecules, such as oxalic acid, were not included due to practical concerns. Oxalic acid is so short, it can only function as a bridging, rather than chelating, molecule. Malonic acid, with a single methyl group between two carboxylic acid groups, has more potential flexibility and was selected as the smallest bifunctional acid additive. Citric acid was also investigated, as it is a very common modifier in cement chemistry (Santa Cruz Chavez et al., 2011; J. Zhang et al., 2014).

Exploratory efforts used a 2.5 g samples of dental cement (physical mixture of 72 wt.% TTCP and 27 wt.% DCPA) were mixed with aliquots of water to find the optimal slurry point. Replicate mixtures using up to 4 wt.% citric acid were prepared, with the 4 wt.% citric acid sample resulting in a noticeably less viscous consistency. When demolded, samples prepared with citric acid were less dense, and tended to crumble. An excessive amount of citric acid was likely responsible for retarding the cure rate beyond a usable point.

A subsequent trial limiting acid content to 1 wt.% was conducted with malonic and citric acids. The citric acid samples required more than five days to solidify (solid remained damp), while the malonic acid samples were fully dry after resting at room temperature for the same period (Figure 5-3). A scale-up reaction was conducted on a 20 g scale of dental cement powder to better observe the macroscopic behavior of the slurry. Within 50 minutes of mixing the powder with 1 wt.% malonic acid solution, the solid had set to a soft, non-flowable state (Figure 5-4). Bifunctional carboxylic acids, rather than citric acid, showed promise for further exploration.

Figure 5-3. Dental cement samples prepared using bifunctional or trifunctional carboxylic acid as a moderator. From left to right, samples are 1% malonic acid, 1% citric acid, 0.5% citric acid and 0.5% malonic acid.

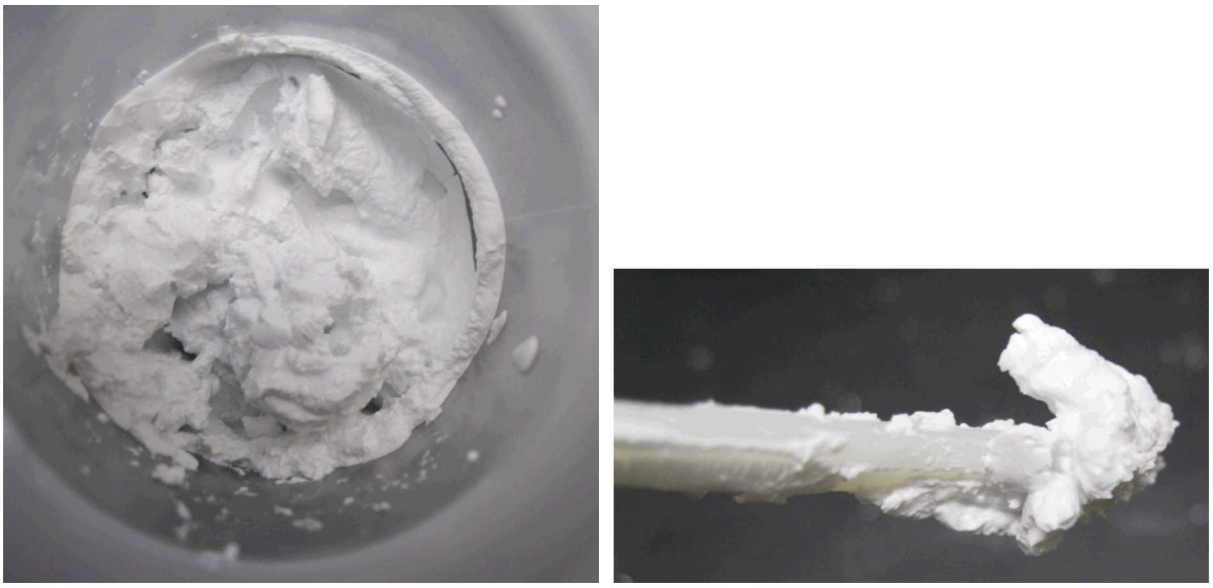

Figure 5-4. Images of 1% malonic acid CPC slurry while still damp.

5.4.2 CPCs with Dicarboxylic Acid Modifiers

A series of bifunctional carboxylic acids (Figure 5-5) was investigated by (Achelhi et al., 2010) as modifiers to hydroxyapatite-based bone cements. The authors reported a potential for calcium oxalate to precipitate, as oxalic acid had the lowest degree of bidentate behavior. Conversely, adipic acid was found to remain

much more integrated into the resulting cement than other acids. The authors postulated that this could be the result of conformational changes in solution allowing for a greater packing density of the crystallite and chelated acid. Further elaboration on this point has not been published thus far. Chain length effects have also been studied by (Zeng et al., 2009), where the adipic acid provided more needle-like hydroxyapatite crystals than acetic acid -based growth medium. Any differences between monofunctional and bifunctional carboxylic groups were not discussed by the authors.

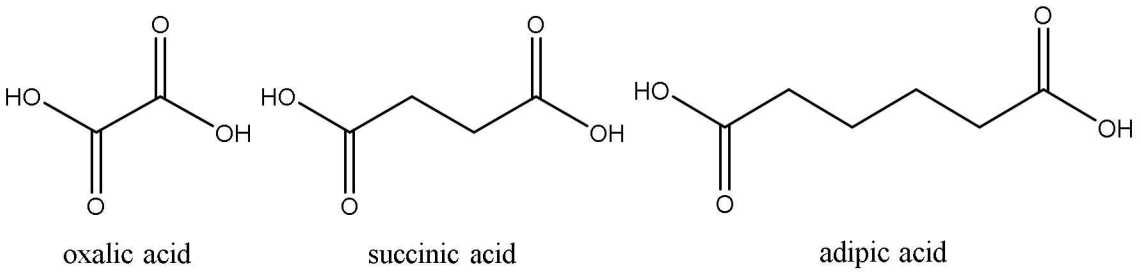

Figure 5-5. Bifunctional carboxylic acids used as hydroxyapatite growth moderators by (Achelhi et al., 2010).

Notably, adipic acid is predicted to be slightly more soluble in octane than water, as it is the first dicarboxylic acid with a predicted positive log (P) value, as shown in **Error! Reference source not found.**-6. Longer chain dicarboxylic acids have recently garnered interest (Tang, Wang, & Wang, 2015) as novel surfactant modifier. The dicarboxylic acid formed an electrostatic interaction with a cationic surfactant in alkaline solution, effectively bridging the surfactant molecules over a larger area, relative to the pure surfactant. Bifunctional surfactants such as these are termed bolaform or bola surfactants and been investigated for a variety of applications. Some notable ones include redox-active selenium-based surfactants for controlled drug delivery (Chen et al., 2019), pH-controllable viscoelastic fluids (Y. Zhang, Kong, An, He, & Liu, 2016), and supramolecular self-assembly (Li et al., 2016). A common theme among these applications is the greater degree of control over rheological properties without the need for labor-intensive specialty surfactant synthesis. A long chain (α,ω)-dicarboxylic acid is appealing as a dual-purpose rheology modifier and calcium chelating additive. Using a single organic compound to accomplish both purposes would reduce the total organic load in the final cement. Dodecanedioic acid (Figure 5-8, DDDA) was selected, as carbon lengths of 12-14 atoms are typically used in surfactant applications (Nardello, Chailloux, Joly, & Aubry, 2006). One significant challenge to this approach was the poor solubility of dodecanedioic acid. Prior reports (Tang et al., 2015) used a strongly alkaline (pH 11) solution to produce the corresponding sodium salt. In order to achieve a less alkaline solution, phosphate buffer solutions were used to dissolve the DDDA.

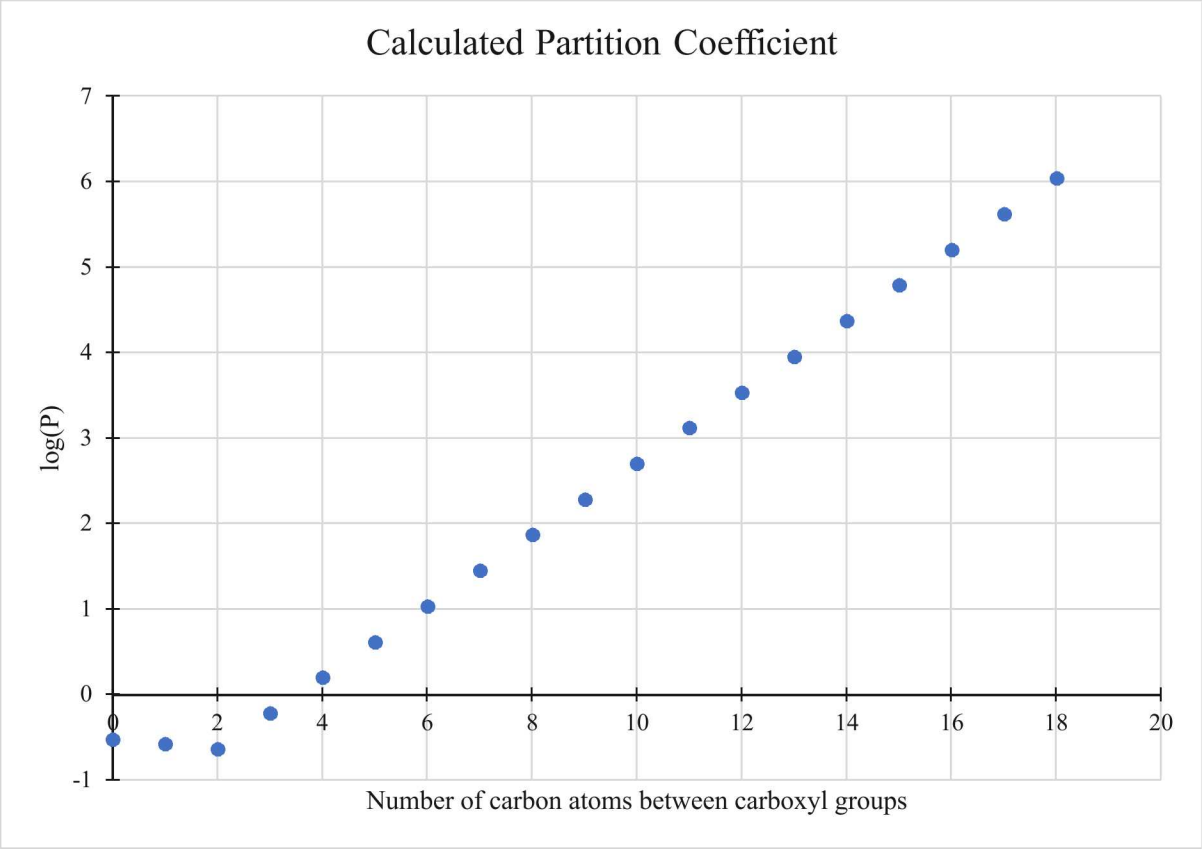

Figure 5-6. Adipic acid (4 carbons between carboxyl groups) is marginally more soluble in octane than water. Increasing chain length dicarboxylic acids are less soluble.

The solubility of DDDA was systematically evaluated in K_3PO_4 and K_2HPO_4 solutions by serial dilution. A ~1 g (4.45 mmol) sample of DDDA was dissolved by adding 1 mL aliquots of a 1 M K_3PO_4 solution until no solids remained. Replicate trials were conducted with serial dilutions of K_3PO_4 solution (0.75 M, 0.5 M) until a minimum solubility molar ratio of 3.5:1 K_3PO_4:DDDA was found. Dibasic and monobasic potassium phosphate solutions were not suitable solvents, as no practical solubility point could be found (Figure 5-7). Further development focused exclusively on tribasic potassium phosphate as a solvent/buffer.

Figure 5-7. Solubility tests (left to right) of 1 mmol DDDA in 1 M K_2HPO_4, 2.5 M K_2HPO_4 and 5 M K_2HPO_4.

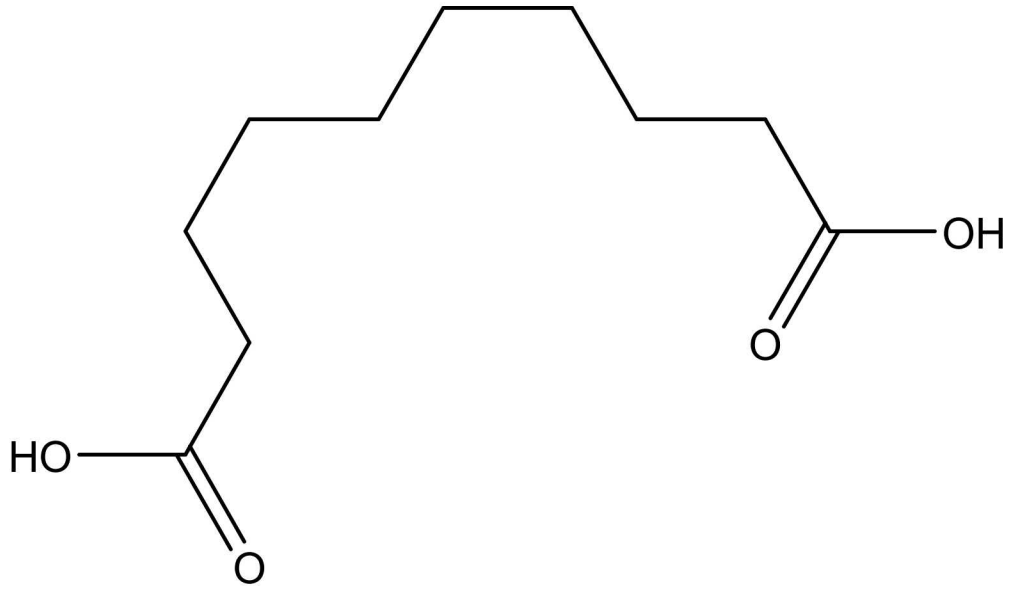

Figure 5-8. Dodecanedioic acid in a bolaform orientation showing both carboxylic acid groups forming a U-shaped surfactant-like shape.

5.4.3 CPCs with DDDA and Phosphate Buffers

A phosphate salt solution was postulated as a mixing aid for the DDDA modifier, with the added potential benefit of shifting equilibrium to favor apatite formation. Stock TTCP was mixed with plain water, and an equivalent volume of 1 M K_3PO_4 solution. The sample prepared in phosphate solution was more easily

wetted due to pronounced wicking behavior. Upon drying, samples exhibited similar consistency. Further efforts to retard solid formation by dispersing the commercial powder in levulinic acid prior to adding 1 M K_3PO_4 were unsuccessful. The reaction was exothermic and rapidly generated a curd-like aggregate. Aliquots extracted from each slurry are shown in Figure 5-9. Mixed salt solutions of equimolar ratios of mono-, di- and tribasic potassium phosphate, and phosphoric acid were also investigated. A trade-off to this approach is the accumulation of phosphate salts in the cured cement. Excessive salt formation may have led to brittle, non-cohesive powders (**Error! Reference source not found.**).

Figure 5-9. Dried aliquots of (left) tetracalcium phosphate in water, (center) tetracalcium phosphate in 1 M K_3PO_4, and (right) tetracalcium phosphate in levulinic acid mixed with 1 M K_3PO_4.

The favorable wetting behavior offered by the potassium phosphate was not sufficient to maintain a flowable slurry with an acceptable cure time. Adding DDDA as a surfactant and growth modifier was necessary to improve slurry flowability and setup time.

For several reasons, minimizing the amount of surfactant used was desirable. First, as a hydrocarbon, DDDA may be subject to radiolytic degradation and subsequent gas generation in a DPC. Secondly, excessive amounts of carboxylic acid, specifically citric acid, were found to be detrimental to the mechanical performance of the CPC. Optimization of the carboxylic acid functional groups (to moderate CPC set time), hydrocarbon chain (to modify slurry rheology) and phosphate solution (to dissolve DDDA and buffer phosphate ion concentration) was approached systematically. The minimum amount of DDDA needed for a given mass of CPC powder was investigated at a constant concentration of 1 M K_3PO_4. The optimized DDDA solubility ratio of 4:1 in 1 M K_3PO_4 was selected as an initial point and compared to an order of magnitude reduction in DDDA. Both samples exhibited a greater percentage of hydroxyapatite relative to starting material based on XRD analyses (Figure 5-10), although the unmodified sample was noticeably more crystalline. The extent of surface modification by residual DDDA was investigated using FTIR spectroscopy (Figure 5-11). Each sample produced from DDDA/phosphate solution exhibited a hydroxyl peak, likely indicating water retention at the surface. Small features in the ~1600 and ~3000 cm^{-1} range corresponding to commercial DDDA were noted.

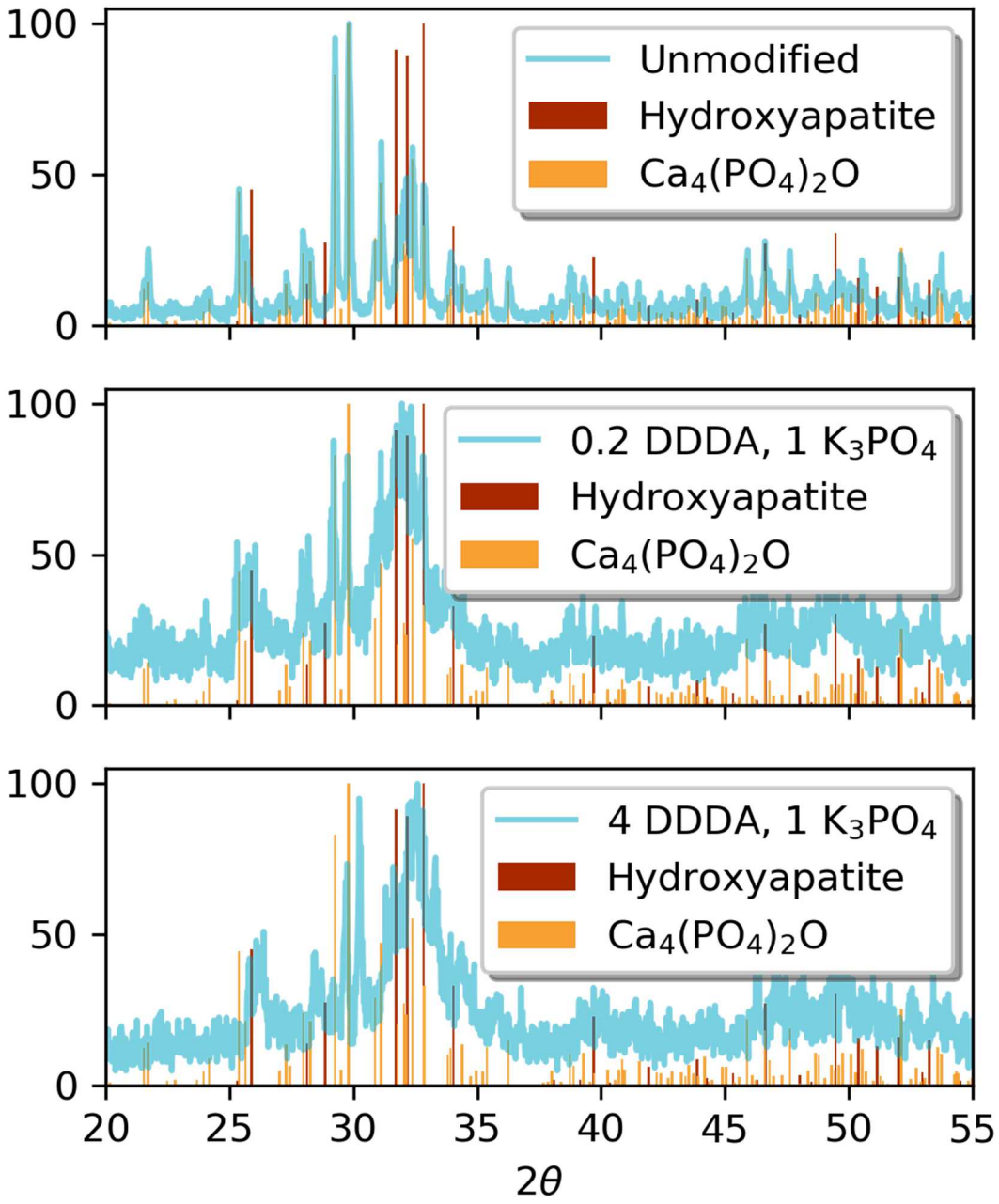

Figure 5-10. XRD patterns comparing DDDA modification at varying concentrations.

The relative efficacy of the surfactant and phosphate solution was evaluated by synthesizing a series of CPC monoliths with varying concentration of potassium phosphate and use of DDDA surfactant. A stock solution of 2 M K_3PO_4 was prepared, and diluted to yield a 1 M solution, with or without 3.5 equivalents of DDDA. Four total solutions were thus prepared: high/low concentration phosphate with/without surfactant. The monoliths were prepared by mixing each solution in a 0.15:1 or 0.15:2 ratio of DDDA to K_3PO_4 and allowed to rest over night at ambient conditions. Each monolith appeared robust when demolded. Analysis of chipped material indicated a mixture of phases, hydroxyapatite and TTCP starting material (Figure 5-13). As described in Section 3 above, hydrothermal stability tests were conducted using

the produced samples. Each of the samples (with and without DDDA) produced from 1 M K_3PO_4 solution largely survived with some dissolution channels evident, while the samples produced from 2 M K_3PO_4 crumbled (Figure 5-14).

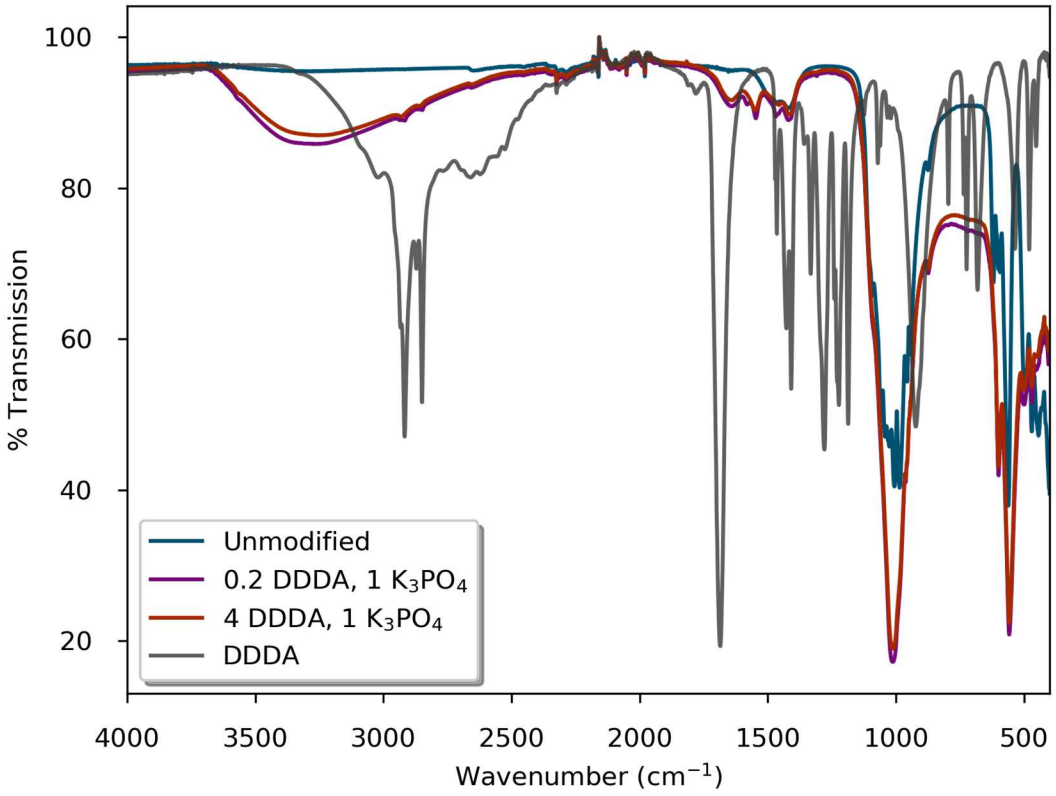

Figure 5-11. FTIR comparison of DDDA-modified CPC samples with unmodified CPC and commercial DDDA. Modified CPC materials show a much greater water (hydroxyl) peak.

Figure 5-12. CPC sample prepared using buffered phosphate (equimolar ratios of K_3PO_4, K_2HPO_4, KH_2PO_4, and H_3PO_4) solution. A stir rod left in the slurry was easily removed and resulted in a fracture across the entire piece, likely due to excessive salt content.

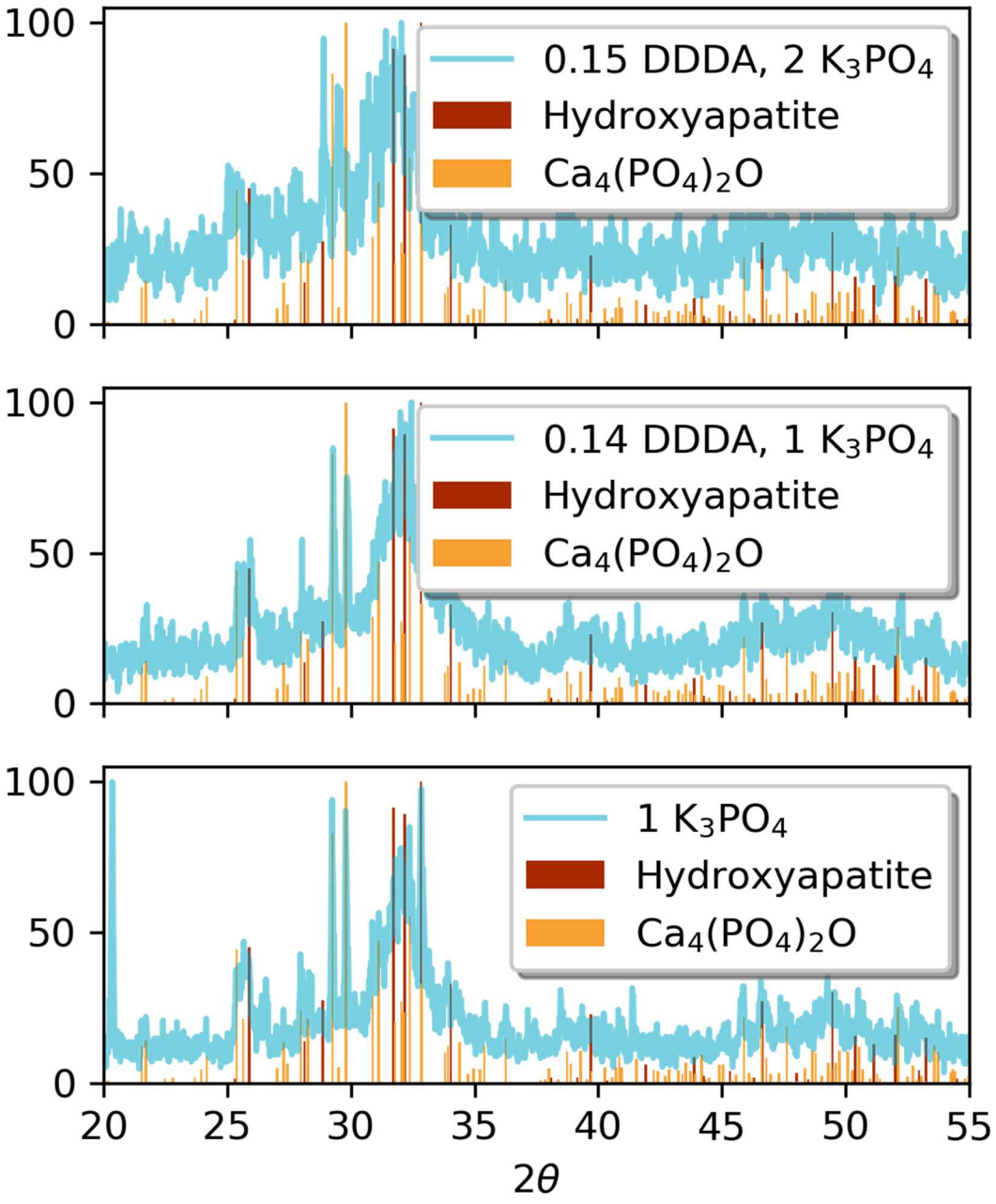

Figure 5-13. XRD patterns of CPC prepared from high (2M) and low (1 M) K_3PO_4 solution with (top) or without (bottom) DDDA surfactant.

Figure 5-14. Sample monoliths after the hydrothermal stability test. Low (1M) concentration K_3PO_4 solution-derived samples survived (right), while high concentration (2 M) derived samples did not (left).

5.4.4 CPCs from Calcium Salts

The production of CPCs by reacting inexpensive and commonly available salts of calcium including calcium carbonate, ($CaCO_3$) calcium nitrate ($Ca(NO_3)_2$) and calcium hypochlorite ($Ca(OCl)_2$) with phosphate salts in water was also explored. Similar to the investigations with TTCP and DCPA described above, it was expected that the rapid formation time of CPC using calcium salts would require the use of a metal chelator as a modifier to control set times. Ascorbic acid was investigated as a chelating, triprotic acid and reducing agent. While not a carboxylic acid, the molecule adopts a chelation geometry that has been widely used for metal chelation (Martell, 1982). A direct synthesis of calcium ascorbate from $CaCO_3$ was attempted, as shown in Figure 5-15. Complete dissolution of the salt was not achieved, as can be noted from the residue in the upper left image. The mixture formed a gel, and a coarse aggregate formed when phosphoric acid was added. A stoichiometric ratio (5 g (0.05 mol) $CaCO_3$ and 17.8 g (0.1 mol) ascorbic acid) was co-dissolved in 25 mL DI H_2O. Despite an effervescent, endothermic reaction, the calcium salt was not fully dissolved. Additional 0.1 g (5.7 mmol) aliquots of ascorbic acid were added while heating on a hotplate until a clear, colorless solution was achieved. The final molar ratio of calcium to ascorbic acid was 1:2.06. An aliquot of the solution (8.3 g) was added to 1 mL 85% H_3PO_4 and stirred to form a cloudy, semifluid gel.

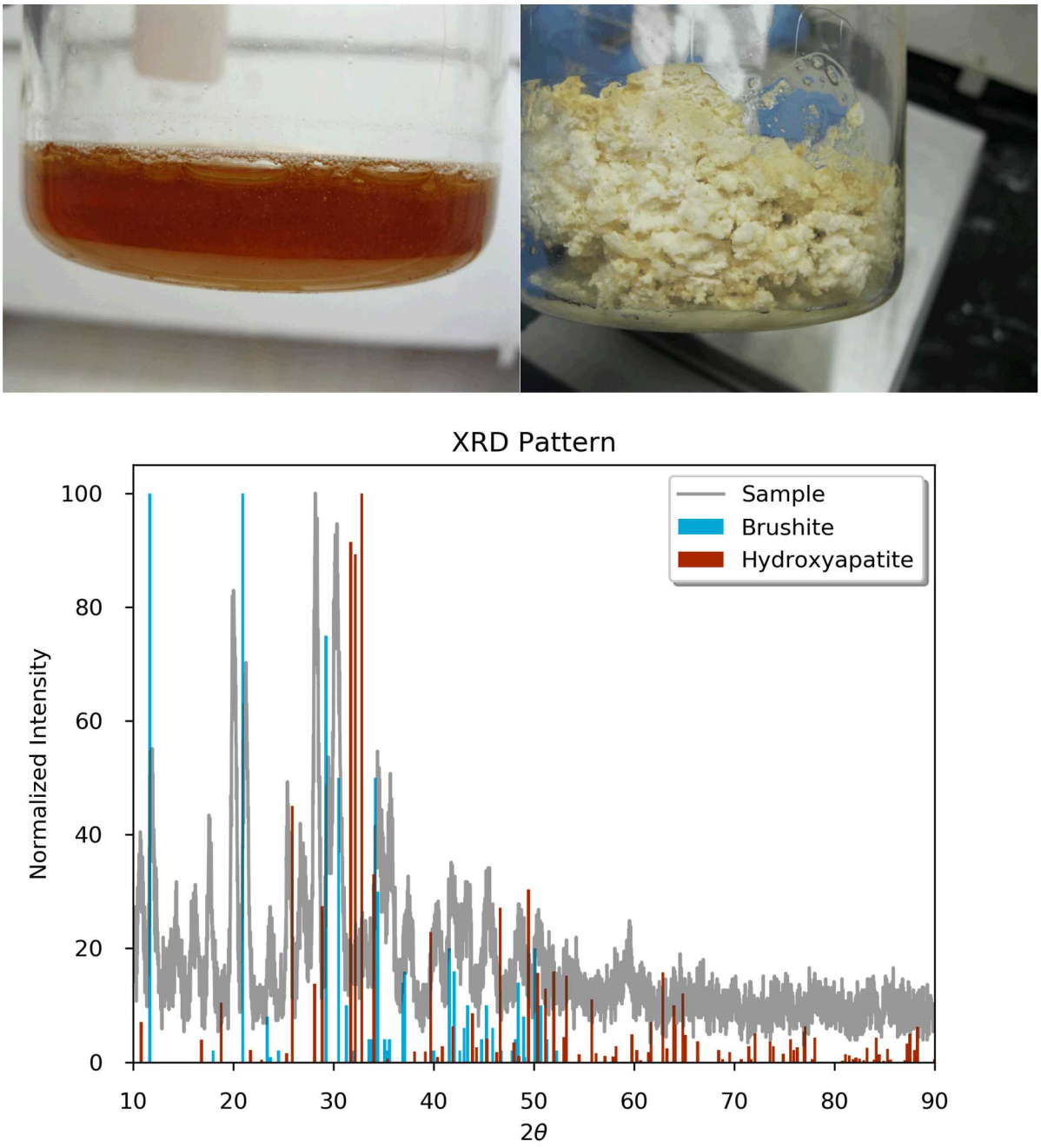

Figure 5-15. Calcium ascorbate gelled precursor (upper left) and product calcium phosphate (upper right). XRD analysis (lower) revealed a poor match to hydroxyapatite.

As an antioxidant, ascorbic acid offers additional processing and post-processing options over citric acid including the fact that ascorbic acid could be used to reduce inexpensive oxidizing calcium salts such as calcium nitrate ($Ca(NO_3)_2$) or calcium hypochlorite ($Ca(OCl)_2$). Without a reducing agent, the corrosivity of these salts would likely be incompatible with long term storage canisters. Aqueous $Ca(NO_3)_2$ (10 mL 0.26 M) was mixed with 2 equivalents of ascorbic acid solution (10 mL 0.5 M) to yield a clear, colorless buffer. Addition of 1.556 mL 1.0035 M K_3PO_4 solution resulted in a short-lived precipitate. The calcium hypochlorite salt was substantially less soluble; an initial effort to dissolve at a 1 molal ratio was

unsuccessful. Additional aliquots of water were added until a total of 80 mL had been reached. The solution remained slightly cloudy but cleared instantly upon the addition of 10 mL 1 molal ascorbic acid solution. Mixing was mildly exothermic, but fine solids precipitated within an hour of resting. While conceptually intriguing, this route was deemed to be impractical due to the unfavorable solubility of the precursors.

5.5 Summary

Dental cement shows promise for use as a filler material and work thus far has identified a plausible composition space for further investigation. Concentrations of DDDA at or near the solubility limit, relative to phosphate salt concentration, produce robust monoliths at a benchtop scale (Figure 5-16). Additional quantification of the reduction in viscosity, increased set time, and extent of residual salt/organic content in the monolith is necessary. Viscosity measurements on the slurry during the pre-cure window have been challenging thus far. Refinement of this technique is underway and will provide insight into the scale-up to filling a container, as well as changes in cure rate as a function of time. Finally, results of the hydrothermal testing indicate that resistance to aqueous dissolution must improve significantly in order for the CPCs using DDDA as a modifier to be considered as potential DPC filler materials.

Figure 5-16. Demolded monolith showing features from mixing beaker.

This page is intentionally left blank.

6. MAGNESIUM POTASSIUM PHOSPHATE FILLERS ($MgKPO_4$)

6.1 MKP ($MgKPO_4$) Cement Overview

Magnesium potassium phosphate (MKP) cements with the general chemical formula ($MgKPO_4$) are high strength materials that are used in a number of construction applications including road repair. They are resistant to temperature swings, road salt, and maintain bond strength better than other construction materials (Wagh, 2016). They tend to cure more slowly than other chemically bonded cement types and could therefore could potentially be used for the large monolithic pours required to fill a DPC.

6.2 MKP Cement Composition Space Studied

Preliminary research on this cement material was initiated using an MKP cement composed of magnesium oxide (MgO) and phosphate salts including monopotassium phosphate (KH_2PO_4) and tricalcium phosphate ($(Ca_3(PO_4)_2$). Sucrose is present as an additive to increase the cure time of the MKP cement. In addition, we examined the addition of boron carbide (B_4C) as a neutron absorbing phase.

The formulations examined below were based on typical industry compositions for MKP cements.

6.3 MKP Cement Fabrication Process

MKP cement consists of fine powders and as a result presents an inhalation hazard. In order to mitigate this hazard, powders were transferred into small resealable zipper storage bags within a fume hood. These storage bags were then transferred into a self-contained LABCONCO Precise® HEPA-filtered glove box where the cement slurries were pre-mixed with their associated liquids to eliminate the presence of dry powders. Once the powders and liquids were fully mixed there was no longer an inhalation hazard and the slurry could safely be transferred out of the glove box.

Once out of the glove box, the pre-mixed slurry was then taken to a kitchen-type planetary mixer for final mixing, which typically lasts 2 minutes when working with small batches (e.g., 114 cm^3 or 7in^3). After final mixing, the slurry was then poured into concrete form tubes with 2.54 cm in internal diameter and 10 cm in length (Figure 6-1), then placed on a vibrating table for a minute to release entrained air. The molds were then covered with sheet of aluminum foil and left to cure for a minimum of 24 hr. The samples were cured for approximately 1 month and then removed from the molds and placed in a storage container.

Figure 6-1. MKP cement being poured into standard molds.

6.4 MKP Cement Additives Examined

The MKP cement resulted in the formation of a dense, hard monolith (Figure 6-2). However, very fast set times were observed after adding water to the dry cement product, on the order of 5 to 10 minutes. After one month of curing, the samples were removed from the molds. A thin layer of cardboard mold material remained tightly bound to the cylindrical monoliths and had to be scraped from the surface.

Known for its neutron capture cross-section and stability to ionizing radiation and most chemicals, B_4C has the potential to be an additive in DPC filler materials. It could reduce the reactivity of DPCs that contain ground water to act as moderator (SNL, 2017). However, its affect on MKP cement curing and post-cure chemical and mechanical properties is unknown. A commercially available MKP cement with the addition of 9% B_4C was used for preliminary testing to assess the cure rate and post-cure properties.

Two batches of the MKP-B_4C cement were mixed with water at 16% and 19% by weight of cement powder. Both resulted in smooth, pourable slurries with the 16% by weight sample being notably more viscous. After filling the concrete form tubes, they were each allowed to set for approximately 1 month. The resulting cylindrical monoliths were removed from the cement molds, examined and photographed. The sample made with 19% water is shown on the right in Figure 6-2.

In a preliminary screening test all the cylindrical monoliths from the baseline MKP formulation and the MKP-B_4C mixes were subjected to immersion in distilled H_2O inside a 1000 ml Nalgene bottle for 24 hours, to assess their resistance to dissolution. All the samples were observed to disaggregate in water covering the bottom of the bottle over this short period of time (see Figure 6-3).

Figure 6-2. Fabricated baseline MKP cement core (left), and baseline MKP cement with boron carbide fabricated core (right). Samples are approximately 2.54 cm (1 in) in diameter and 10.16 cm (4 in) long.

Figure 6-3. MKP cement sample with boron carbide (H_2O added at 19% by weight of powder) after immersion in for 24 hours in distilled water.

6.5 Summary

While our preliminary evaluation of MKP cement demonstrated the mixing and setting of dense monoliths, their consistent disaggregation over a short period of time in water was found to be unsatisfactory for application as a DPC filler material. As work progresses on the filler project into FY20 we will attempt to develop a modified MKP mix with a better resistance to disaggregation and dissolution in H_2O.

7. WOLLASTONITE-ALUMINUM PHOSPHATE BASED FILLERS ($CaSiO_3$-$AlPO_4$)

7.1 Wollastonite Overview

A brief investigation into other ceramic mineral sources revealed wollastonite ($CaSiO_3$) based chemically bonded phosphate ceramics (Wo-CBPCs) as a possible DPC filler materials. Ratios of phosphoric acid to wollastonite between 1.0 and 1.2 can lead to a pH-neutral product. These properties have led Wo-CBPCs to be proposed for the encapsulation of nuclear waste (Colorado et al., 2011; 2015).

Wollastonite has a lower density (on the order of 3 g/cm^3, exact density depends on composition) relative to Al_2O_3 (3.95 g/cm^3) and grains with a higher aspect ratio, both of which suggest a possible lower settling rate and a concomitant increase in working time as compared to corundum-based materials. As mentioned above, wollastonite was previously investigated as a phosphate chemically bonded ceramic (Colorado et al. 2011) but this study examined the use of phosphoric acid rather than a phosphate salt. The latter was used in this work to avoid using a reagent that may cause corrosion of the DPC contents, also, a higher pH phosphate source is likely to have a longer working time than a source with a pH of about 1, such as concentrated H_3PO_4.

7.1.1 Composition Space Studied

Inspired by the work of Colorado et al. (2011) we recognized that it may be possible to directly substitute $CaSiO_3$ for Al_2O_3 to produce a wollastonite aluminum phosphate filler material with desirable properties for a DPC filler application. Applying what we learned in the APC research described in Section 3 we examined several experimental variations using $Al(OH)_3$ or metakaolin as Al sources and H_3PO_4 and ADP ($NH_4H_2PO_4$) as phosphate sources. A small number of experiments were performed to examine this composition space as described below.

7.2 Process Description

Sample reagents were thoroughly mixed and then degassed (as described in Section 3.2.1 above) to remove air entrained as a result of mixing. Mixtures were loaded into glass or PTFE vials or tubes and degassed once more. The vessels were then loosely capped with Al foil in order to prevent condensate from dripping into the tubes, but not hinder transport of steam to and from the samples. The vials or tubes were placed in an oven to cure. After removal and inspection, the samples were removed from their molds and then placed in the oven again for annealing. A representative curing and annealing process is to heat the sample from 82 to 130 °C at 2 °C/hr, then hold the temperature at 130 °C for several hours (typically 7-8 hr). Subsequently, the cured samples were removed from the molds and again placed in an oven for annealing at 250 °C (typically for 7-8 hr). The curing and annealing steps are varied with respect to temperature and duration to explore the effects of these process variables on the consolidation of APC materials.

7.3 Role of Additives and Phase Evolution

An attempt at direct substitution of $CaSiO_3$ for Al_2O_3 (Sample No. 0807d) was made by dry mixing 48.5 g natural wollastonite powder with 3.0 g $Al(OH)_3$. Separately, 0.02 g sodium ligninsulfonate was dissolved in 16.0 mL H_2O; this was followed by 11.5 g H_3PO_4 and 13.8 g $NaH_2PO_4 \bullet H_2O$. This solution was mixed with the dry wollastonite and $Al(OH)_3$. Some foaming ensued; this may be due to release of CO_2 from the rapid H_3PO_4 induced dissolution of possible calcium carbonate ($CaCO_3$) impurities in the wollastonite. However, it should be noted that this impurity can only be present in very small quantities as XRD analyses of the wollastonite revealed no indication of the presence of calcium carbonate. After the foaming ceased, the mixture was degassed and loaded into a 50 mL polypropylene tube. This was loaded into an oven that was then ramped from 82 °C to 130 °C at 2 °C/hr, held at 130 °C for 8 hr, and cooled. After it was removed from the mold, it was baked out at 170 °C for 7 hr.

The result was a very smooth, strong relatively pore-free monolith that broke with difficulty (Figure 7-1). There was no observed expansion or shrinkage during the cure procedure. The top of the monolith was flat and smooth, with no efflorescence. The density of the monolith was 1.63 g/cm^3. This synthesis was repeated as a threefold scaleup to produce 2 larger monoliths (0823f), one of which was annealed at 230 °C. Both 0807d and 0823f were used in water resistance testing.

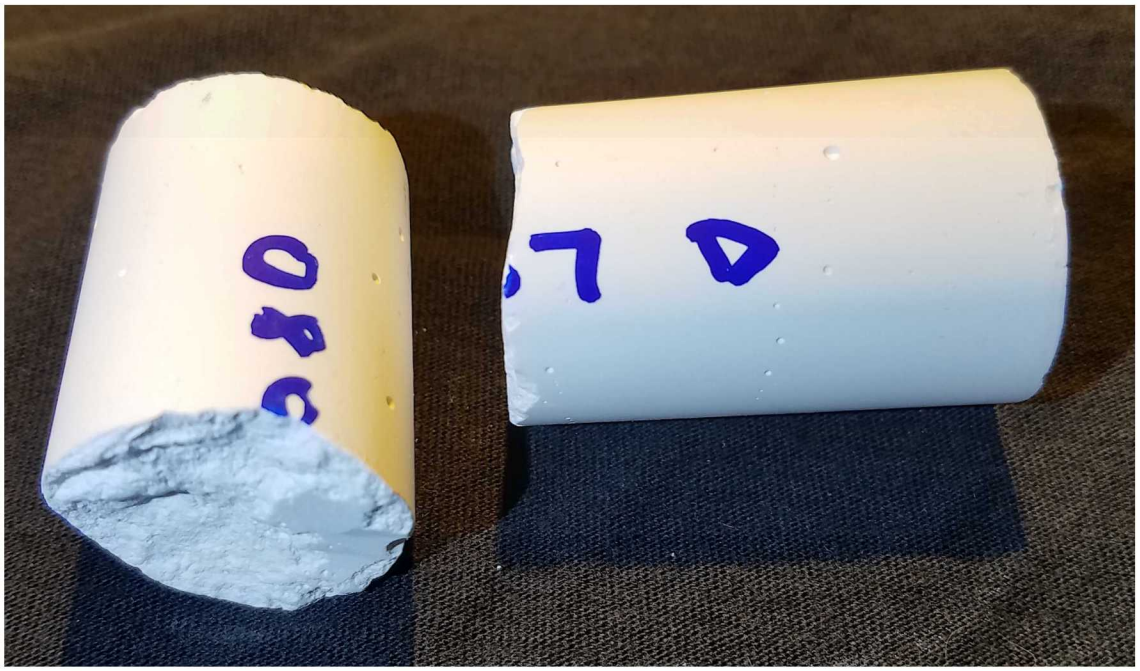

Figure 7-1. Sample No. 0807d. Wollastonite monolith ~ 2.5 cm in diameter and 7.5 cm long. Note the small number of isolated pores ~ 1mm or less in diameter.

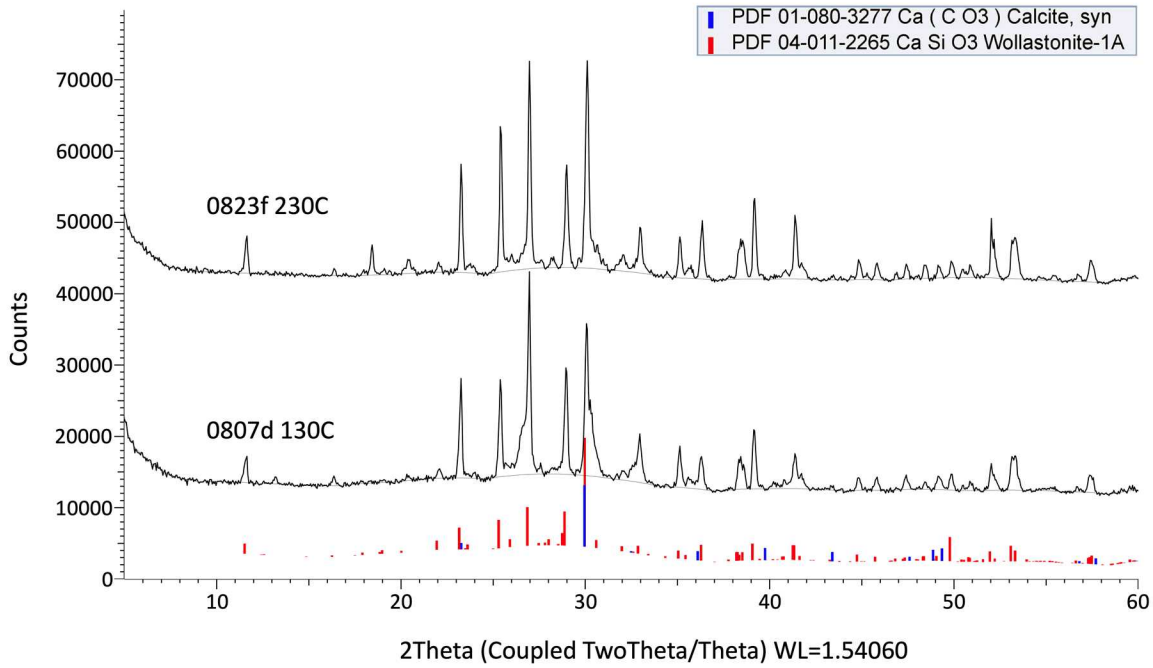

Figure 7-2. Powder XRD patterns of Sample Nos. 0807d and 0823f. Peak comparative analysis indicates both samples are composed primarily of wollastonite.

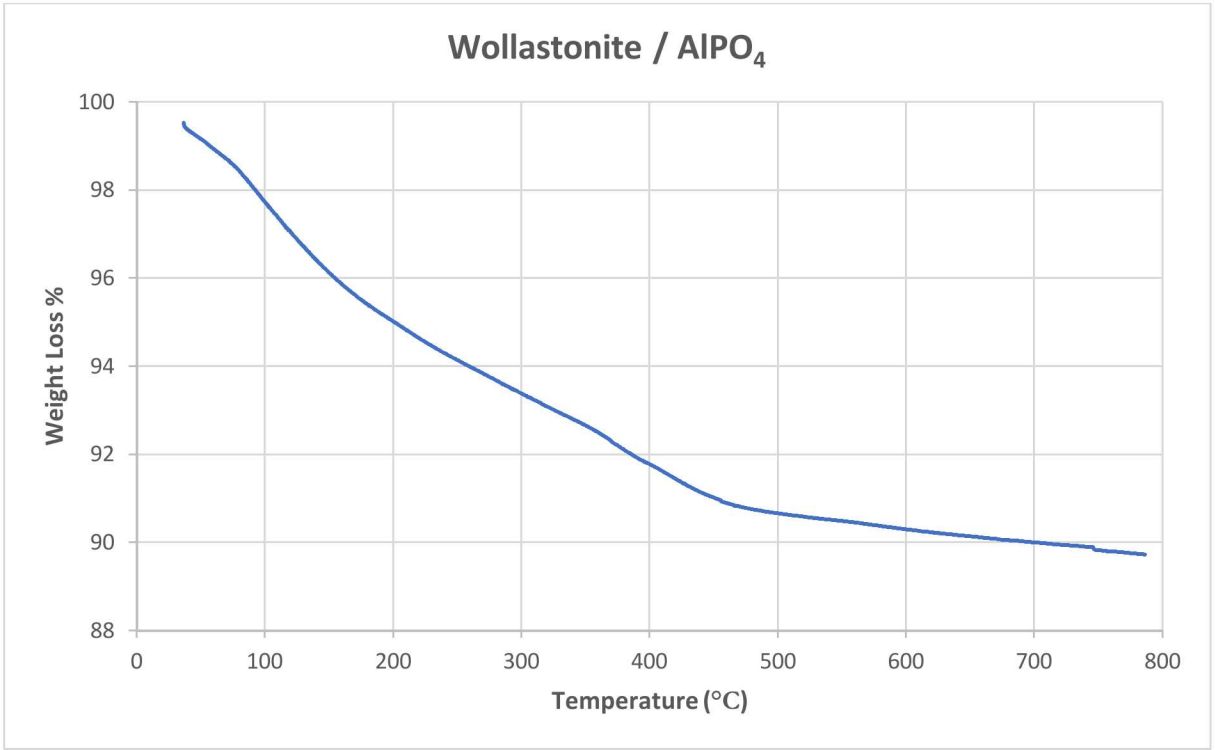

Figure 7-3. TGA of Sample No. 0807d showing approximately 9.5% weight loss between 50 °C and 750 °C. Between 250 and 750 °C there is approximately 4% weight loss.

X-ray diffraction (Cu Kα, λ = 0.15406 nm) showed mostly wollastonite. No calcium phosphate or aluminum phosphate phases were apparent (Figure 7-2). TGA results showed approximately 9.5% weight loss between 50 °C and 750 °C (Figure 7-3). Notably, these data were collected on a sample that had been baked out at 170 °C, and the weight loss between 50 and 170 °C was 4%, so this was moisture that the sample had picked up from ambient humidity.

A second experiment (Sample No. 0814d) using the same composition described above (Sample No. 0807d) was prepared using larger quantities of reactants. Sample No. 0814d made by dry mixing 970 g natural wollastonite powder with 60 g $Al(OH)_3$. Separately, 0.4 g sodium ligninsulfonate was dissolved in 320 mL H_2O; this was followed by 230 g H_3PO_4 and 276 g $NaH_2PO_4 \bullet H_2O$. This solution was mixed with the dry wollastonite and $Al(OH)_3$ and degassed. The resulting mixture was loaded into a steel mold and two polypropylene molds. These were loaded into an oven, ramped from 82 °C to 130 °C at 2 °C/hr, held at 130 °C for 8 hr, and cooled. The product monoliths (Figure 7-4) were 2.5 cm and 9.8 cm in diameter; both had flat tops and showed no signs of expansion, shrinkage, or efflorescence. The measured density of the 9.8 cm diameter large monolith was 1.56 g/cm^3, and there were relatively large pores (approximately 2.3 mm in diameter) from bubbles along the sides of the 2.5 cm diameter monoliths, suggesting outgassing, possibly of CO_2, during the cure cycle. Notably, the 9.8 cm diameter monolith had no such bubbles.

Figure 7-4. Photograph of wollastonite monoliths (Sample No. 0814d).

Two other variants that contained no H_3PO_4 were prepared by dry mixing 100.0 g natural wollastonite powder with 6.0 g $Al(OH)_3$. These variants were prepared with $NaH_2PO_4 \bullet H_2O$ and $NH_4H_2PO_4$ respectively as alternative phosphate sources that are potentially less corrosive to DPC components than the low pH phosphoric acid reagent. In one case (Sample No. 0904c), 0.10 g sodium ligninsulfonate and 40.0 g $NaH_2PO_4 \bullet H_2O$ were separately dissolved in 50 mL H_2O. In the other (Sample No. 0904d), 0.10 g sodium

ligninsulfonate and 25.0 g $NH_4H_2PO_4$ were separately dissolved in 55 mL H_2O. These solutions were mixed with the dry wollastonite and $Al(OH)_3$ mixture and degassed. The resulting slurries were loaded into four polypropylene molds which were loaded into an oven, ramped from 82 °C to 130 °C at 2 °C/hr, held at 130 °C for 8 hr and cooled.

While these compositions may be attractive for applications that are sensitive to low pH conditions, for example the pH of the $NaH_2PO_4 \bullet H_2O$ solution is about 4, the monoliths resulting from these reactions had many 1-2 mm pores (Figure 7-5). It was noted that there was less outgassing during the mixing of the slurry as compared to that observed during the preparation of Sample No. 0807d (described above). Nevertheless, gas evolution in Sample Nos. 0904c and 0904d may have simply been delayed until heating due to the much slower reaction of the $CaCO_3$ impurity with the higher pH phosphate sources. The densities of the NaH_2PO_4 monoliths were approximately 1 g/cm^3, and that of the $NH_4H_2PO_4$ monoliths was approximately 0.9 g/cm^3. Notably, this porosity was not accompanied by significant expansion.

Figure 7-5. Wollastonite-phosphate Sample No. 0904c. Note the large number of irregular pores many of which appear to be interconnected with fracture like features.

The intriguing results with the reaction between wollastonite and acid phosphates led us to consider using talc, nominal formula $Mg_3Si_4O_{10}(OH)_2$. Talc is of interest due to its low density (approx. 2.6-2.8 g/cm^3) and platy crystal habit. Both of these features would be expected to produce a suspension of talc in aqueous phosphate that settles out slowly compared to corundum. A recipe was prepared by dry mixing 145.5 g talc powder with 9.0 g $Al(OH_3)$, then mixing this with a solution of 17.25 g H_3PO_4 (85% aq), 20.71 g $NaH_2PO_4 \bullet H_2O$, 63 g H_2O, and 0.03 g sodium ligninsulfonate (Sample No. 0823g). This was degassed and loaded into two polypropylene tubes. It was noted that expansion and bubbling started even before the tubes were loaded into the oven. The samples were ramped from 82 °C to 130 °C at 2 °C/hr, held at 130 °C for 8 hr, and cooled.

The expansion was of sufficient scale that density could not be conveniently measured (Figure 7-6), The material was a hard and brittle foam. Powder XRD revealed a considerable amount of magnesite ($MgCO_3$) in the product (Figure 7-7) which likely reacted with the H_3PO_4 to generate considerable amounts of CO_2 resulting the observed bubbling and expansion evident in the photograph below.

Figure 7-6. Photograph of Sample No.0823g. Note that the talc-based material foamed considerably upon preparation.

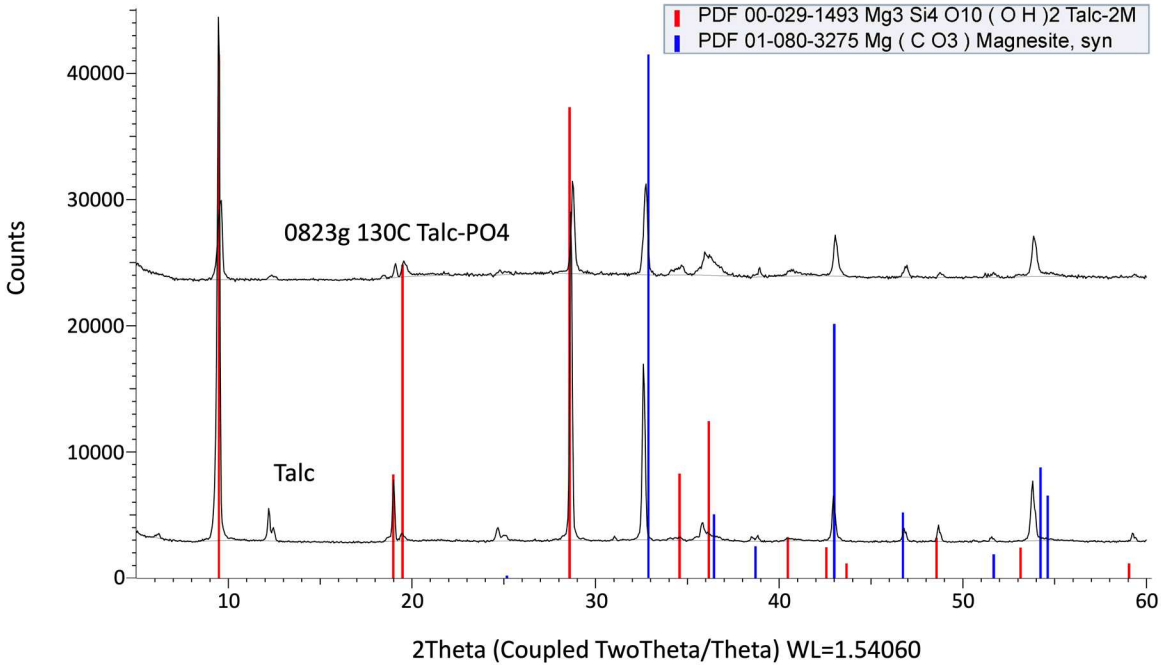

Figure 7-7. Powder XRD pattern of talc-based Sample No. 0823b. In addition to wollastonite, significant amounts of $MgCO_3$ are also present.

7.4 Viscosity Data

Similar to the CPC materials discussed in Section 5 above, the wollastonite aluminum phosphate cement demonstrated a relatively short working time while becoming demonstrably thicker on the order of a few hours. Viscosity as a function of time for the 0814 recipe is provided below.

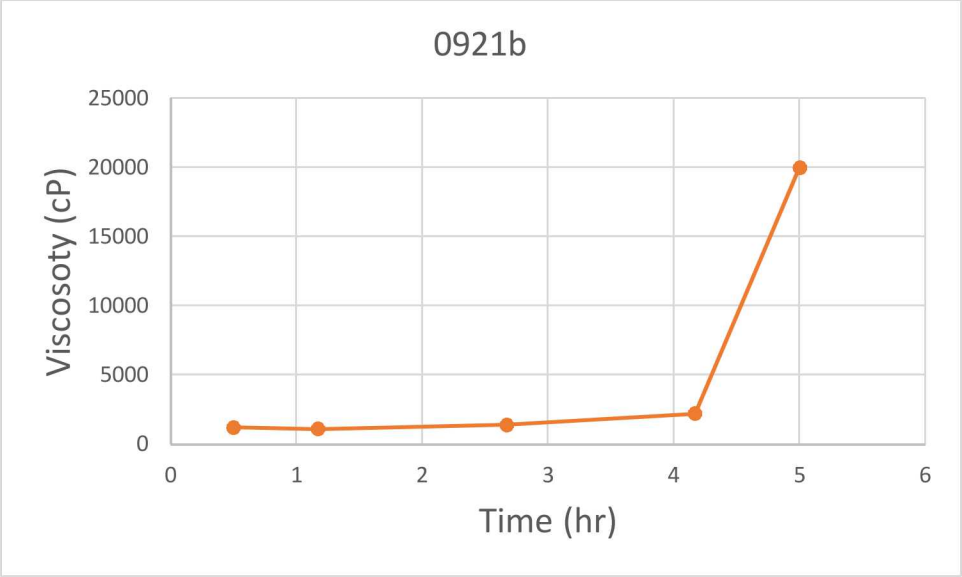

Figure 7-8. Viscosity Data for 0921b

Measured viscosities of the sample slurry 0921b began at 30 minutes and remained reasonably constant at around 1,200 to 1,400 cP for 4 hours and then rapidly increased to over 20,000 cP by 5 hours. This indicates a working time of 4 hours after which the slurry viscosity rapidly increases perhaps as a result of the initiation of setting. This requires further investigation as these materials may slowly set room temperature.

7.5 Wollastonite Aluminum Phosphate Mechanical Properties

A set of basic tests was performed for screening purposes upon small wollastonite phosphate samples. The materials were provided as described below and required machining of the outer diameter, and length to develop the desired right circular cylinders for strength testing. The finished dimensions, density, unconfined compressive strength (UCS), and Young's modulus are given in Table 7-1 below.

The samples were all variants of wollastonite $AlPO_4$. The preparation of 0814 is described above. Sample 0914d was similar to 0814 except that the $Al(OH)_3$ was replaced by metakaolin. Sample 0914e was also similar to 0814, except that it contained neither $Al(OH)_3$ nor metakaolin. Sample 0914f was the same as 0914d except that it used $NH_4H_2PO_4$ as a phosphate source (along with H_3PO_4) instead of NaH_2PO_4. Our goal with these samples was to determine how these compositional variables impact mechanical performance.

Sample No. 0914d was prepared by mixing and degassing 100.0 g natural wollastonite ($CaSiO_3$), 6.0 g Sika MK100 metakaolin, 23.0 g H_3PO_4, 27.6 g $NaH_2PO_4 \bullet H_2O$. This slurry was poured into two 50 mL centrifuge tubes, which were used as molds. These were heated from 82 to 130 °C at 2 °C/hr, then held at 130 °C for 8 hr. After removing the cured samples from their molds, one sample was selected for annealing at 250 °C for 8 hr and subsequent mechanical testing.

Sample Nos. 0914e: 100.0 g natural wollastonite ($CaSiO_3$), 23.0 g H_3PO_4, 27.6 g $NaH_2PO_4 \bullet H_2O$, and 50.0 g H_2O were mixed and degassed. This slurry was poured into two 50 mL centrifuge tubes, which were used as molds. These were heated from 82 to 130 °C at 2 °C/hr, then held at 130 °C for 8 hr. After removing the cured samples from their molds, one sample was selected for annealing at 250 °C for 8 hr.

Sample No. 0914f: 100.0 g natural wollastonite ($CaSiO_3$), 6.0 g Sika MK100 metakaolin, 23.0 g H_3PO_4, 27.6 g $NH_4H_2PO_4$, and 50.0 g H_2O were mixed and degassed. This slurry was poured into two 50 mL centrifuge tubes, which were used as molds. These were heated from 82 to 130 °C at 2°C/hr, then held at 130 °C for 8 hr. After removing the cured samples from their molds, one sample was selected for annealing at 250 °C for 8 hr.

Table 7-1. Mechanical properties data on selected wollastonite phosphate fillers.

Sample ID	Dimension				Weight grams	Density	UCS	Young's Modulus	Poisson's ratio
	Diameter (in)	Diameter (cm)	Length (in)	Length (cm)		g/cc	psi	psi	
0814	0.9114	2.315	2.053	5.215	33.13	1.51	1665	175714	0.9114
0914d	1.263	3.208	2.677	6.800	70.38	1.28	130	8500	1.263
0914e	1.249	3.172	2.946	7.483	79.54	1.34	211	13300	1.249
0914f	1.136	2.885	2.468	6.269	55.8	1.36	478	97333	1.136

Sample No. 0814, which was prepared with $Al(OH)_3$ as the aluminum source and a buffered solution of H_3PO_4 and $NaH_2PO_4 \bullet H_2O$ as the phosphate source, yielded an impressive near net-shape monolith (Figure 7-4). Preliminary evaluation of mechanical properties evaluation revealed a UCS of 1,665 psi, the highest compressive strength tested of any sample in this report. In sharp contrast, the samples fabricated using metakaolin as the Al source (0914d and 0914f) for aluminum phosphate binder formation produced considerably lower UCS values. Finally, Sample No. 0914e, an attempt to produce a calcium phosphate binder from the reaction of wollastonite with H_3PO_4 and $NaH_2PO_4 \bullet H_2O$, also yielded a low compressive strength upon testing.

7.6 Water Resistance Testing

Several of the wollastonite-phosphate samples were selected for water resistance testing (as described in Section 3.3.6 above) in an aqueous environment (Table 7-2). The samples were sealed with water in PFTE sleeves and placed in an Autoclave Engineers 4-liter reactor, into which was poured an additional 2 liters of DI water. After sealing the reactor, it was then heated to 200 °C for 48 hr, subsequently cooled and reopened so the sleeves could be recovered. Upon opening the sleeves, the pH of the water was tested, and if intact, the disc was recovered and dried at 130 °C for 6 hours in order to drive off and residual moisture, and weighed. Low weight loss was anticipated to indicate sample stability and integrity with exposure to hydrothermal conditions. Only the disc was recovered and weighed; any sediment that fell off the disc during the test was considered lost weight.

Table 7-2. Hydrothermal test results of selected wollastonite-phosphate samples.

Sample ID	Starting wt. (g)	pH after test	Wt. after test (g)	% wt. loss
0807d 250 °C	7.23	7	6.65	8.0
0823f 250 °C	6.84	7	6.35	7.2
0814 250 °C	17.5	6	16.31	6.8
0904c 250 °C	15.21	8	14.20	6.6
0914d 250 °C	10.72	7	9.59	10.54
0914e 250 °C	10.55	6	9.01	14.6
0914f 250 °C	13.02	4	12.03	7.6

During the opening and recovery of the wollastonite-phosphate samples after hydrothermal treatment no sediment or sample fragments were observed and hence the discs were recovered intact. However, all three of the samples lost significant weight post-test indicating possible partial sample dissolution. The observed weight losses may simply be from leaching of excess and unreacted phosphate reagents (H_3PO_4, $NaH_2PO_4 \bullet H_2O$ and $NH_4H_2PO_4$) from the samples during hydrothermal treatment. The cause for the weight loss will be investigated in FY20 as work progresses on the evaluation of the Wo-CBPC material system.

Sample Nos. 0807d and 0823f were compositionally identical to 0814, prepared with $Al(OH)_3$ as the aluminum source and a buffered solution of H_3PO_4 and $NaH_2PO_4 \bullet H_2O$. These identical materials consistently exhibited weight loss that may indicates some dissolution has occurred. Sample No. 0904c was composed of wollastonite with $NaH_2PO_4 \bullet H_2O$ as the phosphate source, and no H_3PO_4, and also exhibited weight loss.

The 0914 series as described above in Section 7.5 showed significant weight loss, in particular Sample Nos. 0914d and 0914e. The cause of this is uncertain and these samples will be further evaluated in FY20. However, it should be noted some sediment was lost during the wet test suggesting partial disintegration. The cause of this is likely due to the integrity of the binder.

7.7 Summary

Sample 0814, which was prepared with $Al(OH)_3$ as the aluminum source and a buffered solution of H_3PO_4 and $NaH_2PO_4 \bullet H_2O$ as the phosphate source, yielded an impressive near net-shape monolith (Figure 7-4) with superior mechanical properties and modest water resistance. Metakaolin prove to be a much less effective Al source than $Al(OH)_3$, at least in the limited set of experiments performed to date.

This page is intentionally left blank.

8. CONCLUSIONS AND PATH FORWARD

Based on FY18 Milestone M4SF-18SN010305024 "Recommendations for Filler Material Composition and Delivery Method for Bench-Scale Testing" the following filler compositions were selected for experimental screening work and accelerated testing in FY19. These compositions included the following:

- Aluminum phosphate cements (APCs); more specifically aluminum oxide / aluminum phosphate (Al_2O_3 / $AlPO_4$) cements where Al_2O_3 serves as the filler material bound by an $AlPO_4$ binder formed by the reaction of Al_2O_3 with H_3PO_4;
- Calcium phosphate cements (CPCs); more specifically composed of pure or nearly pure hydroxyapatite ($Ca_5(PO_4)_3(OH)$);
- Magnesium potassium phosphate cements (MKPs) composed of magnesium oxide / magnesium potassium phosphate (MgO / $MgKPO_4$) cements where MgO serves as the filler and $MgKPO_4$ serves as the binder formed by the reaction of MgO with monopotassium phosphate (KH_2PO_4) and tricalcium phosphate (($Ca_3(PO_4)_2$);

Based on the previous milestone, the primary focus of our efforts was focused on the development of promising APC formulations and optimized processing conditions. Work was also initiated on CPCs and MKPs.

Two additional potential cement materials were explored preliminarily as the result of: (1) continued literature investigations into other filler candidates (wollastonite-based phosphate ceramic) and (2) the experimental discovery of a well-consolidated fly ash-based bonded phosphate cement during the evaluation of fly ash as a potential filler material with Al_2O_3 in APCs.

- Fly ash phosphate cements, more specifically where a fly ash material composed primarily of mullite and quartz serves as the filler and is reacted with H_3PO_4 to form amorphous phosphate phase(s) as the binder;
- Wollastonite aluminum phosphate cements, specifically they are wollastonite / aluminum phosphate ($CaSiO_3$ / $AlPO_4$) where $CaSiO_3$ serves as the filler material and $AlPO_4$ serves as the binder formed by $Al(OH)_3$ or metakaolin as Al sources and H_3PO_4 or ADP ($NH_4H_2PO_4$) as phosphate sources.

FY19 research activities focused primarily on the optimization of compositions and subsequent processing of these five materials, with emphasis on APCs, to achieve dense and well-consolidated monolithic samples with relatively low porosity. Once these goals were met basic material properties screening evaluations were performed including an assessment of: (1) cement slurry viscosity and stability over time; (2) dissolution resistance in water at elevated temperature and pressure; and (3) mechanical testing including ultimate compressive strength testing.

Aluminum Phosphate Cements (APCs)

Progress with respect to the APC system initially focused on the examination Al_2O_3 / $AlPO_4$ formed by the reaction between Al_2O_3 with H_3PO_4 may be written as $Al_2O_3 + H_3PO_4 \rightarrow 2AlPO_4 + 3H_2O$ where an excess of Al_2O_3 is reacted with phosphoric acid (H_3PO_4) to form the $AlPO_4$ bonded Al_2O_3 cement. Water is added as necessary to adjust reactant viscosity and form a smooth pourable slurry. The slurry is effectively stable and unreactive at room temperature; heat is required in excess of 130 °C for several hours to drive the reaction to completion and produce a consolidated monolith.

We explored two consolidation pathways with the application of heat: (1) heating under hydrothermal conditions by placing APC samples in containers in a Parr pressure vessel in the presence of liquid water in equilibrium with steam at a pressure of approximately 1 MPa, and (2) heating the sample under ambient pressure without the use of a pressure vessel.

APC Consolidation under Hydrothermal Conditions

We found that the reaction of Al_2O_3 and H_3PO_4 at 170 °C in using the hydrothermal consolidation process is fairly rapid, and at the scales we tested may be substantially complete in less than 24 hr. This reaction produces well-consolidated, monoliths with minor isolated porosity and adequate mechanical strength. The reaction products are principally berlinite, $AlPO_4$–cristobalite, and $AlPO_4 \bullet H_2O$. The data suggest that $AlPO_4$–cristobalite is the decomposition product of $AlPO_4 \bullet H_2O$. It is not clear whether either berlinite or $AlPO_4$–cristobalite or both together function as binder phases in the monoliths. Once we learn this we anticipate being able to alter the reaction conditions to favor one phase over the other. We examined several alternative starting reagents including $Al(OH)_3$ and AlOOH as substitutes for Al_2O_3 and phosphonic acids as substitutes for H_3PO_4. None of these alternatives proved effective as substitutes.

With respect to additives, both fumed aluminum oxide and $Al(OH)_3$ were investigated in combination with Al_2O_3 but neither produced acceptable results. It should be noted that the additive loadings were quite high in these tests (e.g., the Al_2O_3 : $Al(OH)_3$ wt.:wt. was 6:1). In the experiments to produce well-consolidated APCs by heating under ambient pressure conditions (summarized below) much smaller amounts of the $Al(OH)_3$ additive with Al_2O_3 produced very promising results. This suggests the $Al(OH)_3$ additive should be revisited using the hydrothermal process at a wt.:wt. ratio of 19 or more. In addition, boric acid and fly ash were tested as additives to the Al_2O_3 and H_3PO_4 starting materials. Neither additive contributed meaningfully to the mechanical stability of the resulting products.

The viscosity of the Al_2O_3 and H_3PO_4 mixture in water is stable over at least several days. While the viscosities of the reaction mixtures tested were on the order of 2,000 cP, it is likely that higher starting water concentrations and thus lower viscosities are available, since the water in the starting material rapidly comes into equilibrium with steam as the reaction starts.

Recommended future work on hydrothermally produced APCs should focus on fine-tuning the reaction parameters and characterizing the products in greater detail. Specifically work should focus on addressing: (1) the optimization of the APC formulation to improve mechanical performance with concomitant porosity reduction through the use of additives; (2) the evolution of the $AlPO_4$ binder phases (berlinite, $AlPO_4$–cristobalite, and $AlPO_4 \bullet H_2O$) and their effect on mechanical properties and solubility; (3) the effect of reaction rate on volume scaling; and (4) the potential effects of steam-water equilibrium during the hydrothermal reaction.

APC Consolidation under Ambient Pressure Conditions

Preliminary experiments using thermal processing at ambient pressures consistently yielded well-consolidated but highly porous monoliths, a less than ideal outcome for the DPC use case. However, we recognized that adjusting the reactivity of the system through the use of additives may be possible to reduce the evolution of porosity in the system. After a detailed exploration of the composition space and additive effects it appears that well-consolidated APC monoliths lacking large voids can be made by thermal treatment at ambient pressure. The best results were obtained by adding small amounts of metakaolin or $Al(OH)_3$ to the Al_2O_3 (e.g., Al_2O_3:$Al(OH)_3$ = 19:1) starting material. We believe these additives both function by reacting with a portion of the phosphate source at a lower temperature than that at which the phosphate reacts with Al_2O_3 alone. This causes the cement to partially consolidate and enables it to retain shape while allowing the water to escape as steam from the reacting Al_2O_3 and phosphate.

The phosphate sources that are most effective with these additives are $NaH_5(PO_4)_2$ and $NH_4H_5(PO_4)_2$. Of these, $NaH_5(PO_4)_2$ yielded high-quality monoliths more consistently than did $NH_4H_5(PO_4)_2$ and thus the $NaH_5(PO_4)_2$ based APCs with metakaolin and $Al(OH)_3$ additives were subsequently selected for mechanical testing. Of the two additives, metakaolin and $NaH_5(PO_4)_2$ produced monoliths with fewer cracks than did $Al(OH)_3$ and $NaH_5(PO_4)_2$

Viscosity of the Al_2O_3 / metakaolin with $NaH_5(PO_4)_2$ slurry plateaued at around 15,000 cP. The higher viscosities as compared to the simple Al_2O_3 / H_3PO_4 mixtures discussed above are likely a result of the

higher surface area of the metakaolin additive. The simple addition of small amounts of additional water have been shown to reduce viscosities considerably from 15,000 to 5,000 cP.

We have started to investigate the relative compressive strengths of Al_2O_3 / metakaolin and Al_2O_3 / $Al(OH)_3$ monoliths made with the same alumina / additive ratios but do not have sufficient data to draw conclusions favoring one additive over the other.

Recommended future work on APCs thermally cured at ambient pressure should focus on investigating the composition space more thoroughly and characterizing the products in greater detail. The work should focus on addressing: (1) the optimization of the APC formulation to improve mechanical performance with concomitant porosity reduction through the use of additives (in particular metakaolin and $Al(OH)_3$ with $NaH_5(PO_4)_2$); (2) the evolution of the $AlPO_4$ binder phases (berlinite, $AlPO_4$–cristobalite, and $AlPO_4 \bullet H_2O$) and their effect on mechanical properties and solubility; and (3) effects of water content on material properties including compressive strength, density, and volume change from the starting slurry to the final product.

Calcium Phosphate Cements (CPCs)

There are well-established routes using tetracalcium phosphate (TTCP) and dibasic calcium phosphate (DCPA) to prepare CPCs. These are based on its use for clinical applications such as dental appliances and bone replacement. These synthesis routes typically have the disadvantage of fast set times even at room temperature, and because the starting materials are produced in small quantities there is the added disadvantage of relatively high cost.

Attempts to produce a dense well-consolidated CPC on the benchtop with less expensive starting materials, particularly inexpensive calcium salts, were unsuccessful. A variety of potential chelating agents were examined in order to improve the TTCP/DCPA based CPC cement workability and setting time. These chelating additives we tried did not prove viable for increasing set times.

We then focused on modified dental cement formulations using TTCP with DCPA with potassium phosphate salts mixed in H_2O. An alternative chelating agent, dodecanedioic acid (DDDA), a dicarboxylic acid that is soluble in potassium phosphate solutions, was used to increase set times (on the order of several hours). These formulations show some promise. Concentrations of DDDA at or near the solubility limit, relative to phosphate salt concentration, produce robust monoliths at a benchtop scale. However, these monoliths showed a tendancy to disaggregate during water resistance test possibly because there are detectable amounts of TTCP starting material, as indicated by XRD analyses, remaining in the monolith after consolidation.

Recommended future work on CPCs should focus on: (1) additional reduction in the viscosity of the slurry; (2) increasing the slurry set time; and (3) examining the effects of residual salt/organic content CPC mechanical properties and solubility.

Fly Ash Phosphate Cements

The observation that fly ash and H_3PO_4 form hard and pore-free monoliths led us to perform a small set of screening experiments to assess fly ash phosphates as potential candidate fillers. The evaluations completed to date reveal it is possible to produce well-consolidated fly ash phosphate fillers at the bench top scale. Further, these materials can exhibit acceptable compressive strengths for the use case. However, the low pH observed for all samples after the water resistance test, is counter to the use case. Further, the thermochemistry of the system, specifically the evolution of unexpected phosphate phases (hydrogen calcium phosphate hydrate and triclinic $AlPO_4$) and their subsequent conversion to amorphous phosphate phases as a function of temperature is complicated; likely the most complicated of all the systems examined in this report. Further study of the fly ash phosphate system for DPC filler applications is not planned at this time.

Wollastonite Aluminum Phosphate Cements (WAPC)

Inspired by the work of Colorado et al., (2011) on wollastonite cements for radioactive waste disposal applications, we recognized that wollastonite ($CaSiO_3$) might serve as an alternative material for Al_2O_3. Accordingly, we produced a small number of WAPC materials with the goal of replacing the Al_2O_3 as a filler while creating an $AlPO_4$ binder through the addition of a reactive alumina and phosphate source. Metakaolin and $Al(OH)_3$ were studied as sources for alumina and soluble aluminum, with $NaH_5(PO4)_2$ as the phosphate source. Addition of $Al(OH)_3$ and $NaH_5(PO_4)_2$ with wollastonite yielded an impressive near net-shape monolith with very good mechanical properties and modest water resistance. Metakaolin proved to be a much less effective Al source than $Al(OH)_3$, at least in the limited set of experiments performed to date. Of concern with this material system is the weight loss during water resistance testing, which indicates dissolution. In general, they exhibited the greatest weight loss of all the systems studied.

Future work in the WAPC system should involve further exploration of the composition and thermal spaces, and focus on determining the state of phosphate in the product. Specifically, testing should evaluate: (1) the effects of annealing temperature on structure and mechanical performance; (2) the effects of varying the wollastonite : gibbsite ratio; (3) optimizing the WAPC formulations to improve mechanical performance with concomitant porosity reduction through the use of additives; (4) investigation of reactions between calcium aluminates and phosphates on WAPC hydrothermal stability, and mechanical performance; and (5) the cause of relatively high weight loss during water resistance testing which indicates a lack of binder integrity.

9. REFERENCES

Achelhi, K., S. Masse, G. Laurent, A. Saoiabi, A. Laghzizil, & T. Coradin (2010). Role of carboxylate chelating agents on the chemical, structural and textural properties of hydroxyapatite. *Dalton Transactions, 39*(44), 10644-10651. doi:10.1039/C0DT00251H

Alsaed, A., E.L. Hardin, L.L. Price, *Comparative Cost Analysis for Disposal of DPCs Relative to Repackaging*. American Nuclear Society Winter Meeting. Boston MA, November, 2019.

Bahrami, M., M. Ahadi, M. Andisheh-Tadbir, M. Tam. An improved transient plane source method for measuring thermal conductivity of thin films : Deconvoluting thermal contact resistance. International Journal of Heat and Mass Transfer. 2016;96:371-380. doi:10.1016/j.ijheatmasstransfer.2016.01.037.

Bauer, S., A. Urquhart. Thermal and physical properties of reconsolidated crushed rock salt as a function of porosity and temperature. Acta Geotech. 2015. doi:10.1007/s11440-015-0414-8.

Bird, R.B., W.E. Stewart and E.N. Lightfoot. (1960). Transport Phenomena. JohnWiley and Sons Inc. New York, 780 p.

Bohner, M., U. Gbureck & J.E. Barralet (2005). Technological issues for the development of more efficient calcium phosphate bone cements: A critical assessment. *Biomaterials, 26*(33), 6423-6429. doi:https://doi.org/10.1016/j.biomaterials.2005.03.049

Chen, Z., X. Ren, S. Guo, X. Zhang, R. Zhang, M. Zhang, . . . Y. Zhang (2019). Micellization of selenium-containing cationic surfactants with different headgroups in aqueous solution. *Colloid and Polymer Science, 297*(2), 201-211. doi:10.1007/s00396-018-4454-0

Colorado, H.A., C. Hiel, H.T. Hahn and J.-M. Yang (2011). Chemically Bonded Phosphate Ceramic Composites, Metal, Ceramic and Polymeric Composites for Various Uses, Dr. John Cuppoletti (Ed.), ISBN: 978-953-307-353-8, InTech, Available from: http://www.intechopen.com/books/metal-ceramic-andpolymeric-composites-for-various-uses/chemically-bonded-phosphate-ceramic-composites.

Colorado, H.A., J. Pleitt, C. Hiel, J.M. Yang H.T. Hahn and C.H. Castro (2012) Wollastonite based-Chemically Bonded Phosphate Ceramics with lead oxide contents under gamma irradiation. Journal of Nuclear Materials, 425, p.197-204.

Greene, S.R., J.S. Medford, and S.A. Macy, "Storage and Transportation Cask Data for Used Commercial Nuclear Fuel – 2013 U.S. Edition", Advanced Technology Insights, LLC, Knoxville, TN, ATI-TR-13047, August 2013.

Habraken, W., P. Habibovic, M. Epple & M. Bohner (2016). Calcium phosphates in biomedical applications: materials for the future? *Materials Today, 19*(2), 69-87. doi:https://doi.org/10.1016/j.mattod.2015.10.008

Hardin, E.L., L.L. Price, E. Kalinina T. Hadgu, A. Ilgen, C. Bryan, J. Scaglione, K. Banerjee, J. Clarity, R. Jubin, V. Sobes, R. Howard, J. Carter, T. Severynse, AND F. Perry. *Summary of Investigations on Technical Feasibility of Direct Disposal of Dual-Purpose Canister*. FCRD-UFD-2015-000129, Rev.0. Washington, D.C.: U.S. Department of Energy 2015.

Hardin, E.L., P.V. Brady and C. Bryan, "Joint Workplan on Filler Investigations for DPCs," SFWD-SFWST-2018-000481 Rev. 0, SAND2017-13727 R, Sandia National Laboratories, Albuquerque, New Mexico, December 2017.

Hardin, E.L. and P.V. Brady (2018). *Recommendations for Filler Material Composition and Delivery Method for Bench- Scale Testing*. SFWD-SFWST-2018-000490 Rev. 0. U.S. Department of Energy, Office of Spent Fuel and Waste Science and Technology. March, 2018.

Holtec International. "Final Safety Analysis Report on the Hi-Storm 100", REPORT HI-2002444, ML101090397 ML101090397, Non-Proprietary Version, Rev 8, Holtec International, Marlton NJ, January 18, 2010. https://www.nrc.gov/docs/ML1010/ML101090397.pdf

Krogstad, D.V., D. Wang & S. Lin-Gibson (2017). Polyaspartic Acid Concentration Controls the Rate of Calcium Phosphate Nanorod Formation in High Concentration Systems. *Biomacromolecules, 18*(10), 3106-3113. doi:10.1021/acs.biomac.7b00772

Li, Y., H. Li, J. Chai, M. Chen, Q. Yang & J. Hao (2016). Properties and ionic self-assembled structures from mixture of a bola-type strong alkali dication and a branched phosphoric acid. *Journal of Colloid and Interface Science, 472*, 157-166. doi:https://doi.org/10.1016/j.jcis.2016.03.047

Martell, A.E. (1982). Chelates of Ascorbic Acid. In *Ascorbic Acid: Chemistry, Metabolism, and Uses* (Vol. 200, pp. 153-178): AMERICAN CHEMICAL SOCIETY.

Mohammed, M.A., R. Pusch, S. Knutsson and G. Hellstrom, "Rheological Properties of Cement-Based Grouts Determined by Different Techniques," Engineering, 6, 217-229, 2014. http://dx.doi.org/10.4236/eng.2014.65026

Nardello, V., N. Chailloux, G. Joly & J.-M. Aubry (2006). Preparation, amphiphilic properties and lyotropic phase behaviour of new surfactants based on sodium monoalkyl α,ω-dicarboxylates. *Colloids and Surfaces A: Physicochemical and Engineering Aspects, 288*(1–3), 86-95. doi:http://dx.doi.org/10.1016/j.colsurfa.2006.04.026

Owuor, P.S., T. Tsafack, H.Y. Hwang, M. Sajadi, S. Jung, T. Li, . . . P.M. Ajayan (2018). Interconnecting Bone Nanoparticles by Ovalbumin Molecules to Build a Three-Dimensional Low-Density and Tough Material. *ACS Applied Materials & Interfaces, 10*(48), 41757-41762. doi:10.1021/acsami.8b13681

Price, L.L., A.A. Alsaed, P.V. Brady, M. B. Gross, E.L. Hardin, M. Nole, J.L. Prouty K, Banerjee, and G.G. Davidson. *Postclosure Criticality Consequence Analysis – Scoping Phase*, M3SF-19SN010305061, SAND2019-4644 R. Albuquerque, NM: Sandia National Laboratories, 2019.

Price, L.L. *Consequences of Nuclear Criticality in Dual Purpose Canisters After Disposal* American Nuclear Society Winter Meeting. Boston MA, November, 2019.

Santa Cruz Chavez, G., D.L. Alge & T.-M.G. Chu (2011). Additive concentration effects on dicalcium phosphate dihydrate cements prepared using monocalcium phosphate monohydrate and hydroxyapatite. *Biomedical Materials, 6*(6), 065007. doi:10.1088/1748-6041/6/6/065007

SNL (Sandia National Laboratories) 2017. *Joint Workplan on Filler Investigations for DPCs*. SFWD-SFWST-2018-000481 Rev. 0. U.S. Department of Energy, Office of Spent Fuel and Waste Science and Technology. December, 2017.

Sugama, T. 2007. *Advanced Cements for Geothermal Wells*. Report BNL-77901-2007-IR. Brookhaven National Laboratory.

Tang, Y., R. Wang & Y. Wang (2015). Constructing Gemini-Like Surfactants with Single-Chain Surfactant and Dicarboxylic Acid Sodium Salts. *Journal of Surfactants and Detergents, 18*(1), 25-31. doi:10.1007/s11743-014-1632-z

U.S. DEPARTMENT OF ENERGY. *Yucca Mountain Repository License Application*. DOE/RW-0573, Rev. 1. Las Vegas, NV: U.S. Department of Energy, Office of Civilian Radioactive Waste Management 2009.

Wagh, A.S., S. Grover, and S.Y. Jeong, *Chemically Bonded Phosphate Ceramics: II Warm Temperature Process for Alumina Ceramics.* Journal of the American. Ceramic. Society., 86, 1845-1849, 2003.

Wagh, A.S. *Chemically Bonded Phosphate Ceramics: 21st Century Materials with Diverse Applications (1st Edition).* Elsevier Science. 2004.

Wagh, A.S. *Chemically Bonded Phosphate Ceramics: Twenty-First Century Materials with Diverse Applications (2nd edition).* Elsevier. 2016.

Zeng, R., M. Tu, H. Liu, J. Zhao, Z. Zha & C. Zhou (2009). Preparation, structure, drug release and bioinspired mineralization of chitosan-based nanocomplexes for bone tissue engineering. *Carbohydrate Polymers, 78*(1), 107-111. doi:https://doi.org/10.1016/j.carbpol.2009.04.035

Zhang, J., W. Liu, V. Schnitzler, F. Tancret & J.-M. Bouler (2014). Calcium phosphate cements for bone substitution: Chemistry, handling and mechanical properties. *Acta Biomaterialia, 10*(3), 1035-1049. doi:https://doi.org/10.1016/j.actbio.2013.11.001

Zhang, Y., W. Kong, P. An, S. He & X. Liu (2016). CO2/pH-Controllable Viscoelastic Nanostructured Fluid Based on Stearic Acid Soap and Bola-Type Quaternary Ammonium Salt. *Langmuir, 32*(10), 2311-2320. doi:10.1021/acs.langmuir.5b04459